AD_____

Award Number: DAMD17-01-1-0423

TITLE: Assessing Vascular Oxygen Dynamics for Breast Tumor Prognosis: Comparison Between MR BOLD and Near Infrared Method

PRINCIPAL INVESTIGATOR: Hanli Liu, Ph.D
Dr. Yuequing Gu

CONTRACTING ORGANIZATION: The University of Texas at Arlington, Arlington, TX 76019

REPORT DATE: September 2005

TYPE OF REPORT: Annual Summary (Final)

PREPARED FOR: U.S. Army Medical Research and Materiel Command
Fort Detrick, Maryland 21702-5012

REPORT DOCUMENTATION PAGE

Form Approved
OMB No. 0704-0188

1. REPORT DATE *(DD-MM-YYYY)*	2. REPORT TYPE	3. DATES COVERED *(From - To)*
September 2005	Annual Summary (Final)	1 SEP 2001 - 31 AUG 2005

4. TITLE AND SUBTITLE

Assessing Vascular Oxygen Dynamics for Breast Tumor Prognosis: Comparison Between MR BOLD and Near Infrared Method

5a. CONTRACT NUMBER

5b. GRANT NUMBER
DAMD17-01-1-0423

5c. PROGRAM ELEMENT NUMBER

6. AUTHOR(S)

Hanli Liu, Ph.D (mentor); Dr. Yuequing Gu
Professor of Bioengineering
email:Hanli@uta.edu

5d. PROJECT NUMBER

5e. TASK NUMBER

5f. WORK UNIT NUMBER

7. PERFORMING ORGANIZATION NAME(S) AND ADDRESS(ES)

The University of Texas at Arlington
Arlington, TX 76019

8. PERFORMING ORGANIZATION REPORT NUMBER

9. SPONSORING / MONITORING AGENCY NAME(S) AND ADDRESS(ES)

U.S. Army Medical Research and
Materiel Command
Fort Detrick, Maryland 21702-5012

10. SPONSOR/MONITOR'S ACRONYM(S)

11. SPONSOR/MONITOR'S REPORT NUMBER(S)

12. DISTRIBUTION / AVAILABILITY STATEMENT

Approved for public release; distribution unlimited

13. SUPPLEMENTARY NOTES

14. ABSTRACT

The objective of this study is to investigate vascular oxygen dynamics in breast tumors by correlating the results of NIRS and of the BOLD method. In the research, we wish to utilize the NIR technique for a better understanding of the BOLD method in order to improve its clinical use as a diagnostic and/or prognostic tool for breast cancer research and clinical practice.
We have proposed two hypotheses and three aims, as follows:
Hypothesis 1*:** Three-channel NIRS combined with a fiber optical needle can provide spatial information of hemoglobin saturation (SO_2) and concentration (Hb) of breast tumors during intervention. ***Hypothesis 2: Contrast agents in breast tumors based on the BOLD effect can be used to monitor variation in tumor oxygenation.
Aim 1: To investigate heterogeneity of SO_2 in the tumor vascular bed of breast tumors, using a three-channel NIR system against the fiber optic needle measurements. ***Aim 2***: To compare and correlate the measurement results of the breast tumors under 100% O_2 intervention taken simultaneously from the three-channel NIR oximeter and from the BOLD method. ***Aim 3***: To study the influence of several respiratory interventions on SO_2 and BOLD signals of breast tumors using both the three-channel NIR oximeter and the MRI BOLD method.

15. SUBJECT TERMS

technology development, radiologic sciences, tumor therapy planning and prognosis, tumor physiology monitoring

16. SECURITY CLASSIFICATION OF: Unclassified			17. LIMITATION OF ABSTRACT	18. NUMBER OF PAGES	19a. NAME OF RESPONSIBLE PERSON
a. REPORT	b. ABSTRACT	c. THIS PAGE			19b. TELEPHONE NUMBER *(include area code)*
U	U	U	UU	80	USAMRMC

Table of Contents

2001-2005 Final Report

This report presents the specific aims and accomplishments of our breast cancer research project during the years of funding sponsored by the US Department of the Army. It covers our activities from May 2001 to June 2005.

1. Introduction

Tumor oxygenation is believed to be crucial in clinical prognosis as evidenced by needle electrodes. It has been suggested that the Blood Oxygenation Level dependent (BOLD) method can provide a non-invaisve means for tumor oxygenation monitoring. However, interpretation of BOLD measurements is confounded by variation in hemoglobin concentration, oxygen saturation, and blood flow. Near infrared (NIR) spectroscopy (NIRS) can differentiate between changes in hemoglobin saturation and concentration in breast tumors caused by respiratory intervention.

The objective of this study is to investigate vascular oxygen dynamics in breast tumors by correlating the results of NIRS and of the BOLD method. In the research, we wish to utilize the NIR technique for a better understanding of the BOLD method in order to improve its clinical use as a diagnostic and/or prognostic tool for breast cancer research and clinical practice.

Specifically, we have proposed two hypotheses and three aims, as follows:

***Hypothesis 1*:** Three-channel NIRS combined with a fiber optical needle can provide spatial information of hemoglobin saturation (SO_2) and concentration (Hb) of breast tumors during intervention.

Hypothesis 2: Contrast agents in breast tumors based on the BOLD effect can be used to monitor variation in tumor oxygenation.

Aim 1: To investigate heterogeneity of SO_2 in the tumor vascular bed of breast tumors, using a three-channel NIR system against the fiber optic needle measurements.

Aim 2: To compare and correlate the measurement results of the breast tumors under 100% O_2 intervention taken simultaneously from the three-channel NIR oximeter and from the BOLD method.

Aim 3: To study the influence of several respiratory interventions on SO_2 and BOLD signals of breast tumors using both the three-channel NIR oximeter and the MRI BOLD method.

2. Body of the report

The PI along with her research collaborators as well as her graduate students have made significant efforts during the funding period to accomplish the proposed aims, resulting in multiple published journal papers and manuscripts. This report is organized in such a way that we will use our published papers and manuscripts to provide detailed information on specific aspects for each research aim, while the papers and manuscripts are organized as Appendices 1 to 4 for referral, as listed below:

Appendix 1:

Yueqing Gu, Vincent Bourke, Jae Kim, Anca Constantinescu, Ralph P. Mason, Hanli Liu, "Dynamic Response of Breast Tumor Oxygenation to Hyperoxic Respiratory Challenge Monitored with Three Oxygen-Sensitive Parameters," *Applied Optics*, 42(16), 2960-2967 (2003).

Appendix 2:

Hanli Liu, Yueqing Gu, Jae G. Kim, and Ralph P. Mason, "Near Infrared Spectroscopy and Imaging of Tumor Vascular Oxygenation," *Methods in Enzymology: Imaging,* ed. by Michael Conn, vol. 385-386, pp. 349-378 (2004).

Appendix 3:

Yueqing Gu, Ralph Mason, and Hanli Liu, "Estimated fraction of tumor vascular blood contents sampled by near infrared spectroscopy and ^{19}F magnetic resonance spectroscopy," *Optics Express* 13(5), 1724-1733 (2005). http://www.opticsexpress.org/abstract.cfm?URI=OPEX-13-5-1724.

Appendix 4:

Mengna Xia, Yueqing Gu, Hanli Liu, Vikram Kodibagkar, Anca Constantinescu, Ralph Mason, "Tumor oxygen dynamics measured simultaneously by near-infrared spectroscopy and MR EPI imaging," in Biomedical Topical Meetings on CD-ROM (The Optical Society of America, Washington, DC, 2004), ThF33.

Appendix 5:

Yueqing Gu, Mengna Xia, Hanli Liu, Vikram Kodibagkar, Anca Constantinescu, Ralph P. Mason, "Correlation of NIR spectroscopy with BOLD MR imaging of assessing breast tumor vascular oxygen status," in Biomedical Topical Meetings on CD-ROM (The Optical Society of America, Washington, DC, 2004), FB6.

Appendix 6:

Yulin Song, Yueqing Gu, Jae G. Kim, Hanli Liu, Anca Constantinescu, and Ralph P. Mason, "Correlation between total hemoglobin concentration and blood volume of breast tumors measured by NIR spectroscopy and ^{19}F MRS of PFOB," *OSA Biomedical Topical Meetings*, Technical Digest, SuH5, Miami Beach, FL, April 7-10, 2002.

Aim 1*: To investigate heterogeneity of SO_2 in the tumor vascular bed of breast tumors, using a three-channel NIR system against the fiber optic needle measurements.*

For Aim 1, we have designed, implemented, and refined a multi-distance, optical spectroscopic system, which allows us to perform simultaneous measurements of three oxygen-sensitive parameters: arterial hemoglobin oxygen saturation,SaO2, oxygenated hemoglobin concentration, HbO2 in tumor vasculature, and tumor oxygen tension, pO2 in response to hyperoxic respiratory challenge in rat breast tumors. The effects of two hyperoxic gases, oxygen and carbogen (5% CO2 and 95% O2) were compared, by use of two groups of Fisher rats with subcutaneous 13762NF breast tumors implanted in pedicles on the foreback. Also, two different gas-inhalation sequences were compared, i.e., air–carbogen–air–oxygen–air and air–oxygen–air–carbogen–air. The results demonstrate that both of the inhaled, hyperoxic gases significantly improved the tumor oxygen status. Detailed development, experimental descriptions, and data analysis for Aim 1 can be found in **Appendices 1 and 2**.

Aim 2*: To compare and correlate the measurement results of the breast tumors under 100% O_2 intervention taken simultaneously from the three-channel NIR oximeter and from the BOLD method.*

For Aim 2, we have performed animal measurements on Fisher rats with subcutaneous 13762NF breast tumors implanted in pedicles on the foreback using both the NIR oximeter and ^{19}F magnetic resonance spectroscopy. This study introduces an experimental approach to estimate percentage of hemoglobin content and volume sampled by near infrared spectroscopy (NIRS). Carbogen (5% CO2, 95% O2) respiratory intervention was used to induce physiological changes in a group of six Fisher rat breast tumors. Changes in total hemoglobin concentration, $[Hb]_{total}$, and in total blood volume, $\Delta V_{T\text{-}blood}$, of the tumors were measured by NIRS and ^{19}F magnetic resonance spectroscopy of perflubron, respectively. The ratio of $[Hb]_{total}/\ \Delta V_{T\text{-}blood}$ was used to calculate the fraction of hemoglobin contents sampled by NIRS. The results showed that the mean value of estimated fractions is within a range of 15~30% of total hemoglobin content in the tumor tissues. Based on the results, we suggest that NIRS does not sample the entire hemoglobin volume of the tissue vasculature, but is more sensitive to microvasculature. This study helps to understand the blood vascular volume sampled by NIRS, and demonstrates that the low cost, portable NIRS system may be a reliable, non-invasive, real-time, monitoring tool for changes in tumor blood contents. Refer to **Appendix 3** for more details.

Also, we have demonstrated the ability to simultaneously investigate tumor oxygen dynamics by Near-infrared spectroscopy and Fluorocarbon Relaxometry using Echo planar imaging for Dynamic Oxygen

Mapping in breast tumors, with close correlations between the two techniques. More details are given in **Appendices 4 and 6**.

Aim 3*: To study the influence of several respiratory interventions on SO_2 and BOLD signals of breast tumors using both the three-channel NIR oximeter and the MRI BOLD method.*

For Aim 3, we have studied dynamic changes of oxygenated and deoxygenated hemoglobin concentrations in response to hyperoxic gas interventions on rat breast tumors simultaneously measured by near infrared spectroscopy and BOLD (blood oxygenation level dependent) contrast MR imaging. We have demonstrated the ability to correlate NIR and ^{1}H MRI investigations simultaneously. This preliminary study demonstrates that the global signals of breast tumors obtained by NIRS and BOLD MRI in response to respiratory intervention are in good agreement. These two techniques may be complementary to one another for *in vivo* measurements of tumor oxygenation dynamics. MRI can be applied to deep tumors with special pulse sequences, whereas NIRS can be used to monitor acute responses of tumors to different therapeutic interventions. The correlation of NIRS and BOLD MRI techniques could provide a new prognostic tool for assessing efficacy of tumor therapies and could help us better interpret BOLD MRI signals. Furthermore, the heterogeneity of tumor vascular oxygenation dynamics to external interventions can be investigated directly by BOLD MRI, while the development of NIR imaging for tumor oximetry has also great potential to reveal tumor vascular heterogeneities. Please refer to **Appendix 5** for details.

Furthermore, during the course of conducting this proposed research project, we have explored new extra findings, as listed below:

We have investigated the effect of photothermal laser irradiation on rat breast tumor (DMBA-4) vascular contents. An 805-nm diode laser was used in our experiment with a power density ranging from 0.32 to 1.27 W/cm^2. The dynamic changes of oxygenated hemoglobin and total hemoglobin concentrations, $\Delta[HbO_2]$ and $\Delta[Hb]_{total}$, in rat tumors during photothermal irradiation were noninvasively monitored by a near-infrared spectroscopy system. A multichannel thermal detection system was also used simultaneously to record temperatures at different locations within the tumors. Our experimental results showed that: (1) photoirradiation did have the ability to induce hyperthermic effects inside the rat breast tumors in a single exponential trend; (2) the significant changes ($p<0.005$) of $\Delta[HbO_2]$ and $\Delta[Hb]_{total}$ in response to a low dosage of laser irradiation (0.32 W/cm^2) have a single exponential increasing trend, similar to that seen in the tumor interior temperature; and (3) the increase in magnitude of $\Delta[HbO_2]$ is nearly two times greater than that of $\Delta[Hb]_{total}$, suggesting that photoirradiation may enhance tumor vascular oxygenation. The last observation may be important to reveal the hidden mechanism of photoirradiation on tumors, leading to improvement of tumor treatment efficiency. The detailed study is reported in ***Appendix 7***: Yueqing Gu, Wei R. Chen, Mengna Xia, Sang W. Jeong, and Hanli Liu, "Effect of Photothermal therapy on breast tumor vascular contents: non-invasive monitoring by near infrared spectroscopy," *Photochemistry and Photobiology* 81(4), 1002–1009 (2005).

3. Research accomplishments and reportable outcomes

Peer-reviewed papers

1. Yueqing Gu, Wei R. Chen, Mengna Xia, Sang W. Jeong, and Hanli Liu*, "Effect of Photothermal therapy on breast tumor vascular contents: non-invasive monitoring by near infrared spectroscopy," *Photochemistry and Photobiology* 81(4), 1002–1009 (2005).
2. Yueqing Gu, Ralph Mason, and Hanli Liu*, "Estimated fraction of tumor vascular blood contents sampled by near infrared spectroscopy and ^{19}F magnetic resonance spectroscopy," *Optics Express* 13(5), 1724-1733 (2005). http://www.opticsexpress.org/abstract.cfm?URI=OPEX-13-5-1724
3. Hanli Liu*, Yueqing Gu, Jae G. Kim, and Ralph P. Mason, "Near Infrared Spectroscopy and Imaging of Tumor Vascular Oxygenation," *Methods in Enzymology: Imaging*, ed. by Michael Conn, vol. 385-386, pp. 349-378 (2004).
4. Zhiyu Qian, Sunder S. Victor, Yueqing Gu, Cole A. Giller, and Hanli Liu*, " 'Look-Ahead Distance' of a fiber probe used to assist Neurosurgery: Phantom and Monte Carlo study," *Optics Express*, 11(16) 1844-1855, (2003).
5. Yueqing Gu, Vincent Bourke, Jae Kim, Anca Constantinescu, Ralph P. Mason, Hanli Liu*, "Dynamic Response of Breast Tumor Oxygenation to Hyperoxic Respiratory Challenge Monitored with Three Oxygen-Sensitive Parameters," *Applied Optics*, 42(16), 2960-2967 (2003).

Conference papers or abstracts:

1. Mengna Xia, Yueqing Gu, Hanli Liu, Vikram Kodibagkar, Anca Constantinescu, Ralph Mason, "Tumor oxygen dynamics measured simultaneously by near-infrared spectroscopy and MR EPI imaging," in Biomedical Topical Meetings on CD-ROM (The Optical Society of America, Washington, DC, 2004), ThF33.
2. Yueqing Gu, Mengna Xia, Hanli Liu, Vikram Kodibagkar, Anca Constantinescu, Ralph P. Mason, "Correlation of NIR spectroscopy with BOLD MR imaging of assessing breast tumor vascular oxygen status," in Biomedical Topical Meetings on CD-ROM (The Optical Society of America, Washington, DC, 2004), FB6.
3. V. A. Bourke, Y Gu, A. Constantinescu, H. Liu and R. P. Mason, "Dynamic Optical Interrogation Of Oxygenation In The Tumor Microenvironment", The Eighth International Conference on Tumor Microenvironment and Its Impact on Cancer Therapies, Miami (South Beach), Florida, May, 2003.
4. Jae G. Kim, Yueqing Gu, Anca Constantinescu, Ralph P. Mason, Hanli Liu, "Non-Uniform Tumor Vascular Oxygen Dynamics Monitored By Three-Channel Near-Infrared Spectroscopy", *Proc. SPIE-Int. Soc. Opt. Eng.* 4955, 388-396 (2003).
5. Yueqing Gu, Vikram Kodibagkar, Mengna Xia, Zhiyu Qian, Jae. G. Kim, Anca Constantinescu, Ralph P. Mason, Hanli Liu "Simultaneous determination of breast tumor vascular oxygenation and blood volume measured with near infrared spectroscopy and ^{19}F MRS and ^{1}H MRI," presented in *SPIE, Photonics West*, San Jose, CA, Jan. 26-29, 2003.
6. Yulin Song, Yueqing Gu, Jae G. Kim, Hanli Liu, Anca Constantinescu, and Ralph P. Mason, "Correlation between total hemoglobin concentration and blood volume of breast tumors measured by NIR spectroscopy and ^{19}F MRS of PFOB," *OSA Biomedical Topical Meetings*, Technical Digest, SuH5, Miami Beach, FL, April 7-10, 2002.

4. Conclusions

The objective of this study was to investigate vascular oxygen dynamics in breast tumors by correlating the results of NIRS and of the BOLD method. In the research, we have utilized the NIR technique for a better understanding of the BOLD method in order to improve its clinical use as a diagnostic and/or prognostic tool for breast cancer research and clinical practice.

Throughout the study, we have demonstrated that both of the inhaled, hyperoxic gases significantly improved the tumor oxygen status. Arterial hemoglobin oxygen saturation,SaO2, oxygenated emoglobin concentration, HbO2 in tumor vasculature, and tumor oxygen tension, pO2 displayed similar dynamic response in rat breast tumors to two hyperoxic gases, oxygen and carbogen (5% CO2 and 95% O2). But the response times were different: the fastest for arterial SaO2, followed by biphasic changes in tumor vascular HbO2, and then delayed responses for pO2. Both of the gases induced similar changes in vascular oxygenation and regional tissue pO2 in the rat tumors, and changes in HbO2 and mean pO2 showed a linear correlation with large standard deviations, which presumably results from global versus local measurements. Indeed, the pO2 data revealed heterogeneous regional response to hyperoxic interventions. Although preliminary near-infrared measurements had been demonstrated previously in this model, the addition of the pO2 optical fiber probes provides a link between the noninvasive relative measurements of vascular phenomena based on endogenous reporter molecules, with the quantitative, albeit, invasive pO2 determinations.

Also, our preliminary study investigated dynamic changes of oxygenated and deoxygenated hemoglobin concentrations in response to hyperoxic gas interventions on rat breast tumors simultaneously measured by near infrared spectroscopy and BOLD (blood oxygenation level dependent) contrast MR imaging. We have demonstrated the ability to correlate NIR and ^{1}H MRI investigations simultaneously. This preliminary study demonstrates that the global signals of breast tumors obtained by NIRS and BOLD MRI in response to respiratory intervention are in good agreement. These two techniques may be complementary to one another for *in vivo* measurements of tumor oxygenation dynamics. MRI can be applied to deep tumors with special pulse sequences, whereas NIRS can be used to monitor acute responses of tumors to different therapeutic interventions. The correlation of NIRS and BOLD MRI techniques could provide a new prognostic tool for assessing efficacy of tumor therapies and could help us better interpret BOLD MRI signals. Furthermore, the heterogeneity of tumor vascular oxygenation dynamics to external interventions can be investigated directly by BOLD MRI, while the development of NIR imaging for tumor oximetry has also great potential to reveal tumor vascular heterogeneities.

Appendix 1

Yueqing Gu, Vincent Bourke, Jae Kim, Anca Constantinescu, Ralph P. Mason, Hanli Liu, “Dynamic Response of Breast Tumor Oxygenation to Hyperoxic Respiratory Challenge Monitored with Three Oxygen-Sensitive Parameters,” *Applied Optics*, 42(16), 2960-2967 (2003).

Dynamic response of breast tumor oxygenation to hyperoxic respiratory challenge monitored with three oxygen-sensitive parameters

Yueqing Gu, Vincent A. Bourke, Jae G. Kim, Anca Constantinescu, Ralph P. Mason, and Hanli Liu

The simultaneous measurement of three oxygen-sensitive parameters [arterial hemoglobin oxygen saturation (SaO_2), tumor vascular-oxygenated hemoglobin concentration ([HbO_2]), and tumor oxygen tension (pO_2)] in response to hyperoxic respiratory challenge is demonstrated in rat breast tumors. The effects of two hyperoxic gases [oxygen and carbogen (5% CO_2 and 95% O_2)] were compared, by use of two groups of Fisher rats with subcutaneous 13762NF breast tumors implanted in pedicles on the foreback. Two different gas-inhalation sequences were compared, i.e., air–carbogen–air–oxygen–air and air–oxygen–air–carbogen–air. The results demonstrate that both of the inhaled, hyperoxic gases significantly improved the tumor oxygen status. All three parameters displayed similar dynamic response to hyperoxic gas interventions, but with different response times: the fastest for arterial SaO_2, followed by biphasic changes in tumor vascular [HbO_2], and then delayed responses for pO_2. Both of the gases induced similar changes in vascular oxygenation and regional tissue pO_2 in the rat tumors, and changes in [HbO_2] and mean pO_2 showed a linear correlation with large standard deviations, which presumably results from global versus local measurements. Indeed, the pO_2 data revealed heterogeneous regional response to hyperoxic interventions. Although preliminary near-infrared measurements had been demonstrated previously in this model, the addition of the pO_2 optical fiber probes provides a link between the noninvasive relative measurements of vascular phenomena based on endogenous reporter molecules, with the quantitative, albeit, invasive pO_2 determinations.

OCIS codes: 170.1470, 170.3660, 170.4580, 120.3890, 120.1880, 230.2090.

1. Introduction

It is widely recognized that hypoxic regions in solid tumors may limit the efficacy of nonsurgical therapy, including radiotherapy, photodynamic therapy, and chemotherapy.[1–4] Many adjuvant interventions have been tested, including simple strategies such as breathing hyperoxic gases.[5–7] However, a meta-analysis of some 10,000 patients showed only a modest benefit, and this benefit was restricted to specific tumor types.[8] It is thought that the failure of such interventions was largely due to the inability to identify those patients who would benefit. Indeed, there is growing emphasis on tailoring therapy to the individual characteristics of each patient's tumor. Furthermore, carbogen (5% CO_2 and 95% O_2) and oxygen have been used on experimental tumors in animals as well as on clinical trials in patients for many years.[9,10] But the therapeutic benefits of the two kinds of respiratory hyperoxic gases are diverse, depending on the tumor types and individuals.[11–13] Accordingly, accurate assessment of tumor oxygenation at various stages of tumor growth and in response to interventions may provide a better understanding of tumor development and may serve as a prognostic indicator for treatment outcome, potentially allowing therapy to be tailored to individual characteristics.

Various techniques have been developed to measure oxygen tension (pO_2) or vascular oxygenation of tumors.[14] Many methods are invasive, and those requiring biopsy preclude dynamic investigations. Optical techniques based on light absorption of endogenous chromophores, e.g., near-infrared (NIR)

Y. Gu, J. G. Kim, and H. Liu (Hanli@uta.edu) are with the Biomedical Engineering Program, The University of Texas at Arlington, Arlington, Texas 76019. V. A. Bourke, A. Constantinescu, and R. P. Mason are with the Department of Radiology, University of Texas Southwestern Medical Center, Dallas, Texas 75390.

Received 8 September 2002; revised manuscript received 15 January 2003.

0003-6935/03/162960-08$15.00/0

spectroscopy of oxygenated and deoxygenated hemoglobin, are entirely noninvasive and allow real-time monitoring of tumor vascular oxygenation.[15–17] However, NIR has limited spatial resolution, and it remains to be determined whether vascular oxygenation is related to therapeutic outcome. Hitherto, quantitative pO_2 has been shown to have prognostic value,[18–21] but pO_2 represents a balance between oxygen delivery and consumption. Thus, we seek to explore the interplay of vascular and tissue oxygenation. Electrodes have been used widely to study tumor oxygen dynamics with respect to interventions,[22–24] but they are generally limited to a single location and small probes can be fragile. We have ourselves recently shown a correlation between pO_2 and ΔHbO_2 in some tumors, but we noted distinct heterogeneity, and thus, the global NIR measurements were not always related to local pO_2.[25] Multiple fiber-optic probes may be inserted into a tumor,[26–28] and we have now investigated correlation between NIR measurements and multiple (three) simultaneous pO_2 measurements.

We now report simultaneous measurements of three oxygen-related parameters, i.e., arterial hemoglobin oxygen saturation, SaO_2; tumor oxygenated hemoglobin concentration, $[HbO_2]$; and tumor oxygen tension, pO_2, to assess dynamic responses of rat breast tumors to hyperoxic gases. Changes in tumor vascular $[HbO_2]$ were measured by NIR spectroscopy (NIRS) using a photon-migration, frequency-domain device; changes in regional pO_2 were monitored by a fluorescence-quenched, oxygen-sensing, fiber-optic system (FOXY); the arterial SaO_2 values were recorded with a fiber-based, pulse oximeter.

2. Materials and Methods

A. Near-Infrared Spectroscopy System for Measurement of Changes in $[HbO_2]$

NIR light (700 to 900 nm) has considerable tissue penetration depth (several centimeters) and permits *in vivo* sampling of large tissue volumes (e.g., human breast, brain, skeletal muscle, or tumors), since photon transport in tissue is dominated by scattering rather than by absorption. Absorption of NIR light by the oxygenated and the deoxygenated hemoglobin chromophores may be used to determine hemoglobin oxygenation and blood concentration changes. As described in detail previously,[16,25] a homodyne frequency-domain system (NIM, Philadelphia, Pennsylvania) was used to monitor the global changes in oxygenated and deoxygenated hemoglobin concentrations, $\Delta[HbO_2]$ and $\Delta[Hb]$, respectively, in rat breast tumors in response to variations in inhaled gas. Briefly, the light from two NIR laser diodes (758 nm and 785 nm) was coupled into a bifurcated fiber bundle and illuminated on the tumor, and the transmitted light was collected and propagated to a photomultiplier tube (Fig. 1). The fiber bundles were placed on the surface of the tumors in a transmittance mode parallel to the body of the rat. The fiber tips touched firmly on the skin (without compression) in the middle parts of the tumors, providing optimal geometry to interrogate deep tumor tissue.

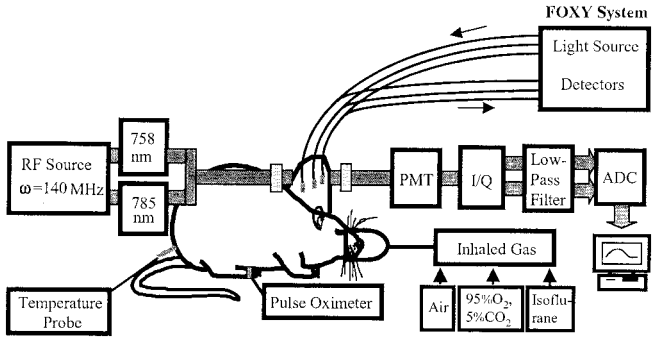

Fig. 1. Experimental setup for simultaneous oximetry. The 3-mm-diameter fiber bundles of the NIRS system deliver and detect the laser light through the tumor in transmittance geometry. PMT represents a photomultiplier tube. I/Q is an in-phase and quadrature phase demodulator for retrieving amplitude and phase information. The FOXY system comprises three fiber-optic oxygen-sensing probes that are inserted into different regions of the tumor. The pulse oximeter probe is placed on the hind foot of the rat.

Based on modified Beer–Lambert's law,[29] changes in oxygenated and deoxygenated hemoglobin concentrations, $\Delta[HbO_2]$ and $\Delta[Hb]$, due to respiratory intervention were derived from the measured amplitudes at the two wavelengths and calculated with the following equations[25]:

$$\Delta[HbO_2] = \frac{-10.63 \log\left(\frac{A_B}{A_T}\right)^{758} + 14.97 \log\left(\frac{A_B}{A_T}\right)^{785}}{d}, \quad (1)$$

$$\Delta[Hb] = \frac{8.95 \log\left(\frac{A_B}{A_T}\right)^{758} - 6.73 \log\left(\frac{A_B}{A_T}\right)^{785}}{d}, \quad (2)$$

where A_B and A_T are the baseline and transient amplitudes measured from the NIR system, respectively; d is the source–detector separation; the unit for both $\Delta[HbO_2]$ and $\Delta[Hb]$ is millimolar per differential path-length factor (DPF); and the DPF is for tumor tissues. As demonstrated in our previous study, normalization of $\Delta[HbO_2]$ and $\Delta[Hb]$ to their maximal values can eliminate the effects of d and DPF on the results.[25]

B. Fiber-Optic Oxygen-Sensing System for Measurement of Changes in pO_2

Regional pO_2 in tumors was monitored with a multichannel, fiber-optic, oxygen-sensing system (FOXY, Ocean Optics, Inc., Dunedin, Florida).[30] Three fluorescence-quenched, optical fiber probes (AL300, tip diameter 410 μm) were inserted into different regions of the tumors (Fig. 1). Probes were positioned so that at least one was in a poorly oxygenated region (low baseline pO_2) and at least one in a well-oxygenated region (high baseline pO_2). If necessary,

the probes were gently moved through the tumor until such diverse regions were located. In some cases, the mean pO_2 derived from the three individual measurements is presented. Although this is a commercial system, few details have been published previously,[31] and no applications to *in vivo* tumor oximetry have been published to our knowledge. Light from a pulsed blue LED (475 nm) was coupled into one branch of a bifurcated optical fiber bundle and propagated to the probe tip. The distal end of the probe is coated with a thin layer of a hydrophobic solgel material, where an oxygen-sensing ruthenium complex is effectively trapped. Illumination of the ruthenium complex causes fluorescence at ~600 nm. If the excited ruthenium complex encounters an oxygen molecule, the excess energy is transferred to the oxygen molecule in a nonradiative transition, decreasing or quenching the fluorescence signal. The degree of quenching correlates with the oxygen concentration, and hence, pO_2.

The fluorescence response of the ruthenium crystal complex is highly temperature dependent, so to accomplish probe calibration it was necessary to stream gases of known oxygen concentrations (100%, 20.9%, 10%, 2%, and 0%) through a cylindrical water jacket heated to 37 °C. Calibration curves were automatically calculated by means of the vendor-supplied software, with the second-order, polynomial calibration:

$$\frac{I_0}{I} = 1 + K_1[O] + K_2[O]^2 \qquad (3)$$

where, I_0 is the fluorescence intensity at zero oxygen concentration (nitrogen), I is the measured intensity of fluorescence at a pressure of oxygen, $[O]$ represents the oxygen concentration (related to pO_2), K_1 and K_2 are the first- and the second-order coefficients and are automatically supplied by the curve-fitting routine from the calibration measurements.

C. Pulse Oximeter for Measurement of Arterial S_aO_2

Arterial SaO_2 of the breast-tumor-bearing rats was also monitored with a fiber-optic pulse oximeter (Nonin Medical, Inc., Plymouth, Minnesota) placed on the hind foot of the rats. The system consisted of two optical fibers used for delivering and receiving the light. The tips were placed on either side of the foot in transmission mode.

D. Animal Model

Mammary adenocarcinomas 13762NF (originally obtained from the Division of Cancer Therapeutics, NIH, Bethesda, Maryland) were implanted in skin pedicles[32] on the foreback of adult female Fisher 344 rats (~150 g). Once the tumors reached 1–2 cm diameter, rats were anesthetized with 150-μl ketamine hydrochloride (100 mg/ml, i.p.) and maintained under general gaseous anesthesia with 1.3% isoflurane in air (1 dm^3/min). Body temperature was maintained at 37 °C by a warm water blanket. Tumors were shaved to improve optical contact for transmitting NIR light. The tumor diameters along the three major orthogonal axes (a, b, c) were measured with calipers and volume estimated with an ellipsoid approximation with the formula: $V = (\pi/6)(abc)$.

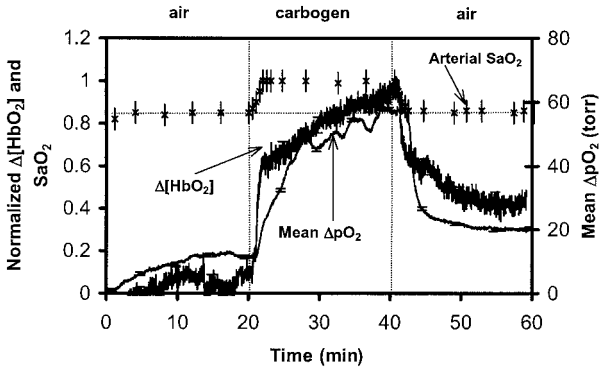

Fig. 2. Time profile of the three oxygen-sensitive parameters, i.e., the normalized changes of tumor $\Delta[HbO_2]$, the mean changes of tumor ΔpO_2, and the arterial SaO_2 with respect to carbogen breathing in a representative 13762NF rat breast tumor (No. 1, 3.2 cm^3).

Two groups of rats ($n = 7$ in each group) were used to compare the effects of carbogen and oxygen on vascular oxygenation of breast tumors. Group 1 experienced the gas-inhalation sequence of air–carbogen–air–oxygen–air. Group 2 was exposed to the reverse sequence of air–oxygen–air–carbogen–air. Each gas was maintained for 20 min. In addition, the FOXY pO_2 probes were applied to five rats from Group 1, and the dynamics of the three oxygen-related parameters were measured simultaneously.

3. Results

A. Dynamic Responses of Three Oxygen-Related Parameters to Carbogen Intervention

Typical time profiles of the normalized $\Delta[HbO_2]$, mean ΔpO_2, and SaO_2 in response to carbogen intervention are shown for a representative 13762NF breast tumor (No. 1, 3.2 cm^3) in Fig. 2. When the inspired gas was switched from air to carbogen, the SaO_2 readings increased rapidly and significantly from the baseline value of 85% to the maximum of 100% within 2.5 minutes ($p < 0.0001$). The normalized $\Delta[HbO_2]$ showed a sharp initial rise in the first minute ($p < 0.0001$) followed by a slower, gradual, but further significant increase over the next 19 min ($p < 0.001$). Mean ΔpO_2 increased rapidly by approximately 50 Torr within 8 min ($p < 0.0005$) and also continued a slower and gradual increase over the next 12 min ($p < 0.005$). Return to breathing air produced a significant decline for all three signals ($p < 0.0001$).

SaO_2 and pO_2 displayed a single-phase dynamic behavior in response to carbogen intervention, whereas $\Delta[HbO_2]$ showed an apparent biphasic response. These dynamics may be characterized by time constants of a single-exponential response. For the tumor in Fig. 3, SaO_2 had the fastest response, with a time constant of $\tau(SaO_2) = 1.1 \pm 0.2$ min ($R =$

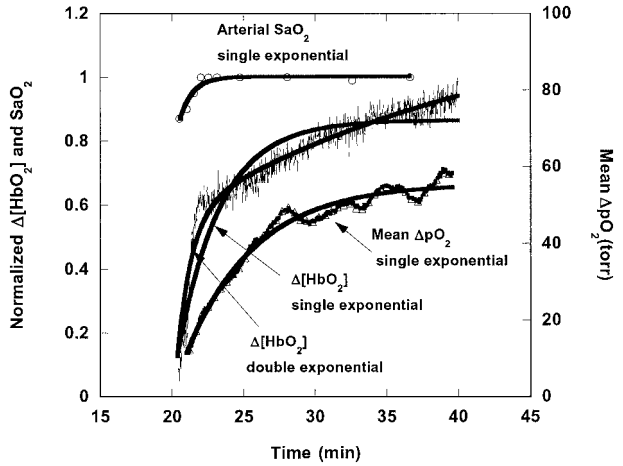

Fig. 3. Dynamic responses of the three oxygen-sensitive parameters to carbogen intervention in a rat breast tumor (No. 1, 3.2 cm^3). Single-exponential curve fitting yielded SaO_2 = $0.204\{1 - \exp[-(t - 20.02)/1.1]\} + 0.85$ ($R = 0.93$), $\Delta[HbO_2]$ = $0.655\{1 - \exp[-(t - 20.36)/2.59]\} + 0.125$ ($R = 0.89$), and $\Delta pO_2 = 42.68\{1 - \exp[-(t - 21.01)/4.56]\} + 16.66$ ($R = 0.98$); biexponential fitting resulted in $\Delta[HbO_2] = 0.373\{1 - \exp[-(t - 20.36)/0.61]\} + 0.648\{1 - \exp[-(t - 20.36)/21]\}$ ($R = 0.97$).

0.93), followed by $[HbO_2]$ with $\tau(\Delta[HbO_2]) = 2.59 \pm 0.06$ min ($R = 0.89$), whereas ΔpO_2 yielded the slowest response $\tau(\Delta pO_2) = 4.56 \pm 0.06$ min ($R = 0.98$). Time constants for Group 1 are listed in Table 1. In every case $\tau(SaO_2) < \tau(\Delta[HbO_2]) < \tau(\Delta pO_2)$, based on the single-exponential fitting. No apparent relation between the time constant and the tumor volume was observed.

It is clear that the response of ΔHbO_2 is not well represented by a single exponential, and thus, a double-exponential expression with two time constants, τ_1 and τ_2, was also used (Fig. 3). Comparison between the biexponential fitting for $\Delta[HbO_2]$ and the single-exponential results for both SaO_2 and ΔpO_2 in the first five rat tumors (Table 1) shows that the time constants of SaO_2 ($\sim 1.2 \pm 0.4$ min) are similar to those of the first phase of $\Delta[HbO_2]$ ($\sim 0.5 \pm 0.2$ min), whereas the second phase is longer and highly variable ($\sim 14 \pm 11$ min). No significant correlations were found between any of the time constants in Table 1.

Time delay, t_d, between the time when the gas intervention was initiated and the time when the changes in signals were detected, reveals another difference among the three oxygen-sensitive parameters. For tumor 1 (Fig. 2), the SaO_2 signal was the first to respond to the intervention. Change in $\Delta[HbO_2]$ was observed 30 s later with $t_d = 30$ s, followed by changes in ΔpO_2 another 30 s later ($t_d = 60$ s). Similarly, when the gas was returned from carbogen to air, the SaO_2 signal decreased immediately, followed by declines in $\Delta[HbO_2]$ and in ΔpO_2 with t_d of 30 and 120 s later, respectively. As expected, changes in SaO_2 always preceded ΔHbO_2, and ΔpO_2 occurred last for all tumors.

B. Comparison of the Effects of Carbogen and Oxygen Intervention on Tumor Oxygenation

Switching from air breathing to carbogen or oxygen produced similar changes in ΔHbO_2 [Fig. 4(a)]. However, the time course was substantially different, requiring a biphasic exponential fit for carbogen, but a single exponential for oxygen [Fig. 4(b)]. For the seven tumors in Group 1, there was no significant difference ($p > 0.3$) in the maximum magnitude of $\Delta[HbO_2]$ caused by carbogen or oxygen interventions [Fig. 4(c)].

To examine the possible effect of preconditioning required that Group 2 experience a reversed gas intervention, with exposure to oxygen prior to carbogen [Fig. 5(a)]. In this case, the time constants of the normalized tumor vascular $\Delta[HbO_2]$ were now similar for both gas challenges: indeed, for six of seven tumors, carbogen no longer induced the biphasic behavior. Figure 5(b) shows that changes in $(\Delta HbO_2)_{max}$ were similar to those in Group 1, and again, the two gases did not produce significantly different response in $(\Delta HbO_2)_{max}$. This is emphasized for both Groups 1 and 2 by a strong linear correlation (slope $\cong 1.16$) between the $\Delta[HbO_2]_{max}$ values observed in response to each of the two con-

Table 1. Time Constants of SaO_2, $\Delta[HbO_2]$, and ΔpO_2 Response to Carbogen and Oxygen Intervention in the Breast Tumors[a]

Breast Tumors Volume (cm^3)	Single-Exponential Fitting of SaO_2, $\Delta[HbO_2]$ and ΔpO_2 (Carbogen Intervention)						Double-Exponential Fitting for $\Delta[HbO_2]$ (Carbogen Intervention)			Single-Exponential Fitting of $\Delta[HbO_2]$ (O_2 Intervention)	
	SaO_2		$\Delta[HbO_2]$		ΔpO_2						
	τ (min)	R	τ (min)	R	τ (min)	R	$\tau 1$ (min)	$\tau 2$ (min)	R	τ (min)	R
No. 1 (3.2)	1.1 ± 0.2	0.93	2.59 ± 0.06	0.89	4.56 ± 0.04	0.98	0.61 ± 0.03	21 ± 3	0.97	0.35 ± 0.01	0.92
No. 2 (3.0)	1.6 ± 0.2	0.98	3.40 ± 0.07	0.91	4.6 ± 0.1	0.82	0.62 ± 0.06	11 ± 1	0.96	0.51 ± 0.01	0.91
No. 3 (4.6)	1.2 ± 0.2	0.97	2.12 ± 0.06	0.76	2.26 ± 0.02	0.98	0.6 ± 0.1	37 ± 3	0.96	1.52 ± 0.02	0.89
No. 4 (2.6)	1.9 ± 0.3	0.98	2.68 ± 0.05	0.93	3.5 ± 0.1	0.86	0.12 ± 0.02	5.2 ± 0.1	0.98	1.71 ± 0.03	0.94
No. 5 (5.6)	0.8 ± 0.2	0.91	2.68 ± 0.05	0.74	4.51 ± 0.02	0.99	0.17 ± 0.03	12.5 ± 0.6	0.99	5.49 ± 0.03	0.98
No. 6 (1.9)	0.9 ± 0.2	0.81	1.62 ± 0.01	0.95	nd	/	0.63 ± 0.08	2.3 ± 0.1	0.96	5.16 ± 0.06	0.93
No. 7 (0.72)	1.0 ± 0.5	0.95	3.60 ± 0.03	0.93	nd	/	0.61 ± 0.02	10.5 ± 0.3	0.98	3.54 ± 0.03	0.95
Mean	1.2 ± 0.4		2.7 ± 0.6		4 ± 1		0.5 ± 0.2	14 ± 11		2.5 ± 2	

[a]Under the inhalation sequence of air–carbogen–air–oxygen–air.
[b]nd, not determined.

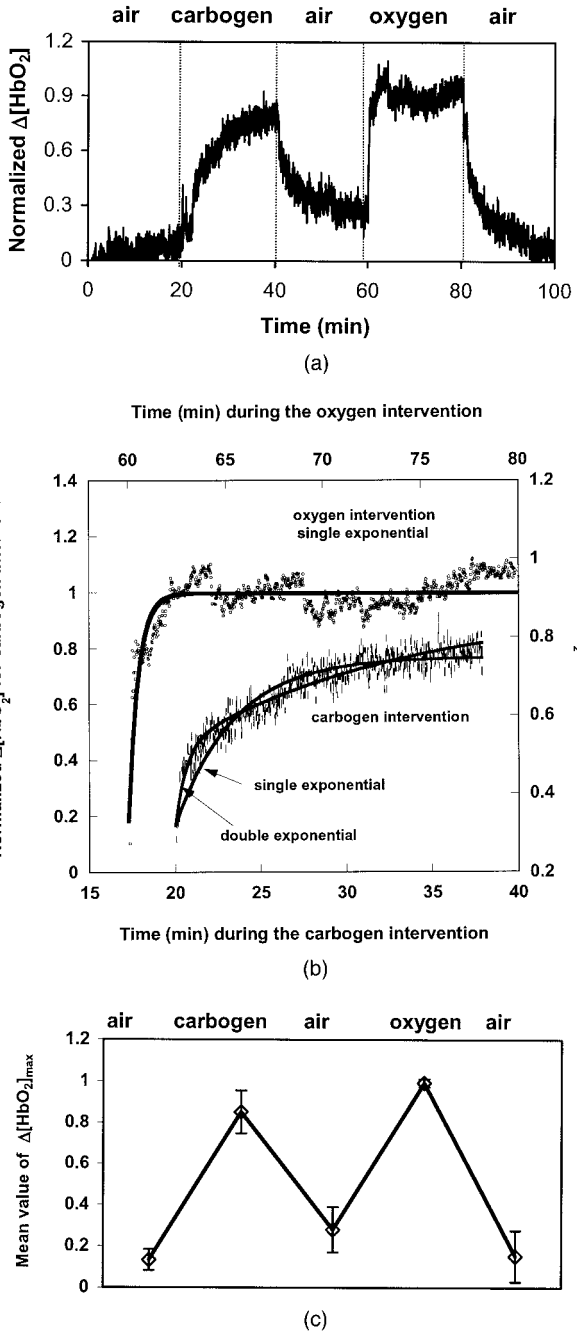

Fig. 4. (a) Time course of changes in tumor vascular $\Delta[HbO_2]$ for a representative 13762NF breast tumor from Group 1 (No. 2, 3.0 cm^3) with respect to altering inhaled gas. (b) Respective curve fits for the carbogen and oxygen interventions. (c) Average maximum values of normalized $\Delta[HbO_2]$ for the seven breast tumors in Group 1.

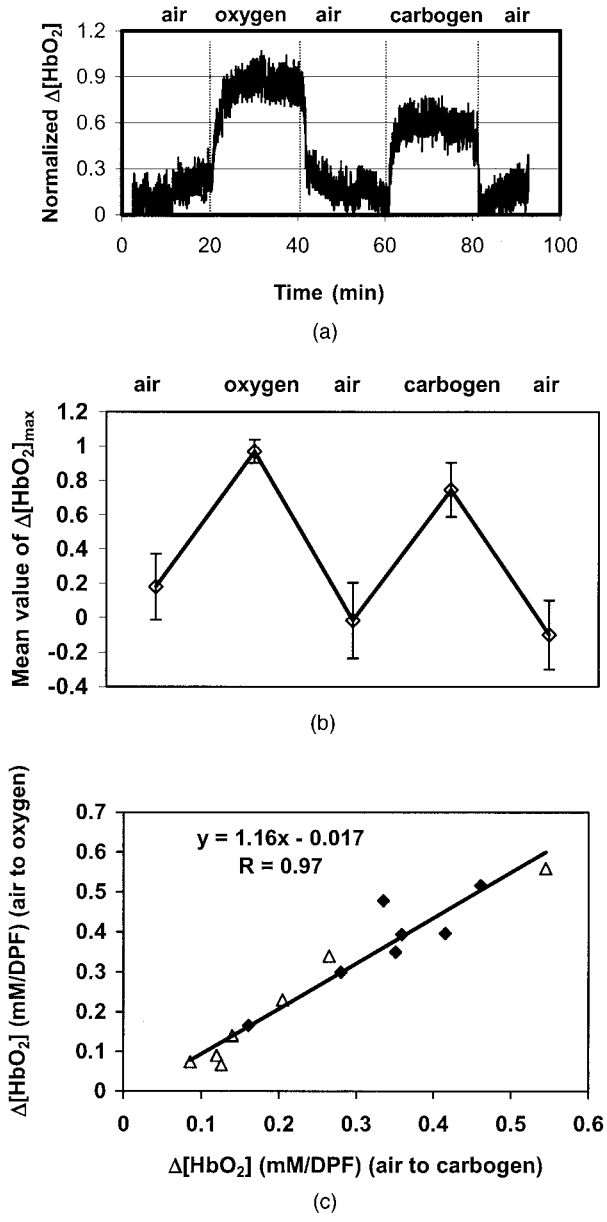

Fig. 5. (a) Dynamic changes in tumor vascular $\Delta[HbO_2]$ for a representative 13762NF breast tumor from Group 2 (No. 9, 2.6 cm^3) with gas-inhalation sequence reversed compared with Group 1. (b) Average maximum values of normalized $\Delta[HbO_2]$ for Group 2. Gas-inhalation sequence reversed compared with Group 1. (c) Correlation between maximum $\Delta[HbO_2]$ achieved with carbogen inhalation versus that with oxygen (R = 0.97): ◆, carbogen first; △, oxygen first.

secutive interventions [Fig. 5(c)]. In this case, nonnormalized data are shown for specific comparison of the absolute $\Delta[HbO_2]_{max}$ produced by oxygen and carbogen for each of the tumors.

C. Tumor pO_2

The FOXY pO_2 probes generally indicated distinct heterogeneity in pO_2. Moreover, response to the hyperoxic gas was diverse: those probes that indicated apparently well-oxygenated regions usually showed a large and rapid response, whereas those with lower baseline pO_2 often showed little change [Fig. 6(a)]. The pO_2 responses to the two interventions showed a highly consistent behavior at each individual location [Fig. 6(b)]. There was also a distinct correlation between the global NIR measurements and the mean ΔpO_2 (Fig. 7). Because of heterogeneity in regional pO_2, the standard deviations of the mean pO_2 values were large.

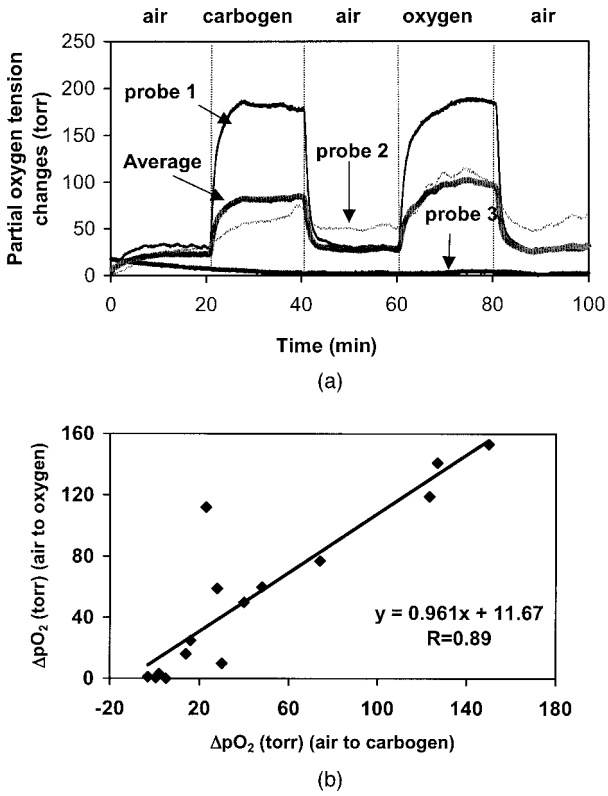

Fig. 6. (a) Time profiles of tumor ΔpO_2, measured with the three channels of the FOXY fiber-optic, oxygen-sensing system with respect to different gas inhalations for breast tumor No. 3 (4.6 cm^3). The mean signal for the three channels was calculated and is plotted by the thicker trace. (b) Correlation between ΔpO_2 at individual locations in the tumors in response to carbogen or oxygen for the five tumors in Group 1 ($R > 0.8$).

4. Discussion

In this study, we have simultaneously measured the arterial SaO_2, the global changes in the $\Delta[HbO_2]$ of tumor vasculature, and the regional changes in the ΔpO_2 of tumor tissue, in response to hyperoxic (i.e., carbogen and oxygen) gas interventions with a pulse oximeter, an NIRS system and a multichannel, fiber-optic, oxygen-sensing system, respectively. All three oxygen-sensitive indicators displayed similar dynamic tendency in response to carbogen intervention (Fig. 2).

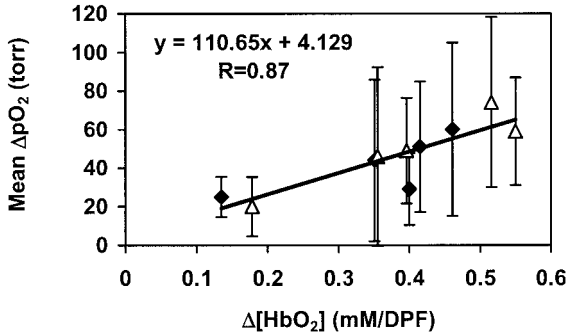

Fig. 7. Correlation between mean ΔpO_2 and $\Delta[HbO_2]$ for the five breast tumors ($R > 0.86$): ◆, transition from air to carbogen; △, transition from air to oxygen.

The simultaneous measurements demonstrate the compatibility of the NIRS system with the FOXY fiber-optic oxygen-sensing system, without interference. Both systems are relatively inexpensive and provide real-time measurements, but the multichannel FOXY fiber-optic system monitors ΔpO_2 in specific locations, whereas the NIRS system provides global measurements. Whether ΔHbO_2 determined with this methodology will be a clinically useful predictor for tumor response to oxygen-dependent interventions and therapies remains to be determined. However, it is established that measurements of pO_2 have prognostic value in the clinic[18,20] so that correlations between pO_2 and NIR measurements would be very important.

We have previously applied a polarographic oxygen electrode simultaneously with NIR.[25] However, that study provided only a single local pO_2 value, and in some cases correlations with global NIR measurements were very poor. The optical fiber system used here allows multiple locations to be interrogated simultaneously. The device can be expanded to many channels, but our system uses four channels. Unfortunately, probes are fragile, and the oxygen-sensitive coating on the tips is readily damaged. Thus, we only had three probes available for this study. Indeed, fiber-optic probe fragility is a well-recognized problem, and our previous experience with the more expensive OxyLite system was also restricted to three channels owing to probe damage.[26]

The FOXY system (~$13k) is much less expensive than the OxyLite (~$48k), and its mode of action is also simpler, detecting fluorescent signal intensity rather than fluorescence lifetime. It seems capable of measuring pO_2 across the whole range of atmospheric oxygen tensions (0–760 Torr), whereas the OxyLite is restricted and becomes very insensitive above approximately 100 Torr. However, our experience shows that although the FOXY system provides precise measurements of ΔpO_2, absolute values of pO_2 may not be reliable. We continue to perform validation experiments. By contrast, the OxyLite system seems to give very accurate pO_2 values.

Our experience shows that the FOXY probes are much easier to use than electrodes, particularly, in terms of calibration and stability. Since the probes are fragile, we insert them into tumors through a fine needle (25 gauge), which readily punctures the surrounding skin and penetrates tough fibrous tissues. The needle is then backed up from the tip to facilitate measurements. The probes often require a few minutes to settle at a stable baseline value, but then show good baseline stability and rapid response to interventions [Figs. 2 and 6(a)]. They are easily moved within the tumor to locate regions, presenting a particular pO_2 of interest, e.g. hypoxic or well oxygenated. In the search for appropriate locations, probes are moved forward to interrogate fresh tissues rather than in reverse, since blood may pool in the tracks owing to vascular damage. However, we observe

minimal bleeding on removal of the probes from the tumors.

We have found no interference between the NIR and FOXY instruments, although any tumor motion associated with moving the fiber probes can alter the optical contact of the NIR optrodes, and thus, alter apparent ΔHbO_2. Thus, baseline ΔHbO_2 is determined once the fiber probes are situated. New fiber-optic probes of the FOXY system have a thick coating of fluorescent gel and a black covering, but this wears with use and gradually allows reception of the NIR light. Since the LEDs of the two systems operate at very different wavelengths, viz. 475 versus 760 nm, there is no interference for detection. The detection of local NIR light by the FOXY probe opens the exciting possibility of detecting regional hemoglobin oxygen saturation. We believe the FOXY optical probes could be moved within the tumor to map the distribution and path of the transmitted NIR light, helping to explore and validate the optical characteristics of the tumor. This can simultaneously provide a correlation between local ΔHbO_2 and ΔpO_2.

In this study, we have examined a much larger group of rats than previously.[16,25] We have now shown rigorously that the two hyperoxic gases induce similar changes in vascular oxygenation (NIR) and regional tissue pO_2 (FOXY) in this type of rat breast tumor. These data are consistent with our previous observations using ^{19}F NMR imaging (FREDOM)[33] in this tumor type and also in rat prostate tumors.[34,35] If the two gases are indeed equivalent in terms of manipulation of tumor oxygenation, it could have great therapeutic benefit since the popular carbogen, which is in use in clinical trials,[36] can cause respiratory discomfort.

The current data show that ΔHbO_2 and ΔpO_2 are correlated (Fig. 7), and thus, such noninvasive observations could have value in the clinic. The major deficiency in our current NIR approach is lack of spatial discrimination, and thus efforts to implement NIR imaging will be of great value. It will also be interesting to correlate other measurements, such as blood-oxygen-level-dependent (BOLD) proton magnetic resonance imaging, which provide high spatial resolution, but which are sensitive to vascular flow and volume as well as oxygenation.[37]

The biphasic response of ΔHbO_2 to carbogen is intriguing, and we believe it represents the distinct vascular compartments of arterioles (high flow) and capillaries. However, the change to monophasic behavior, when carbogen is administered second, requires further exploration; in the future, we propose to test various concentrations of oxygen and carbon dioxide and air to separate the components of the response. The carbogen dioxide component of carbogen is known to be vasoactive; however, the specific effects may depend on tumor type, site of growth, and other factors.[9,38]

In terms of vascular oxygen delivery, the data in Table 1 reveal the progressive movement of oxygen: t_d (SaO_2) $<$ t_d ($\Delta[HbO_2]$) $<$ t_d (ΔpO_2). As expected, switching to hyperoxic gas caused the systemic arterial SaO_2 to increase, as a result of the immediate combination of deoxyhemoglobin with oxygen. The highly oxygenated blood circulated in the systemic vasculature of the rats (including the capillary bed of the tumor tissue), resulting in a delayed increase in $[HbO_2]$ in the tumor vasculature, and led to an unloading of oxygen to the tumor tissue. For the biexponential model of $\Delta[HbO_2]$, the fast component has a similar time constant to the SaO_2 measured with the pulse oximeter on the hind leg, strongly suggesting that it represents arteriolar oxygenation in the tumor. In this study, tumor volumes do not show any direct relation with time constants or changes of amplitude in response to hyperoxic gas interventions.

It is increasingly evident that oxygen and hypoxia play important roles in tumor development and response to therapy.[18] NIR offers an attractive noninvasive means of investigating tumor oxygenation, particularly in terms of dynamic response to interventions, but we had previously shown a potential mismatch between global ΔHbO_2 and local ΔpO_2.[25] The data presented here indicate a correlation between the global NIR measurements and mean pO_2 values with even as few as three representative locations per tumor. This does suggest that it will be important to develop regional NIR measurements and that even relatively crude mapping could reveal heterogeneity. In the meantime, we believe these studies provide further evidence for the value of NIRS to explore tumor physiology.

This study was supported in part by the Department of Defense Breast Cancer Research grants BC000833 (YG) and BC990287 (HL), and NIH RO1 CA79515 (RPM) and RO1 supplement CA79515-S (VB). We are grateful to Mengna Xia and Dawen Zhao for their assistance with data processing. We gratefully acknowledge Weina Cui for helpful discussions.

References

1. R. S. Bush, R. D. T. Jenkin, W. E. C. Allt, F. A. Beale, A. J. Dembo, and J. F. Pringle, "Definitive evidence for hypoxic cells influencing cure in cancer therapy," Br. J Cancer **37**(suppl 3), 302–306 (1978).
2. E. J. Hall, *Radiobiology for the Radiologist*, 4th ed. (Lippincott, Philadelphia, Pa., 1994).
3. M. Nordsmark and J. Overgaard, "A confirmatory prognostic study on oxygenation status and loco-regional control in advanced head and neck squamous cell carcinoma treated by radiation therapy," Radiother. Oncol. **57,** 39–43 (2000).
4. O. Thews, D. K. Kelleher, and P. Vaupel, "Erythropoietin restores the anemia-induced reduction in cyclophosphamide cytotoxicity in rat tumors," Cancer Res. **61,** 1358–1361 (2001).
5. J. H. A. M. Kaanders, L. A. M. Pop, H. A. M. Marres, R. W. M. van der Maazen, A. J. van der Kogel, and W. A. J. van Daal, "Radiotherapy with carbogen breathing and nicotinamide in head and neck cancer: feasibility and toxicity," Radiother. Oncol. **37,** 190–198 (1995).
6. M. I. Saunders, P. J. Hoskin, and K. Pigott, "Accelerated radiotherapy, carbogen and nicotinamide (ARCON) in locally advanced head and neck cancer: a feasibility study," Radiother. Oncol. **45,** 159–166 (1997).
7. J. A. Kruuv, W. R. Inch, and J. A. McCredie, "Blood flow and

oxygenation of tumors in mice. I. Effects of breathing gases containing carbon dioxide at atmospheric pressure," Cancer. **20,** 51–59 (1967).
8. J. Overgaard and M. R. Horsman, "Modification of hypoxia-induced radioresistance in tumors by the use of oxygen and sensitizers," Semin. Radiat. Oncol. **6,** 10–21 (1996).
9. P. Vaupel, D. K. Kelleher, and O. Thews, "Modulation of tumor oxygenation," Int. J. Radiat. Oncol. Bio. Phys. **42,** 843–848 (1998).
10. S. Dische, "What we learnt from hyperbaric oxygen?" Radiother. Oncol. **20**(Suppl.), 71–74 (1991).
11. S. Dische, M. I. Saunders, and R. Sealy, "Carcinoma of the cervix and the use of hyperbaric oxygen with radiotherapy: a report of a randomized controlled trial," Radiother. Oncol. **53,** 93–98 (1999).
12. V. M. Laurence, R. Ward, I. F. Dennis, and N. M. Bleehen, "Carbogen breathing with nicotinamide improves the oxygen status of tumors in patients," Br. J Cancer **72,** 198–205 (1995).
13. L. Martin, E. Lartigau, and P. Weeger, "Changes in the oxygenation of head and neck tumors during carbogen breathing," Radiother. Oncol. **27,** 123–130 (1993).
14. H. B. Stone, J. M. Brown, T. Phillips, and R. M. Sutherland, "Oxygen in human tumors: correlations between methods of measurement and response to therapy," Radiat. Res. **136,** 422–434 (1993).
15. E. L. Hull, D. L. Conover, and T. H. Foster, "Carbogen induced changes in rat mammary tumor oxygenation reported by near infrared spectroscopy," Br. J. Cancer **79,** 1709–1716 (1999).
16. H. Liu, Y. Song, K. L. Worden, X. Jiang, A. Constantinescu, and R. P. Mason, "Noninvasive investigation of blood oxygenation dynamics of tumors by near-infrared spectroscopy," Appl. Opt. **39,** 5231–5243 (2000).
17. R. G. Steen, K. Kitagishi, and K. Morgan, "*In vivo* measurement of tumor blood oxygenation by near-infrared spectroscopy: immediate effects of pentobarbital overdose or carmustine treatment," J. Neuro-Oncol. **22,** 209–220 (1994).
18. M. Höckel and P. Vaupel, "Tumor hypoxia: definitions and current clinical, biologic, and molecular aspects," J. Natl. Cancer Inst. **93,** 266–276 (2001).
19. L. Gray, A. Conger, M. Ebert, S. Hornsey, and O. Scott, "The concentration of oxygen dissolved in tissues at time of irradiation as a factor in radio-therapy," Br. J. Radiol. **26,** 638–648 (1953).
20. A. W. Fyles, M. Milosevic, R. Wong, M. C. Kavanagh, M. Pintile, A. Sun, W. Chapman, W. Levin, L. Manchul, T. J. Keane, and R. P. Hill, "Oxygenation predicts radiation response and survival in patients with cervix cancer," Radiother. Oncol. **48,** 149–156 (1998).
21. D. Zhao, A. Constantinescu, E. W. Hahn, and R. P. Mason, "Measurement of tumor oxygen dynamics predicts beneficial adjuvant intervention for radiotherapy in Dunning prostate R3327-HI tumors," Radiat. Res. (to be published) (2003).
22. C. Song, I. Lee, T. Hasegawa, J. Rhee, and S. Levitt, "Increase in pO_2 and radiosensitivity of tumors by Fluosol and carbogen," Cancer Res. **47,** 442–446 (1987).
23. D. Cater and I. Silver, "Quantitative measurements of oxygen tension in normal tissues and in the tumors of patients before and after radiotherapy," Acta Radiol. **53,** 233–256 (1960).
24. D. Zhao, A. Constantinescu, E. W. Hahn, and R. P. Mason, "Differential oxygen dynamics in two diverse Dunning prostate R3327 rat tumor sublines (MAT-Lu and HI) with respect to growth and respiratory challenge," Int. J. Radiat. Oncol. Biol. Phys. **53,** 744–756 (2002).
25. J. G. Kim, Y. Song, D. Zhao, A. Constantinescu, R. P. Mason, and H. Liu, "Interplay of tumor vascular oxygenation and pO_2 in tumors using NIRS, ^{19}F MR pO_2 mapping, and pO_2 needle electrode," J. Biomed. Optics **8,** 53–62 (2003).
26. D. Zhao, A. Constantinescu, E. W. Hahn, and R. P. Mason, "Tumor oxygen dynamics with respect to growth and respiratory challenge: investigation of the Dunning prostate R3327-HI tumor," Radiat. Res. **156,** 510–520 (2001).
27. J. Bussink, J. H. A. M. Kaanders, A. M. Strik, B. Vojnovic, and A. J. van der Kogel, "Optical sensor-based oxygen tension measurements correspond with hypoxia marker binding in three human tumor xenograft lines," Radiat. Res. **154,** 547–555 (2000).
28. J. R. Griffiths, "The OxyLite: a fibre-optic oxygen sensor," Br. J. Radiol. **72,** 627–630 (1999).
29. Y. Gu, Z. Qian, J. Chen, D. Blessington, N. Ramanujam, and B. Chance, "High resolution three dimensional scanning optical image system for intrinsic and extrinsic contrast agents in tissue," Rev. Sci. Instrum. **73,** 172–178 (2002).
30. Ocean Optics Inc., Dunedin, Fla., March 2003. http://www.oceanoptics.com/products/foxysystem.asp
31. C. B. Allen, B. K. Schneider, and C. J. White, "Limitations to oxygen diffusion in *in vitro* cell exposure systems in hyperoxia and hypoxia," Am. J. Physiol. Lung Cell Molec. Physiol. **281,** L1021–L1027 (2001).
32. E. W. Hahn, P. Peschke, R. P. Mason, E. E. Babcock, and P. P. Antich, "Isolated tumor growth in a surgically formed skin pedicle in the rat: a new tumor model for NMR studies," Magn. Reson. Imaging **11,** 1007–1017 (1993).
33. Y. Song, A. Constantinescu, and R. P. Mason, "Dynamic breast tumor oximetry: the development of prognostic radiology," Technol. Cancer Res. Treat. **1,** 1–8 (2002).
34. S. Hunjan, D. Zhao, A. Constantinescu, E. W. Hahn, P. P. Antich, and R. P. Mason, "Tumor oximetry: demonstration of an enhanced dynamic mapping procedure using Fluorine-19 echo planar magnetic resonance imaging in the Dunning prostate R3327-AT1 rat tumor," Int. J. Radiat. Oncol. Biol. Phys. **49,** 1097–1108 (2001).
35. D. Zhao, A. Constantinescu, L. Jiang, E. W. Hahn, and R. P. Mason, "Prognostic radiology: quantitative assessment of tumor oxygen dynamics by MRI," Am. J. Clin. Oncol. **24,** 462–466 (2001).
36. J. H. Kaanders, J. Bussink, and van der A. J. Kogel, "ARCON: a novel biology-based approach in radiotherapy," Lancet Oncol. **3,** 728–737 (2002).
37. F. A. Howe, S. P. Robinson, L. M. Rodrigues, and J. R. Griffiths, "Flow and oxygenation dependent (FLOOD) contrast MR imaging to monitor the response of rat tumors to carbogen breathing," Magn. Reson. Imaging. **17,** 1307–1318 (1999).
38. T. J. Dunn, R. D. Braun, W. E. Rhemus, G. L. Rosner, T. W. Secomb, G. M. Tozer, D. J. Chaplin, and M. W. Dewhirst, "The effects of hyperoxic and hypercarbic gases on tumour blood flow," Br. J. Cancer **80,** 117–126 (1999).

Appendix 2

Hanli Liu, Yueqing Gu, Jae G. Kim, and Ralph P. Mason, “Near Infrared Spectroscopy and Imaging of Tumor Vascular Oxygenation,” *Methods in Enzymology: Imaging,* ed. by Michael Conn, vol. 385-386, pp. 349-378 (2004).

ICP. Such processes include hydrocephalus, pseudotumor cerebri, intracranial mass lesions, and toxic–metabolic encephalopathy (where a depressed level of consciousness may or may not correspond to an increased ICP). MR–ICP measurement may prevent unnecessary invasive monitoring in an increased risk setting. Single time measurement of ICP may also be helpful in the evaluation of patients with possible ventriculoperitoneal shunt malfunction—particularly young children who present with nonspecific complaints and/or who are unable to communicate their symptoms. The MRI-based technique would limit exposure to harmful radiation from repeated CT scans. Also, a finding of normal ICP by the MRI-based method might prevent unnecessary shunt exploration.

If proven accurate and reliable, noninvasive, MRI-based measurement of intracranial compliance and pressure and TCBF may provide a valuable adjunct to the evaluation of patients with various neurologic problems. In the setting of TBI, a finding of increased ICP may provide an early warning signal for a physician to adjust therapy. This tool also may prove valuable in situations where external factors confound clinical evaluation (i.e., drug intoxication), where "coma" does not necessarily reflect an increased pressure state (i.e., diffuse axonal injury), or where coexisting medical problems make placement of an invasive monitor too dangerous (i.e., bleeding disorders). In each case, noninvasive MR–ICP measurement would enhance the array of currently available evaluation modalities, providing a novel adjunct to patient diagnosis and serial monitoring with limited expense and morbidity.

[17] Near-Infrared Spectroscopy and Imaging of Tumor Vascular Oxygenation

By HANLI LIU, YUEQING GU, JAE G. KIM, and RALPH P. MASON

Introduction

Current Development in Optical Methods for Vascular Hemoglobin Oxygenation

In recent years, a large number of investigations have been conducted in both laboratory and clinical settings to noninvasively monitor tissue vascular oxygenation using near-infrared (NIR) spectroscopy (NIRS) and imaging. Although the NIR imaging techniques are limited by their spatial resolutions, they have a great potential to be developed as a new imaging

0076-6879/04 $35.00

modality because of their capabilities to provide functional images. NIR spectroscopy and imaging research has been mainly focused on two organs: (1) the brain and (2) the breast.

The NIR studies of the brain include detection of brain injury or trauma,[1] determination of cerebrovascular hemodynamics and oxygenation,[2,3] and functional brain imaging in response to a variety of neurologic activations.[4–7] NIR functional brain imaging increasingly has become of great interest in studying hemodynamic response to brain activation.[8] This is mainly because the optical signals of the NIR techniques are able to noninvasively penetrate through the scalp and skull of an adult human and are sensitive to changes in the concentration of oxygenated (HbO) and deoxygenated hemoglobin (Hb). Although it is difficult to obtain very accurate quantification of cerebral HbO and Hb concentrations from the NIR imaging techniques due to rigorous requirements of theory and boundary conditions,[9] the techniques can offer relatively accurate measurements of changes of HbO and Hb, thus providing quantitative changes in total cerebral blood volume (CBV, which is assumed to be proportional to total hemoglobin concentration, HbT, where HbT = HbO + Hb).

The objective of NIR breast imaging is to develop a novel functional imaging modality for early breast cancer detection and diagnosis beyond currently available techniques. Various efforts by several research groups[10–15] have been made in either laboratory or clinical studies. For example, the research groups of Paulsen and colleagues[12] and of Jiang[15]

[1] S. Gopinath, C. S. Robertson, R. G. Grossman, and B. Chance, *J. Neurosurg.* **79,** 43 (1993).
[2] C. Cheung, J. P. Culver, K. Takahashi, J. H. Greenberg, and A. G. Yodh, *Phys. Med. Biol.* **46,** 2053 (2001).
[3] G. Zhang, A. Katz, R. R. Alfano, A. D. Kofinas, P. G. Stubblefield, W. Rosenfeld, D. Beyer, D. Maulik, and M. R. Stankovic, *Phys. Med. Biol.* **45,** 3143 (2000).
[4] M. Fabiani, G. Gratton, and P. M. Corballis, *J. Biomedi. Opti.* **1,** 387 (1996).
[5] R. Wenzel, H. Obrig, J. Ruben, K. Villringer, A. Thiel, J. Bernarding, U. Dirnagl, and A. Villringer, *J. Biomed. Opt.* **1,** 399 (1996).
[6] B. Chance, E. Anday, S. Nioka, S. Zhou, L. Hong, K. Worden, C. Li, T. Murray, Y. Ovetsky, D. Pidikiti, and R. Thomas, *Opt. Express.* **2,** 411 (1998).
[7] D. A. Boas, T. Gaudette, G. Strangman, X. Cheng, J. J. A. Marota, and J. B. Mandeville, *Neuroimage* **13,** 76 (2001).
[8] D. A. Boas, G. Jasdzewski, G. Strangman, J. P. Culver, and R. Poldrack, "OSA Biomedical Topical Meetings, Technical Digest," p. 307. Miami, FL, April 7–10, 2002.
[9] J. C. Hebden, E. M. C. Hillman, A. Gibson, N. Everdell, R. M. D. Yusof, D. T. Delpy, S. R. Arridge, T. Austin, and J. H. Meek, "OSA Biomedical Topical Meetings, Technical Digest," p. 587. Miami, FL, April 7–10, 2002.
[10] B. Tromberg, N. Shah, R. Lanning, A. Cerussi, J. Espinoza, T. Pham, L. Svaasand, and J. Butler, *Neoplasia* **2,** 26 (2000).
[11] S. Fantini, S. A. Walker, M. A. Franceschini, M. Kaschke, P. M. Schlag, and K. T. Moesta, *Appl. Opt.* **37,** 1982 (1998).

have developed a frequency-domain (FD) 16-source, 16-detector breast imager and have reported their *in vivo* results of optical properties of abnormalities from female volunteers and patients. The research group led by Chance has employed a time-domain (TD) 32-channel imaging system in conjunction with magnetic resonance imaging (MRI) to increase specificity and sensitivity of breast cancer detection.[13] Because of simplicity and low cost in comparison to the FD and TD imaging systems, continuous-wave (CW) NIR breast imaging systems also have been developed by the groups of Barbour *et al.*[14] and Chance.[16] These systems are currently under clinical tests for better breast cancer detection and diagnosis.

Although Hb, HbO, and HbT concentrations and light-scattering properties of tumors may be different from those of surrounding tissues, the optical contrast between tumor and surrounding tissue is about 2–3-fold at most in absorption, and much less in light scattering.[17] Thus much effort on increasing the optical contrast between tumor and healthy surrounding tissues also has been made using fluorescence imaging[18] or molecular beacons[16] to detect and diagnose cancer or tumor with improved sensitivity and specificity.

However, efforts in using NIR techniques to monitor tumor responses to therapeutic interventions[19–21] and therapy, such as to chemotherapy[22] or photodynamic therapy,[23] are very limited and preliminary. Moreover,

[12] T. O. McBride, B. W. Pogue, S. Jiang, U. L. Österberg, and K. D. Paulsen, *Opt. Lett.* **26,** 822 (2001).

[13] V. Ntziachristos and B. Chance, "SPIE Proceedings of Optical Tomography and Spectroscopy of Tissue III," Vol. 3597, p. 565, 1999.

[14] R. L. Barbour, C. H. Schmitz, H. L. Graber, and Y. Pei, "OSA Biomedical Topical Meetings, Technical Digest," p. 456. Miami, FL, April 7–10, 2002.

[15] X. Gu, N. Iftimia, Y. Xu, H. Jiang, and L. L. Fajardo, "OSA Biomedical Topical Meetings, Technical Digest," p. 468. Miami, FL, April 7–10, 2002.

[16] B. Chance, "OSA Biomedical Topical Meetings, Technical Digest" p. 450. Miami, FL, April 7–10, 2002.

[17] J. B. Fishkin, O. Coquoz, E. R. Anderson, M. Brenner, and B. J. Tromberg, *Appl. Opt.* **36,** 10 (1997).

[18] R. H. Mayer, J. S. Reynolds, and E. M. Sevick-Muraca, *Appl. Opt.* **38,** 4930 (1999).

[19] H. Liu, Y. Song, K. L. Worden, X. Jiang, A. Constantinescu, and R. P. Mason, *Appl. Opt.* **39,** 5231 (2000).

[20] J. G. Kim, Y. Song, D. Zhao, A. Constantinescu, R. P. Mason, and H. Liu, *J. Biomed. Opt.* **8,** 53 (2003).

[21] E. L. Hull, D. L. Conover, and T. Foster, *Br. J. Cancer* **79,** 1709 (1999).

[22] D. B. Jakubowski, A. E. Cerussi, F. Bevilacqua, N. Shah, and B. J. Tromberg, "OSA Biomedical Topical Meetings, Technical Digest," p. 456. Miami, FL, April 7–10, 2002.

[23] H. Wang, T. C. Zhu, M. Solonenko, S. M. Hahn, J. Metz, A. Dimofte, J. Mile, and A. G. Yodh, "OSA Biomedical Topical Meetings, Technical Digest." Miami, FL, April 7–10, 2002.

few reports have been found on using NIR spectroscopy and imaging as a prognostic tool for therapy planning and optimization, or for tumor prognosis. Based on the existing knowledge and development of NIR spectroscopy and imaging for the brain and breast, we were motivated a few years ago by the possibility of using NIRS as an efficient, real-time, noninvasive means to monitor tumor vascular oxygenation during respiratory interventions. The recent results in our study were obtained from animal breast and prostate tumors *in vivo* with a one-channel NIR spectrometer. The data have demonstrated that the NIR techniques could have applications as a prognostic means accompanying cancer therapy.[19,20,24]

Tumor Oxygenation as an Indicator for Tumor Response to Interventions

The presence and significance of tumor hypoxia has been recognized since the 1950s. Hypoxic cells *in vitro* and in animal tumors *in vivo* are documented to be three times more resistant to radiation-induced killing compared with aerobic cells.[25] Recent studies have shown that tumor hypoxia is a possible prognostic indicator and is related to the aggressiveness of a tumor, the clinical stage, and poor clinical outcome.[26–30] To improve the efficacy of oxygen-dependent treatment modalities, one possible strategy is the reduction of tumor hypoxia by raising the arterial oxygen partial pressure, P_aO_2 to overcome diffusion-limited hypoxia. Raising the arterial pO_2 by breathing hyperoxic or hyperbaric gas mixtures could be effective.[31,32] However, attempts to apply increased oxygen breathing in the clinic have not always been successful, and this may be attributed to the inability to identify those patients with hypoxic tumors.[33] More specifically, it may be

[24] Y. Gu, V. Bourke, J. G. Kim, A. Constantinescu, R. P. Mason, and H. Liu, *Appl. Opt.* **42,** 2960 (2003).

[25] S. M. Evans, W. T. Jenkins, M. Shapiro, and C. J. Koch, *Adv. Exp. Med. Biol.* **411,** 215 (1997).

[26] M. Höckel, K. Schlenger, B. Aral, M. Mitze, U. Schäffer, and P. Vaupel, *Cancer Res.* **56,** 4509 (1996).

[27] E. K. Rofstad and T. Danielsen, *Br. J. Cancer* **80,** 1697 (1999).

[28] A. W. Fyles, M. Milosevic, R. Wong, M. C. Kavanagh, M. Pintile, A. Sun, W. Chapman, W. Levin, L. Manchul, T. J. Keane, and R. P. Hill, *Radiother. Oncol.* **48,** 149 (1998).

[29] D. M. Brizel, S. P. Scully, J. M. Harrelson, L. J. Layfield, J. M. Bean, L. R. Prosnitz, and M. W. Dewhirst, *Cancer Res.* **56,** 941 (1996).

[30] J. H. A. M. Kaanders, K. I. E. M. Wijffels, H. A. M. Marres, A. S. E. Ljungkvist, L. A. M. Pop, F. J. A. van den Hoogen, P. C. M. de Wilde, J. Bussink, J. A. Raleigh, and A. J. van der Kogel, *Cancer Res.* **62,** 7066 (2002).

[31] S. Dische, *Br. J. Radiol.* **51,** 888 (1979).

[32] O. Thews, D. K. Kelleher, and P. Vaupel, *Radiother. Oncol.* **62,** 77 (2002).

attributed to the inability to identify those patients who would benefit from such interventions. Therefore evaluation of tumor oxygenation distributions and their changes during various stages of tumor growth, during therapeutic interventions, and during therapy is needed. Such evaluation can provide a better understanding of tumor development and tumor response to therapy, potentially allowing therapy to be planned to individual characteristics.

Numerous studies on tumor oxygen tension (pO_2) measurements have been conducted in recent years using a variety of methods,[34–36] such as microelectrodes,[37] optical reflectance,[38] electron spin resonance (EPR),[39,40] or MRI.[36,41–45] The latter two methods have advantages of making repeated measurements of pO_2 noninvasively, and MRI has the further advantage of providing dynamic maps of pO_2, which can reveal tumor heterogeneity.[46] Although NIRS does not quantify pO_2, it can indicate dynamic changes in vascular oxygenation and has the advantage of being entirely noninvasive, providing real-time measurements, and being cost-effective and portable. Our recent studies have revealed the need for NIR imaging of tumor vasculatures to study tumor heterogeneous response to therapeutic interventions and therapy. In the following sections, we briefly introduce basic algorithms used to quantify tumor hemoglobin oxygenation, followed by the NIR instrument description, system calibration, and experimental methods. Then, we provide several representative results taken

[33] J. Overgaard, *in* "Progress in Radio-Oncology V" (H. D. Kogelnik, ed.), p. 469. Monduzzi Editore, Bologna, Italy, 1995.
[34] H. B. Stone, J. M. Brown, T. Phillips, and R. M. Sutherland, *Radiat. Res.* **136,** 422 (1993).
[35] R. P. Mason, S. Ran, and P. E. Thorpe, *J. Cell. Biochem.* **87,** 45 (2002).
[36] D. Zhao, L. Jiang, and R. P. Mason, *Methods Enzymol.* **386,** 378 (2004).
[37] O. Thews, D. K. Kelleher, B. Lecher, and P. Vaupel, *Adv. Exp. Med. Biol.* **428,** 123 (1996).
[38] F. Steinberg, H. J. Röhrborn, K. M. Scheufler, S. Asgari, H. A. Trost, V. Seifert, D. Stolke, and C. Streffer, *Adv. Exp. Med. Biol.* **428,** 553 (1996).
[39] P. E. James, J. A. O'Hara, O. Y. Grinberg, T. Panz, and H. M. Swartz, *Adv. Exp. Med. Biol.* **428,** 97 (1996).
[40] J. A. O'Hara, F. Goda, J. F. Dunn, and H. M. Swartz, *Adv. Exp. Med. Biol.* **411,** 233 (1996).
[41] D. Le, R. P. Mason, S. Hunjan, A. Constantinescu, B. R. Barker, and P. P. Antich, *Magn. Reson. Imaging* **15,** 971 (1997).
[42] S. Hunjan, R. P. Mason, A. Constantinescu, P. Peschke, E. W. Hahn, and P. P. Antich, *Int. J. Radiat. Oncol. Biol. Phys.* **41,** 161 (1998).
[43] D. Zhao, A. Constantinescu, L. Jiang, E. W. Hahn, and R. P. Mason, *Am. J. Clin. Oncol.* **24,** 462 (2001).
[44] D. Zhao, A. Constantinescu, C.-H. Chang, E. W. Hahn, and R. P. Mason, *Radiat. Res.* **159,** 621 (2003).
[45] D. Zhao, S. Ran, A. Constantinescu, E. W. Hahn, and R. P. Mason, *Neoplasia* **5,** 308 (2003).
[46] R. P. Mason, A. Constantinescu, S. Hunjan, D. Le, E. W. Hahn, P. P. Antich, C. Blum, and P. Peschke, *Radiat. Res.* **152,** 239 (1999).

from both prostate and breast tumors under hyperoxic respiratory interventions, using both one-channel and multichannel NIR systems, as well as one-channel and three-channel pO_2 fiber optic needle probes. At the end, we wish to demonstrate that the NIR techniques are complementary with tumor pO_2 readings and can be used as a new prognostic means for cancer therapy prognosis and therapy planning.

Theory and Algorithms

It is well known that hemoglobin concentrations and oxygen saturation in tissue vasculature can be determined using NIRS, since light absorptions of HbO and Hb in the NIR range are distinct. As with our previous work,[19,20] we assumed that HbO and Hb are the major significant absorbing species in tissue vasculature, including tumors, within the selected NIR range of 700–900 nm. Although diffusion theory has been a well-accepted theoretical approach to mathematically quantify light–tissue interaction,[6,7,10,47] no analytical solution has been available for solid tumors because of their finite size and high heterogeneity. While our future work will use the finite element method to obtain numerical solutions for the diffusion equation, our current approach is based on modified Beer–Lambert's law to account for light scattering in tumor tissue.

For a nonscattering medium, Beer–Lambert's law gives rise to the following expressions for the relationships between the absorption coefficient, μ_a, and the extinction coefficient for deoxyhemoglobin (ε_{Hb}) and oxyhemoglobin (ε_{HbO}):

$$\mu_a^{758} = 2.3\{\varepsilon_{Hb}^{758}[Hb] + \varepsilon_{HbO}^{758}[HbO]\} \quad (1)$$

$$\mu_a^{785} = 2.3\{\varepsilon_{Hb}^{785}[Hb] + \varepsilon_{HbO}^{785}[HbO]\} \quad (2)$$

where [HbO] and [Hb] are concentrations of HbO and Hb, respectively, the factor of 2.3 results from the different definitions of μ_a and ε in relation to the incident and detected optical intensities. The conventional definitions for μ_a and ε are $I = I_0 e^{-\mu aL}$ and $I = I_0 10^{-\varepsilon CL}$, respectively, where I_0 and I are the incident and detected optical intensities in transmission measurement from a nonscattering medium, C is the concentration of hemoglobin measured in m*M*/L, and L is the optical pathlength through the medium in cm. By eliminating I and I_0 in these two expressions, we arrived at a relationship of $\mu_a = 2.3\ \varepsilon C$.

[47] M. S. Patterson, B. Chance, and B. C. Wilson, *Appl. Opt.* **28,** 2331 (1989).

Because of light scattering in tissue, Beer–Lambert's law cannot be applied directly to biologic tissue, such as tumors. By taking an empiric approach to modify Beer–Lambert's law, we arrived at $\mu_a = 2.3\varepsilon C = 2.3/L_S \log(I_0/I)$, where L_S represents the optical pathlength in a scattering medium and is no longer equal to the physical distance between the source and detector, d. In a highly light-scattering medium, L_S is much longer than d. Specifically, in the tumor study, we use I_0 and I to represent the incident and detected light intensities, when the tissue sample is without and with light absorption from [HbO] and/or [Hb]. Then, changes in absorption coefficient of the tumor, $\Delta\mu_a$, between baseline and transient conditions under respiratory intervention can be expressed as

$$\Delta\mu_a = \mu_{aT} - \mu_{aB} = 2.3\log(I_B/I_T)/L_S \tag{3}$$

where I_B and I_T are baseline and transient light intensities of the measured optical signals, respectively.

Using the transmitted light intensities at $\lambda_1 = 758$ nm and $\lambda_2 = 785$ nm and manipulating Eqs. (1)–(3), we can quantify the changes of tumor [HbO] and [Hb] due to an intervention as follows:

$$\Delta[\mathrm{HbO}] = -11.73 \times \frac{\log(I_B/I_T)^{\lambda 1}}{L_S^{\lambda 1}} + 14.97 \times \frac{\log(I_B/I_T)^{\lambda 2}}{L_S^{\lambda 2}} \tag{4}$$

$$\Delta[\mathrm{Hb}] = 8.09 \times \frac{\log(I_B/L_T)^{\lambda 1}}{L_S^{\lambda 1}} - 6.73 \times \frac{\log(I_B/I_T)^{\lambda 2}}{L_S^{\lambda 2}} \tag{5}$$

where $L_S^{\lambda 1}$ and $L_S^{\lambda 2}$ are optical path lengths between the source and detector at the respective wavelengths. The units of Δ[HbO] and Δ[Hb] in Eqs. (4) and (5) are mM. The constants given in the equations were computed with the extinction coefficients for oxygenated and deoxygenated hemoglobin at the two wavelengths used.[48]

In principle, $L_S^{\lambda 1}$ and $L_S^{\lambda 2}$ in Eqs. (4) and (5) are variables, depending on the actual separation of source and detector, as well as the optical properties of tumor. Previously, a differential pathlength factor (DPF), (i.e., $L_S = d \times DPF$) has been introduced to associate L_S with d.[49] The DPF values of blood-perfused tissues have been studied intensively for muscles[50] and

[48] W. G. Zijlstra, A. Buursma, and W. P. Meeuwsen-van der Roest, *Clin. Chem.* **37,** 1633 (1991).

[49] D. T. Delpy, M. Cope, P. van der Zee, S. Arridge, S. Wray, and J. Wyatt, *Phys. Med. Biol.* **33,** 1433 (1988).

[50] M. Ferrari, Q. Wei, L. Carraresi, R. A. De Blasi, and G. Zaccanti, *J. Photochem. Photobiol.* **16,** 141 (1992).

brains[51] with approximate values of 4–6 and 5–6, respectively. However, little is known about DPF for tumors, although a DPF value of 2.5 has been used by others.[52] In our approach, we made two assumptions: (1) DPF is the same for both Δ[HbO] and Δ[Hb] at 785 nm (i.e., $DPF = DPF^{785}_{HbO} = DPF^{785}_{Hb}$). This assumption was based on the fact that the absorption difference between oxygenated and deoxygenated blood at 785 nm is much smaller than that at 758 nm. The maximal relative error caused by this assumption in tumor oxygen interventions was estimated to be less than 12%, and detailed justification and discussion were given by Liu *et al.*[19] Furthermore, we associated L_S to μ_a by $L = \sqrt{3}/2d\sqrt{\mu_s'/\mu_a}$, where μ_s' is the reduced scattering coefficient, according to Sevick-Muraca *et al.*[53] and Liu.[54] The second assumption was $\mu_s'(758\text{ nm}) \cong \mu_s'(785\text{ nm})$ because of weak wavelength dependence of light scattering from tissue. With all the conditions mentioned and further derivation, as given in details by Kim *et al.*[20] we arrived at the final expressions for Δ[HbO] and Δ[Hb]:

$$\Delta[\mathrm{HbO}] = \frac{-10.63 \cdot \log\left(\frac{A_B}{A_T}\right)^{758} + 14.97 \cdot \log\left(\frac{A_B}{A_T}\right)^{785}}{d} \tag{6}$$

$$\Delta[\mathrm{Hb}] = \frac{8.95 \cdot \log\left(\frac{A_B}{A_T}\right)^{758} - 6.73 \cdot \log\left(\frac{A_B}{A_T}\right)^{785}}{d} \tag{7}$$

where d is the direct physical distance between source and detector. $\Delta[\mathrm{Hb}]_{total}$ is followed by adding Eqs. (6) and (7), as

$$\Delta[\mathrm{Hb}]_{total} = \Delta[\mathrm{HbO}] + \Delta[\mathrm{Hb}] \tag{8}$$

Equations (6) to (8) will be used in calculating Δ[HbO], Δ[Hb], and $\Delta[\mathrm{Hb}]_{total}$ in tissue phantoms and tumors during gas interventions in later sections.

The units for Δ[HbO], Δ[Hb], and $\Delta[\mathrm{Hb}]_{total}$ in Eqs. (6) to (8) are m*M*/DPF, which still depends on the optical properties of tumor at a particular wavelength. Because our focus is on dynamic changes in [HbO] due to respiratory challenges, in some cases, we normalize Δ[HbO] at its maximal

[51] P. van der Zee, M. Cope, S. R. Arridge, M. Essenpreis, L. A. Potter, A. D. Edwards, J. S. Wyatt, D. C. McCormick, S. C. Roth, E. O. R. Reynolds, and D. T. Delpy, *Adv. Exp. Med. Biol.* **316,** 143 (1992).

[52] R. G. Steen, K. Kitagishi, and K. Morgan, *J. Neurooncol.* **22,** 209 (1994).

[53] E. M. Sevick-Muraca, B. Chance, J. Leigh, S. Nokia, and M. Maris, *Anal. Biochem.* **195,** 330 (1991).

[54] H. Liu, *Appl. Opt.* **40,** 1742 (2001).

value (i.e., $\Delta[HbO]/\Delta[HbO]_{max}$) to eliminate the effect of DPF on our results.

Experimental Methods

One-Channel and Multichannel NIR System

A dual-wavelength (at 758 and 785 nm), one-channel NIR system (NIM, Inc., Philadelphia, PA) uses an in-phase and quadrature-phase chip (IQ chip). As shown in Fig. 1, the NIR system starts with a radiofrequency (RF) source to modulate the light intensities of two laser diodes (LD_1 and LD_2) at 140 MHz through a time-sharing system. The light passes through a bifurcated fiber optic probe, is transmitted through the tumor tissue, and is collected by a second fiber bundle. The light is then amplified by a photomultiplier tube (PMT), demodulated by the IQ circuit, and filtered by a lowpass filter (LPF) for passing only the direct current (DC) components. The signals are digitized by an analog-to-digital converter (ADC) and stored in a laptop computer. The measured DC signals at the IQ branches

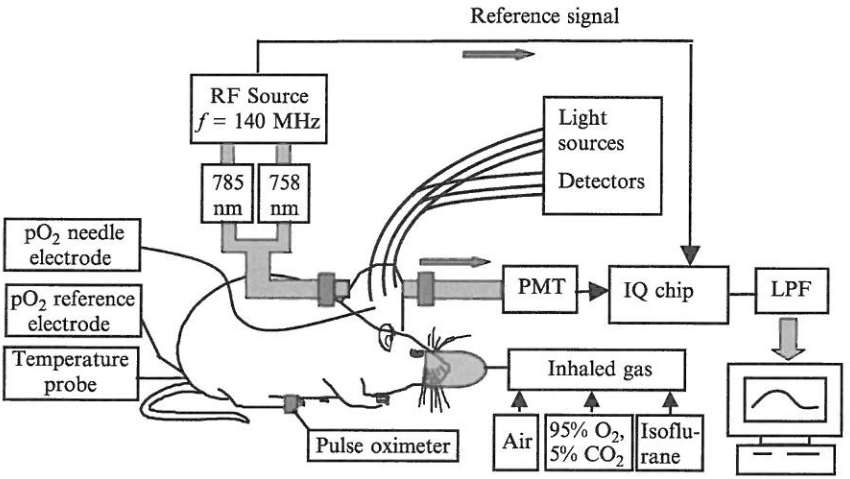

FIG. 1. Experimental setup for simultaneous tumor oximetry, using an NIRS system with either a needle electrode or a three-channel fiber-optic FOXY system. The NIR system consists of two laser diodes modulated at 140 MHz, two fiber bundles for light delivery and collection, a photomultiplier tube (PMT), an in-phase and quadrature-phase demodulator (IQ chip), and lowpass filter (LPF) for retrieving amplitude and phase information. The FOXY system comprises three fiber-optic, oxygen-sensing probes that are inserted into different regions of the tumor. Alternatively, a needle electrode probe can be inserted into the tumor for single-channel pO_2 reading.

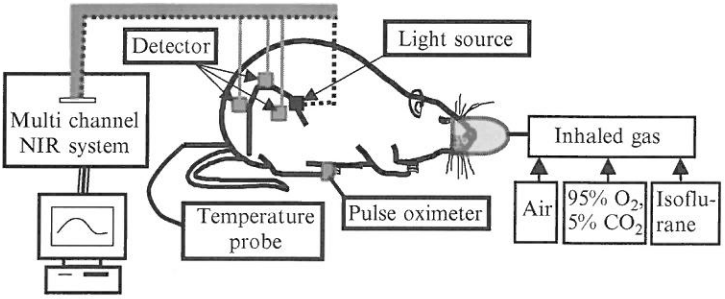

FIG. 2. Schematic experimental setup for three-channel NIRS experiments. One of the three detectors was placed opposite to the light source in order to detect light in transmission mode, and the other two detectors were set in the semireflection mode on the tumor surface.

at the measured wavelengths, $I_{bc}(\lambda)$ and $Q_{bc}(\lambda)$, lead to the quantification of optical amplitudes, $A(\lambda)$, and phase, $\theta(\lambda)$, that have passed through the tumor tissues[55]:

$$A(\lambda) = \sqrt{\mathrm{I}(\lambda)_{\mathrm{DC}}^2 + Q(\lambda)_{\mathrm{DC}}^2} \tag{9}$$

$$\theta(\lambda) = \arctan\left(\frac{Q(\lambda)_{\mathrm{DC}}^2}{I(\lambda)_{\mathrm{DC}}^2}\right) \tag{10}$$

where λ represents the respective wavelengths used in the NIR system. Then, changes in light intensity through the tumor caused by hyperoxic interventions are used to compute changes in tumor vascular [HbO] and [Hb]. Whether the readings of $\theta(\lambda)$ can be linked to tumor physiology remains to be further explored.

Besides a one-channel NIR system, we have also used a multichannel NIR system (Fig. 2) to explore and reveal intratumoral vascular heterogeneity by having simultaneous readings at several separations of the source and detectors. Unlike the single-channel system, the multichannel system uses two laser diodes at 730 and 850 nm with constant light intensities (i.e., DC light) and three photo detectors. These detectors are placed along the circumference together with the light source, with three different source–detector separations in order to detect different depths within the tumor volume, as demonstrated in Fig. 3.

Following the same procedures as those described in the previous section, we arrived at the expression of Δ[HbO] for the multichannel system with the two wavelengths of 730 and 830 nm, as follows:

[55] Y. Yang, H. Liu, X. Li, and B. Chance, *Opt. Eng.* **36,** 1562 (1997).

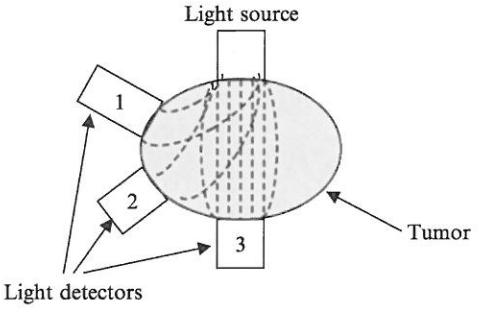

FIG. 3. A schematic diagram showing the locations of the three detectors and possible internal tumor volumes interrogated by the different detectors.

$$\Delta[\mathrm{HbO}] = \frac{-0.674 \cdot \log\left(\frac{A_B}{A_T}\right)^{730} + 1.117 \cdot \log\left(\frac{A_B}{A_T}\right)^{830}}{d} \tag{11}$$

where d is the direct source–detector separation in cm, and the unit of Δ[HbO] is mM/DPF.

System Testing and Calibration

It is important to characterize and verify linearity of the NIRS system before any animal experiment starts. We have performed two critical system tests: (1) to quantify the output voltage range, within which the NIR system has a linear response, and (2) to perform liquid phantom measurements to confirm the physiologic readings derived from the optical NIRS system.

Linearity Testing Associated with Crosstalk Between the Amplitude and Phase. In principle, changes in amplitude of an FD photon migration system should be independent of its changes in phase (i.e., the crosstalk between amplitude and phase should be minimal for an ideal NIR system): However, in reality, it is difficult to have such a perfect condition for an actual instrument, so it is necessary to conduct the crosstalk test. We altered the optical densities (O.D.) of optical filters in front of the two light sources (758 and 785 nm) to attenuate the detected amplitude, so we could see whether changes in amplitude and phase were correlated. The test showed that phase–amplitude crosstalk exists, if the measured output intensity is either too small (<50 mV) or too large (>380 mV), as shown in Fig. 4A and 4B for 758 nm and 785 nm, respectively. We also plotted O.D. values of the filters versus log (amplitude of the output signal) to see the electrical attenuation of the system output in response to the optical

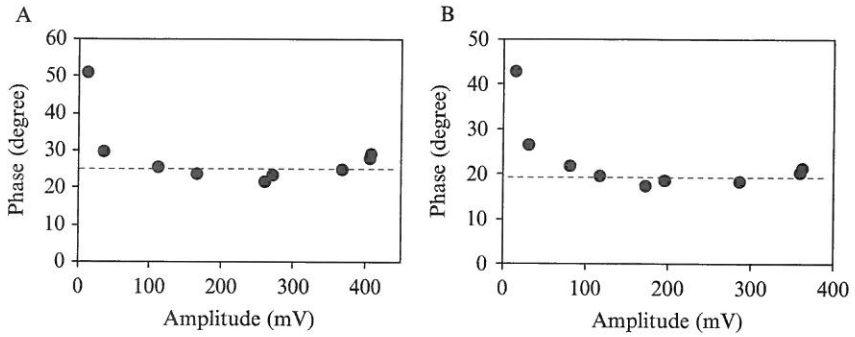

FIG. 4. Relationships between the output amplitude (mV) and phase (in degree) of the NIR single-channel system at (A) 758 nm and (B) 785 nm.

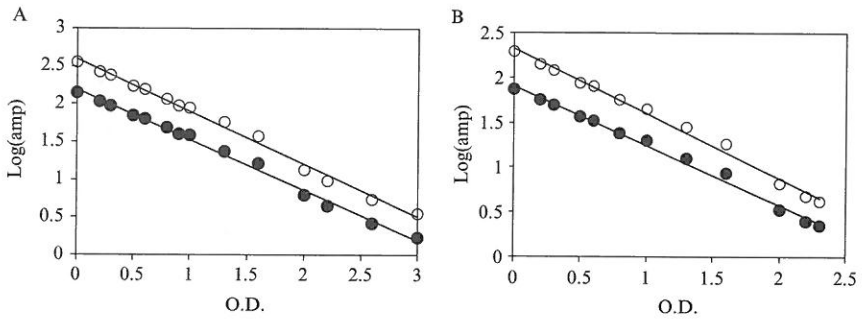

FIG. 5. Linearity tests for the NIR system between the optical input attenuation and electrical output signals at 758 nm (open circles) and 785 nm (solid circles). The X variable is the optical density (O.D. = $\log[I_0/I]$) of the filters, which were inserted before the detector to attenuate the light intensity. Cases (A) and (B) correspond to a higher (350 mV for 758 nm) and lower (193 mV for 758 nm) output voltage, respectively. Both 350 and 193 mV were obtained when the measurement was performed without any optical attenuation.

attenuation. It was found that as long as the output is in the range 100–350 mV, good linearity is achieved for the system response, as shown in Fig. 5A and 5B.

Blood Phantom Study. To calibrate the NIRS system for quantifying hemoglobin concentrations, we used human blood for tissue phantom experiments. Two packets of Sigma (St. Louis, MO) P-3813 phosphate buffered saline (PBS) (pH 7.4) powder was used to make a 2-liter buffer, and 100 ml of 20% intralipid was added into the buffer for a 1% intralipid solution, as shown in Fig. 6A. Then 14 g of baking yeast was mixed with tap

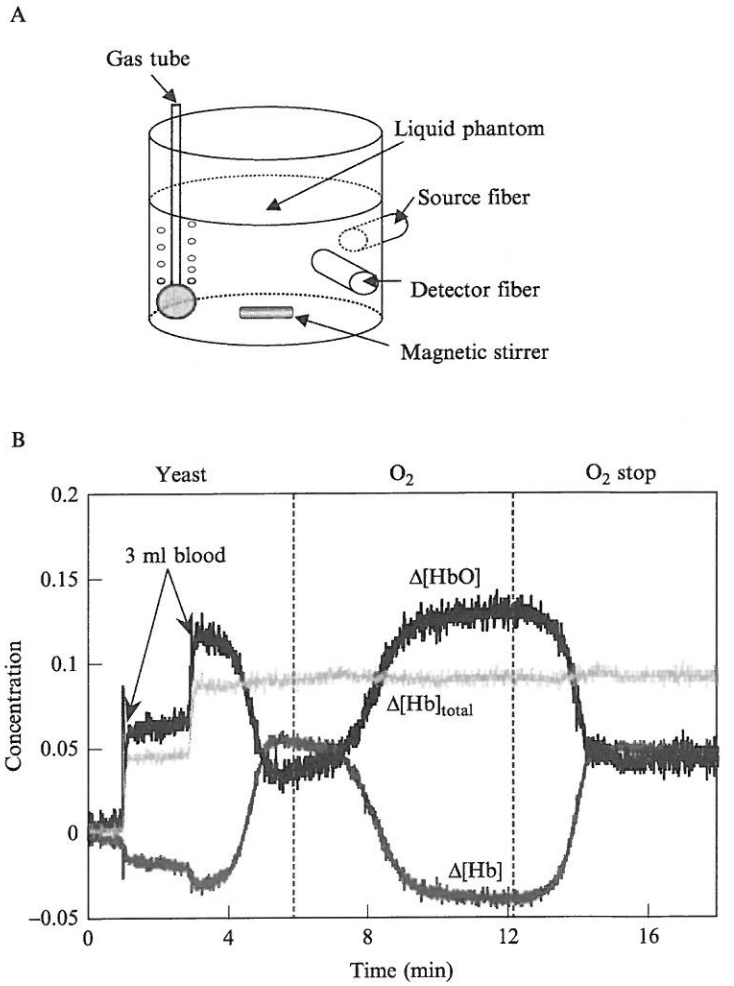

FIG. 6. (A) Experimental setup for system calibration using a liquid phantom with 1% Intralipid and baker's yeast in saline buffer. The NIRS probes were placed in reflectance geometry, while the gas bubbler was placed opposite to minimize liquid movement effects. (B) Simultaneous dynamic changes of Δ[HbO], Δ[Hb], and $\Delta[Hb]_{total}$ in the phantom solution measured using the NIR single-channel system. The dark solid curve is for Δ[HbO], the lighter solid line is for $\Delta[Hb]_{total}$, and the gray solid line shows Δ[Hb] in the phantom solution. Blood was deoxygenated by the yeast's oxygen consumption and oxygenated by bubbling O_2. During the oxygenation and deoxygenation process, $\Delta[Hb]_{total}$ was maintained as a constant.[20]

water before being added into the 2-liter buffer solution to deoxygenate the tissue phantom solution. Amount of blood for each addition to the solution was 3 ml for two additions after the yeast was well mixed in the solution.

When the blood was fully deoxygenated by yeast, pure oxygen was introduced in the solution to oxygenate the blood. After the blood was fully oxygenated, oxygen blowing was stopped in order to re-deoxygenate the solution by yeast again. The gas tube for oxygen delivery was placed far from the NIRS probes to minimize any liquid movement effects, as shown in Fig. 6A. Source and detector probes for the NIRS system were placed in reflection geometry with a direct separation of ~3 cm. The solution was stirred constantly with a magnetic stirrer to maintain homogeneity.

After getting the raw amplitude data from the experiment, we used Eqs. (6) to (8) to calculate Δ[HbO], Δ[Hb], and $\Delta[\mathrm{Hb}]_{\mathrm{total}}$. As shown in Fig. 6B, $\Delta[\mathrm{Hb}]_{\mathrm{total}}$ remained constant, as expected, whereas Δ[HbO] and Δ[Hb] altered in opposite directions during the oxygenation and deoxygenation cycle. This demonstrates that the two assumptions used to derive Eqs. (6) and (8) are correct and necessary to compensate the differences in DPF caused by two different wavelengths.[20] Notice that there appears to be a delay between the gas switch and responses of Δ[HbO] and Δ[Hb] as shown in Fig. 6B. This delay is possibly caused by the entire process of transporting oxygen gas from the tube to the solution, oxygenating/deoxygenating the solution, and reaching a homogeneous state near the detectors.

Animal Models

In the prostate tumor study, Dunning prostate R3327-HI rat tumors (originally obtained from Dr. Peter Peschke, DKFZ Heidelberg) were implanted in pedicles on the foreback of adult male Copenhagen rats.[56] In the breast tumor study, rat mammary adenocarcinomas 13762NF (originally obtained from the Division of Cancer Therapeutics, National Cancer Institute [DCT NCI]) grown in the hindlimb of adult female Fisher 344 rats (~200 g) were used. Once the tumors reached approximately 1–2 cm in diameter, the rats were anesthetized with 0.2 ml ketamine hydrochloride (100 mg/ml; Aveco, Fort Dodge, IA) and maintained under general gaseous anesthesia with isoflurane in air (1.3% isoflurane at 1 dm^3/min air) through a mask placed over the mouth and nose. Tumors were shaved to improve optical contact for transmitting light. Body temperature was maintained by a warm water blanket and was monitored by a rectally

[56] E. W. Hahn, P. Peschke, R. P. Mason, E. E. Babcock, and P. P. Antich, *Magn. Reson. Imaging* **11,** 1007 (1993).

inserted thermal probe (see Fig. 1) connected to a digital thermometer (Digi-Sense, Model 91100–50; Cole-Parmer Instrument Company, Vernon Hills, IL). A pulse oximeter (Model 8600; Nonin, Inc., Plymouth, MN) was placed on the hindfoot to monitor arterial oxygenation (S_aO_2). Tumor volume V (in cm^3) was estimated as $V = 4\pi/3(L + W + H/6)^3$, where L, W, and H are the three respective orthogonal dimensions.

In general, the source–detector fiber separation was about 1–1.5 cm in transmittance geometry, and thus the tumor volume interrogated by NIR light can be estimated as follows. The radius of probe is 0.4 cm, which makes the volume of the cylinder 0.5–0.75 cm^3. By diffusion approximation, the optical penetration depth is about one third of the direct distance between the source and detector, which makes an additional spherical volume with a radius from 0.5–0.75 cm. Therefore the total tumor volume interrogated by NIR light can be estimated in the range of 1.0–2.5 cm^3, depending on the actual source–detector separation.[20]

Measurements of pO_2 Using Oxygen Needle Electrode and Fiber-Optic Fluorescence-Quenched Probe

Needle Electrode. We used a needle-type oxygen electrode for local pO_2 readings in several tumors. Linear two-point calibrations were performed with air (21% O_2) and pure nitrogen (0% O_2) saturated saline buffer solutions before the animal experiments, and we estimated an instrumental precision of 2–3 mmHg. After calibration, the needle electrode was inserted carefully into the tumor with the reference electrode being placed rectally, as described in detail previously.[20] Both the sample and reference electrodes were connected to a picoammeter (Chemical Microsensor; Diamond Electro-Tech, Inc., Ann Arbor, MI) and polarized at −0.75 V. Measurement points of pO_2 were manually recorded, whereas the NIRS data were acquired automatically. Measurements of pO_2 and NIRS were initiated, while rats breathed air for ~10 min to demonstrate a stable baseline. The inhaled gas was then switched to carbogen (5% CO_2 and 95% O_2) or oxygen for 15 min and switched back to air.

Fiber-Optic Fluorescence-Quenched Probe. For multiple pO_2 readings, we used a multichannel, fiber-optic, oxygen-sensing system (FOXY; Ocean Optics, Inc.). We calibrated the three fluorescence-quenched, optical fiber probes initially and then inserted them into different regions of the tumors to monitor the changes of oxygen tension (ΔpO_2) in response to the respiratory challenges as described previously.[24] The probes were placed in such a way that at least one was in a relatively poorly oxygenated region (low baseline pO_2) and at least one was in a relatively well-oxygenated region (high baseline pO_2). A mean ΔpO_2 of the tumor was obtained by

averaging the three readings. A typical FOXY channel used a pulsed blue light-emitting diode (LED) at ~475 nm and was coupled into one branch of a bifurcated optical fiber bundle. Then, the fluorescent light was propagated to the FOXY probe tip. Each probe had two 300-μm-diameter optical fibers with an aluminum jacket. The distal end of the probes was coated with a thin layer of a hydrophobic sol-gel material, so that an oxygen-sensing ruthenium complex was effectively trapped and protected from water. The ruthenium complex at the probe tips was excited by the blue LED and emitted fluorescence at ~600 nm. If the excited ruthenium complex encountered an oxygen molecule, the excess energy would be transferred to the oxygen molecule in a nonradiative transition, decreasing or quenching the fluorescence signal.

The fluorescence response of the ruthenium complex was highly temperature dependent, so the probe calibration was accomplished by streaming gases of known oxygen concentrations (100, 20.9, 10, 2, and 0%) through a cylindrical water jacket heated to 37°. Calibration curves were calculated by the vendor-supplied software, using the second-order, polynomial calibration:

$$\frac{I_0}{I} = 1 + K_1[O] + K_2[O]^2 \tag{12}$$

where I_0 is the fluorescence intensity at zero concentration (nitrogen), I is the measured intensity of fluorescence at a pressure p of oxygen, $[O]$ represents the oxygen concentration (related to pO_2), and K_1 and K_2 are the first- and second-order coefficients and are automatically supplied by the curve-fitting routine from the calibration measurements. After the system calibration, the oxygen concentration in tumor–tissue sample measurements was deduced using Eq. (12).

NIR Measurements of Breast–Prostate Tumors Under Interventions

We conducted all animal experiments in a darkened room, and the measurements were initiated while the rats breathed air for 10 min to get a stable baseline. The inhaled gas was switched to carbogen (5% CO_2 and 95% O_2) or pure oxygen for 15–20 min, and then back to air for 15 min. Sometimes, repeated cycles were taken either to check the reproducibility or to minimize preconditioning effects. Raw amplitude data from either the one-channel or three-channel detectors were recorded simultaneously during the experiments, processed, and displayed through the computer to obtain tumor Δ[HbO] and $\Delta[Hb]_{total}$. The dynamic data were fitted with a single-exponential and/or double-exponential expression, using Kaleidagraph software (Synergy Software, Reading, PA), to obtain time constants

and amplitudes. Those fitted parameters allowed us to further develop a two-region tumor model, which will be discussed in a later section.

In many cases, we performed simultaneous measurements of changes in tumor HbO and in tumor pO_2, using either the needle electrode or the fiber-optic FOXY system along with the NIRS readings, as shown in Fig. 1, for both breast and prostate tumors.

Results and Model Development

HbO and pO_2 Changes in Prostate Tumors Under Carbogen Intervention

We have measured relative changes of [HbO], $[Hb]_{total}$, and tumor tissue pO_2 from several Dunning prostate R3327-HI tumors, and Fig. 7 shows two representative data sets. Figure 7A shows the temporal profiles of Δ[HbO] and pO_2 in a Dunning prostate R3327-HI tumor (3.6 cm^3) measured simultaneously with the NIRS and pO_2 needle electrode during carbogen respiratory challenge. After the breathing gas was switched from air to carbogen, Δ[HbO] increased rapidly, whereas $\Delta[Hb]_{total}$ seemed to have much smaller responses. In this case, tumor tissue pO_2 increased at a much slower rate, from a baseline of 60 mmHg to ~80 mmHg during the entire carbogen intervention. Figure 7B is obtained from another prostate tumor (3.1 cm^3); the electrode readings showed a slower pO_2 response from ~15 to 40 mmHg, whereas the NIRS response was biphasic, a sharp rise in Δ[HbO] followed by a further slow, gradual significant increase over the next ~15 min. In this case, $\Delta[Hb]_{total}$ showed little change, ~2% of the maximum in Δ[HbO]. The biphasic feature of Δ[HbO] has been a commonly observed dynamic characteristic under tumor vascular oxygenation, as reported previously.[19,20,24]

HbO and pO_2 Changes in Breast Tumors Under Carbogen and Oxygen Intervention

For a representative 13762NF breast tumor (3.2 cm^3), typical time profiles of the normalized Δ[HbO] and mean ΔpO_2 in response to carbogen and then oxygen intervention are shown in Fig. 8. When the inspired gas was switched from air to carbogen, the normalized Δ[HbO] showed a sharp initial rise in the first minute ($p < 0.0001$), followed by a slower, gradual, but further significant increase over the next 19 min ($p < 0.001$). The mean ΔpO_2 profile was averaged over the three individual ΔpO_2 readings (FOXY), and it increased rapidly by about 50 torr (= mmHg) within 8 min ($p < 0.0005$) and also continued a slower and gradual increase over the next 12 min ($p < 0.005$). Return to breathing air produced a significant

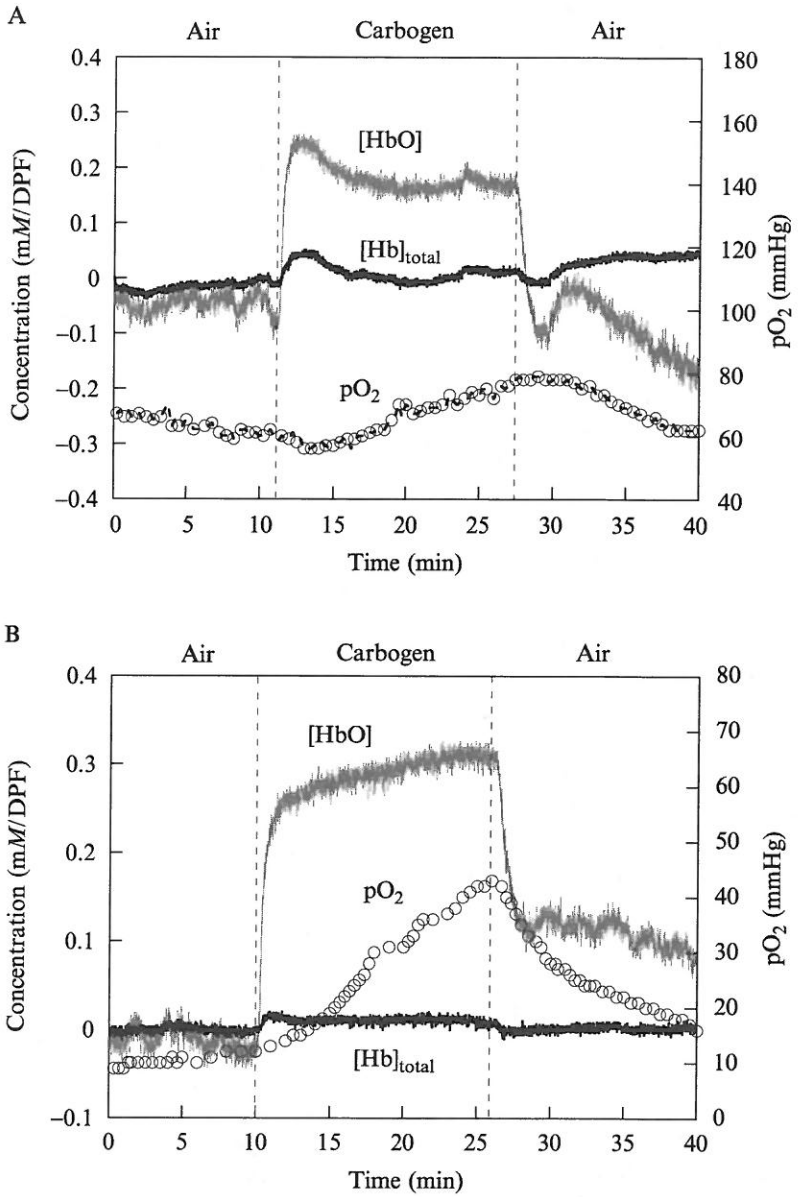

FIG. 7. Simultaneous dynamic changes of Δ[HbO] and pO_2 in R3327-HI rat prostate tumors using NIRS and pO_2 needle electrode. (A) A representative tumor (3.6 cm^3) showed a rapid NIR response, whereas (B) another tumor (3.1 cm^3) showed a clear biphasic feature in Δ[HbO] with a slow pO_2 response. The unit of Δ[HbO] is m*M*/DPF, where DPF is equal to the optical pathlength divided by the source–detector separation. Dotted vertical line marks the time when the gas was changed.

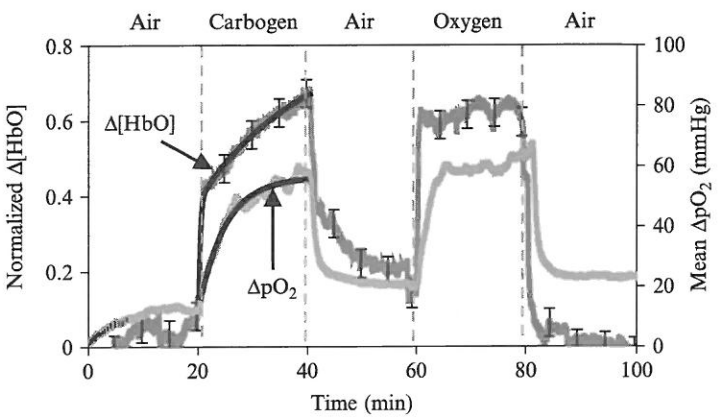

FIG. 8. Dynamic responses of Δ[HbO] and mean ΔpO_2 to hyperoxic gas intervention in a rat breast tumor (3.2 cm^3). In response to carbogen breathing, single-exponential curve fitting yielded $\Delta pO_2 = 42.68\ \{1 - \exp[-(t-21.01)/4.56]\} + 16.66$ ($r = 0.98$), and biexponential fitting resulted in $\Delta[HbO] = 0.373\ \{1 - \exp[-(t-20.36)/0.61]\} + 0.648\ \{1-\exp[-(t-20.36)/21]\}$ ($r = 0.97$). The smooth black curves plotted along with the data are obtained according to the previous exponential expressions, respectively.

decline for both signals ($p < 0.0001$). When the hyperoxic intervention was repeated with pure oxygen, the dynamic features of Δ[HbO] and ΔpO_2 remained consistent, except that the biphasic behavior of Δ[HbO] was less apparent. A detailed investigation on Δ[HbO] differences in response to carbogen and oxygen interventions has been given in our earlier study.[24]

In response to carbogen intervention, the pO_2 profile displayed a single-phase dynamic behavior, whereas Δ[HbO] showed an apparent biphasic response. These dynamics may be characterized by time constants of single- and double-exponential responses, respectively. A single exponential fitting gives rise to a slow ΔpO_2 response of $\tau(\Delta pO_2) = 4.56 \pm 0.06$ min ($r = 0.98$). A double-exponential expression with two time constants, τ_1 and τ_2, was used to fit the normalized Δ[HbO], yielding fast and slow time constants of 0.61 min and 21 min, respectively. Figure 8 plots the fitted curves along with the experimental data. During the course of our study, we have often observed biphasic characteristic of Δ[HbO], which motivated us to develop a model to interpret the experimental finding, to be described in a later section.

The advantage of using FOXY pO_2 probes is to detect distinct heterogeneity in tumor pO_2. The individual responses at different locations within the tumor to the hyperoxic gas were diverse: those probes that indicated

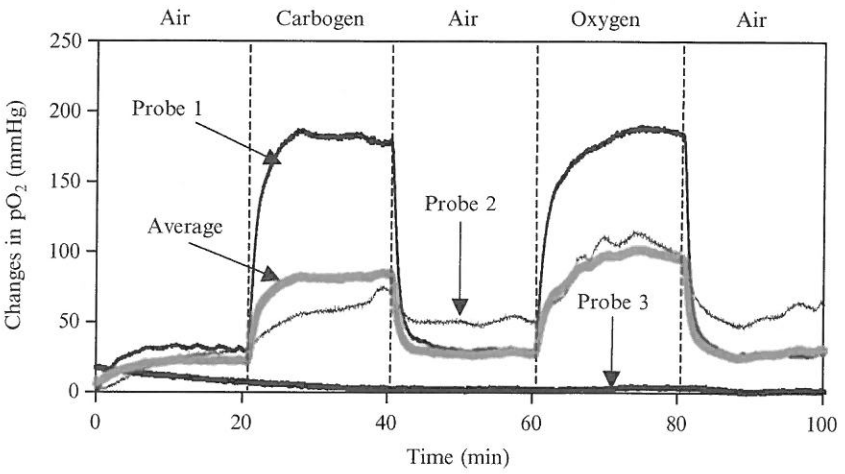

FIG. 9. Time profiles of tumor oxygen tension changes, ΔpO_2, measured with three channels of a FOXY fiber-optic, oxygen-sensing system with respect to different gas inhalations for a breast tumor (4.6 cm^3). The mean signal for the three channels was calculated and plotted by the thicker trace. Modified from Gu *et al.*[24]

apparently well-oxygenated regions usually showed a large and rapid response, whereas those with lower baseline pO_2 often showed little change (Fig. 9). By studying a group of five rats with both carbogen and oxygen interventions, we obtained a distinct correlation between the maximal values of global Δ[HbO] and the mean ΔpO_2, as shown in Fig. 10. Because of heterogeneity in regional pO_2, the standard deviations of the mean pO_2 values were quite large.

Tumor Heterogeneity Observed by a Multichannel NIRS System

To study tumor heterogeneity, the multichannel NIRS system also has been used to detect changes in [HbO] with different source-detector separations. Fig. 11A shows three temporal profiles of Δ[HbO] obtained from three detectors in a breast tumor (16.6 cm^3), with a source–detector separation of 1.5 cm for detector 1, 2.5 cm for detector 2, and 2.8 cm for detector 3, respectively (Fig. 3). The measurement uncertainties are plotted at discrete times in Fig. 11A. After 10 min of air breathing measurement as the baseline, the inhaled gas was switched from air to carbogen, causing a sharp increase in Δ[HbO] ($p < 0.0001$ after 1 min from gas switch), followed by a further gradual, but significant, increase over the next 15 min ($p < 0.0001$).

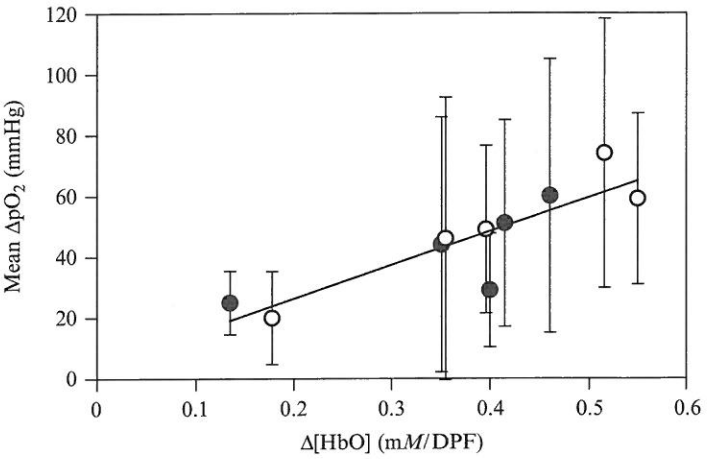

FIG. 10. Correlation between mean ΔpO_2 and ΔHbO for five breast tumors ($r > 0.86$) with a linear relationship of $\Delta pO_2 = 110.65\ \Delta HbO + 4.1285$. Solid circles are for transition air to carbogen, whereas open circles are for transition air to oxygen.[24]

As with the single-channel NIRS measurement, the biphasic features appear clearly in the multichannel results. The rising parts of $\Delta[HbO]$ from detectors 1, 2, and 3 after gas switch to carbogen are shown in Fig. 11B–11D, respectively, along with the fitted curves. The two equations used for the curve fitting are

$$\Delta[HbO]_{single} = A\{1 - \exp[-(t - t_0)/\tau]\} \tag{13}$$

$$\Delta[HbO]_{double} = A_1\{1 - \exp[-(t - t_0)/\tau_1]\} + A_2\{1 - \exp[-(t - t_0)/\tau_2]\} \tag{14}$$

respectively, for the single-exponential and double-exponential expressions. It is clear that the double-exponential expression gives a much better fit, as confirmed by the respective chi squared (χ^2) and R^2 values. Table I summarizes all the fitted parameters for the respective detectors.

Mathematical Model Development to Interpret Data

As shown in the last section, the temporal profiles of tumor $\Delta[HbO]$ caused by respiratory challenge can be well fitted with a double-exponential equation, represented by two time constants (fast and slow). To understand these time constants and to interpret the experimental findings, we further developed a hemoperfusion model,[19] briefly described as follows.

A
Δ[HbO] (mM/DPF)
Air
Carbogen
Air
Detector 1
Detector 2
Detector 3
Time (min)
B
Δ[HbO]–D1 (mM/DPF)
Gas switch
(air→carbogen)
Double-exponential fitting
Single-exponential fitting
Time (min)
C
Δ[HbO]–D2 (mM/DPF)
Gas switch
(air→carbogen)
Double-exponential fitting
Single-exponential fitting
Time (min)
D
Δ[HbO]–D3 (mM/DPF)
Gas switch
(air→carbogen)
Double-exponential fitting
Single-exponential fitting
Time (min)

TABLE I
SUMMARY OF VASCULAR OXYGEN DYNAMICS FROM THREE DETECTORS FROM FIG. 11

Double-exponential fitting $\Delta HbO_2 = A_1[1 - \exp(-t/\tau_1)] + A_2[1 - \exp(-t/\tau_2)]$			
Parameters	Detector 1	Detector 2	Detector 3
Separation: d (cm)	1.5	2.5	2.8
A_1 (mM/DPF)	0.037 ± 0.001	0.0125 ± 0.0002	0.0134 ± 0.0002
τ_1 (min)	0.24 ± 0.01	0.30 ± 0.02	0.27 ± 0.01
A_2 (mM/DPF)	0.020 ± 0.001	0.0130 ± 0.0004	0.0060 ± 0.0002
τ_2 (min)	8.27 ± 0.72	9.87 ± 0.84	7.00 ± 0.58
χ^2	0.005	0.001	0.0005
R^2	0.95	0.96	0.95
$\gamma_1/\gamma_2 = A_1/A_2$	1.85 ± 0.07	0.96 ± 0.05	2.23 ± 0.08
τ_1/τ_2	0.029 ± 0.004	0.030 ± 0.004	0.039 ± 0.005
$f_1/f_2 = (A_1/A_2)/(\tau_1/\tau_2)$	64 ± 9	32 ± 5	58 ± 9

Following an approach used to measure regional cerebral blood flow (rCBF) with diffusible radiotracers,[57–59] we made an analogy to evaluate tumor hemodynamics, using the respiratory intervention gas as a tracer.

In response to respiratory intervention, a sudden small change introduced in arterial O_2 saturation (S_aO_2) results in an increase in arterial HbO concentration (ΔHbO^{artery}). This increase in HbO^{artery} can be considered as an intravascular tracer.[60] Following Kety's method and assuming that changes in dissolved O_2 are negligible,[60] we have

$$\frac{d}{dt}\left(\Delta HbO^{vasculature}\right) = f\left(\Delta HbO^{artery} - \frac{\Delta HbO^{vasculature}}{\gamma}\right) \qquad (15)$$

[57] S. S. Kety, *Pharmacol. Rev.* **3,** 1 (1951).
[58] S. S. Kety, *Israel J. Med. Sci.* **23,** 3 (1987).
[59] H. Watabe, M. Itoh, V. Cunningham, A. A. Lammertsma, P. Bloomfield, M. Mejia, T. Fujiwara, A. K. P. Johes, T. Johes, and T. Nakamura, *J. Cerebr. Blood Flow Metab.* **16,** 311 (1996).
[60] A. D. Edwards, C. Richardson, P. van der Zee, C. Elwell, J. S. Wyatt, M. Cope, D. T. Delpy, and E. O. R. Reynolds, *J. Appl. Physiol.* **75,** 1884 (1993).

FIG. 11. (A) Dynamic changes of [HbO] measured at three detectors from a rat breast tumor (volume: 16.6 cm^3). Dotted vertical lines mark the points when the gas was changed. The rising parts of Δ[HbO] obtained from three detectors were fitted using both single-exponential and double-exponential expressions, and (B) to (D) are from detectors 1 to 3, respectively.

where f represents blood perfusion rate, and γ is defined as a vasculature coefficient of the tumor. The coefficient, γ, is the ratio of HbO concentration change in the vascular bed to that in veins and equals $(\Delta HbO^{vasculature})/(\Delta HbO^{vein})$.

In Eq. (15), whereas f and γ are constants, $\Delta HbO^{vasculature}$ is a time-dependent variable. In principle, $\Delta HbO^{vasculature}$ can be solved rigorously given a constant input, H_0, for ΔHbO^{artery} after time 0. Our previous study demonstrates that changes in arterial HbO (S_aO_2) are much faster than that in the vascular bed.[19] Then we arrive at Eq. (16):

$$\Delta HbO^{vasculature}(t) = \gamma \times H_0 \times \left(1 - e^{-ft/\gamma}\right) \tag{16}$$

Equation (16) indicates that the change in oxygenated hemoglobin concentration in tumor vasculature, $\Delta HbO^{vasculature}(t)$, depends on the blood perfusion rate, f, the arterial oxygenation input, H_0, and the vasculature coefficient of the tumor, γ.

Our NIR instrument indeed measures changes in vascular HbO concentration (i.e., $\Delta[HbO]^{vasculature}$). Then, Eq. (16) can be used to interpret the NIR measurements, since it gives the same exponential form as Eqs. (13) and (14), used to fit the experimental data. The comparison between Eqs. (13) and (16) reveals that the measured time constant is closely associated with the blood perfusion rate, f, and the vasculature coefficient of the tumor, γ in the measured volume. Furthermore, if the measured volume involves two distinct regions, then the detected signal will involve two different blood perfusion rates, f_1 and f_2, and/or two different vasculature coefficients, γ_1 and γ_2. In this case, it is reasonable to assume that the measured signal results from both of the regions, as illustrated in Fig. 12A. Consequently, Eq. (16) can be modified with a two-exponential expression and two time constants:

$$\begin{aligned}\Delta HbO^{vasculature}(t) &= \gamma_1 \times H_0 \times \left(1 - e^{-f_1 t/\gamma_1}\right) + \gamma_2 \times H_0 \times \left(1 - e^{-f_2 t/\gamma_2}\right) \\ &= A_1 \times \left(1 - e^{-f_1 t/\gamma_1}\right) + A_2 \times \left(1 - e^{-f_2 t/\gamma_2}\right)\end{aligned} \tag{17}$$

where f_1 and γ_1 are the blood perfusion rate and vasculature coefficient from region 1, respectively, f_2 and γ_2 are from region 2, and $A_1 = \gamma_1 \times H_0$ and $A_2 = \gamma_2 \times H_0$. The two time constants are equal to $\tau_1 = \gamma_1/f_1$ and $\tau_1 = \gamma_2/f_2$, respectively. When A_1, A_2, and the two time constants are determined from our NIR measurements, we arrive at the ratios for the two vasculature coefficients and the two blood perfusion rates:

$$\frac{\gamma_1}{\gamma_2} = \frac{A_1}{A_2}; \qquad \frac{f_1}{f_2} = \frac{A_1/A_2}{\tau_1/\tau_2} \tag{18}$$

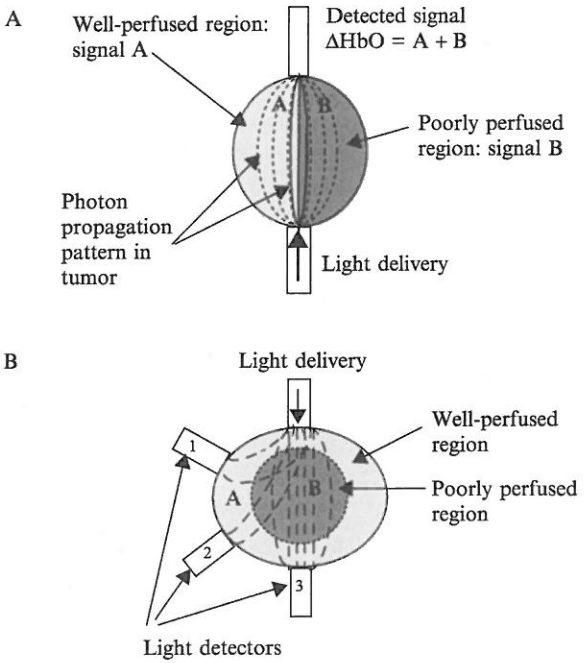

FIG. 12. (A) Schematic diagram to show a tumor model with two vascular perfusion regions, along with the light patterns propagating within the tumor tissue. "A" represents a portion of the detected signal interrogating the well-perfused region, and "B" represents another portion of the detected signal, mainly passing through the poorly perfused region. Our assumption is that the total detected signal is a sum of A and B. (B) A more realistic tumor tissue model with the center poorly perfused (leading to signal A) and the periphery well perfused (leading to signal B). It demonstrates possible tumor volumes interrogated by the multichannel detectors. The total detected signal is still a sum of A plus B.

In this way, by quantifying these two ratios, we are able to obtain insight into the tumor vasculature and blood perfusion. For example, a rather uniform vascular structure will result in a ratio of γ_1/γ_2 near 1, whereas the coexistence of two time constants possibly reveals two mechanisms of regional blood perfusion in the tumor. A large time constant implies a slow perfusion through a poorly perfused area, whereas a small time constant indicates a fast perfusion through a well-perfused area. In the meantime, we can determine the ratio of the perfusion rates in these two areas after obtaining the ratios of amplitudes and time constants from the two-exponential curve fitting. In this way, we have developed a hemodynamic model for the NIR data interpretation, which allows us to associate tumor

blood oxygenation dynamics with regional blood perfusion and vascular structures of the tumor within the measured volume.

Discussions

NIRS is noninvasive and provides a real-time assessment of changes in tumor vascular hemoglobin oxygenation. In this chapter, we basically provide demonstration of the ease and utility of NIRS studies of tumors. By switching the inhaled gas from air to carbogen, the NIRS measurement produces a rapid biphasic elevation in Δ[HbO]. The rapid time constant is in the range of seconds to a minute, whereas the slow component (10 to 50 times slower) continues for many minutes (see Figs. 7B and 8). The elevated oxygenation process is completely reversible upon returning air breathing, but still present 10 to 20 min after the baseline inhalation in many cases (see Figs. 7B and 8). The high reproducibility of results suggests that one can apply repeated interventions to explore the efficacy of interventions designed to alter tumor vascular oxygenation (e.g., vascular targeting agents). Our recent study has also shown that tumor response to oxygen was much more rapid and fit well to a monoexponential curve. For almost every tumor in a group of seven breast tumors, the time to reach 80% of maximum elevation in Δ[HbO] was longer with carbogen intervention than with oxygen breathing.[24]

With single-channel and multichannel NIRS, we have measured relative changes in $[Hb]_{total}$ and [HbO] in breast and prostate rat tumors in response to hyperoxic respiratory intervention. We observed that respiratory challenge caused Δ[HbO] to rise promptly and significantly in both breast and prostate tumors. However, the total concentration of hemoglobin did not always behave consistently. The dynamic changes of tumor oxygenation can be modeled by a two-exponential expression with a fast and slow time constant. Based on the model, we suggest that the NIRS measurement can "see" two vascular mechanisms during tumor oxygenation under hyperoxic gas intervention. By fitting the two-exponential model with the NIR experimental data, we can determine the two time constants and their corresponding amplitudes, leading to the relationships between the two perfusion rates and between the vascular structures, as expressed in Eq. (18).

With this tumor model, we are able to obtain information on the blood perfusion of tumor: a large time constant usually represents a slow blood perfusion, whereas a small time constant indicates a fast blood perfusion. A combination of well-perfused and poorly perfused mechanisms in tumor vasculature will result in coexistence of two time constants. Indeed, some tumor lines have been reported with only 20–85% of vessels

perfused,[61] and it is known that tumor structures and oxygen distribution are highly heterogeneous.[46,62] Therefore it is highly possible that our NIRS readings often detect a mixture of both well-perfused and poorly perfused regions in the tumor, depending on the locations of sources and detectors of the NIR system.

In the process of developing the model, we introduced a vasculature coefficient, γ. We expect that γ depends on (1) oxygen consumption and (2) capillary density of the tumor. Further studies are underway to quantify more about this coefficient and to confirm our speculations.

As an example to demonstrate the direct use of the newly developed model, the multichannel NIR results are fitted with the model, and the corresponding fitted parameters are listed in Table I. It is reasonable to expect that the central region of a solid tumor is close to necrosis (i.e., a poorly perfused region), whereas the tumor peripheral region is highly vascularized. Then, Fig. 12B can be used to schematically illustrate possible tumor volumes interrogated by the multichannel detectors. Close inspection of Table I reveals that the tumor structure ratios of γ_1/γ_2 from the three respective detectors are significantly different, whereas the perfusion ratios of f_1/f_2 from detectors 1 and 3 are almost doubled with respect to that from detector 2. Besides the results presented here, we have observed similar ΔHbO profiles and fitted parameters from other breast tumors. In such a way, we can obtain more details of tumor heterogeneity by having more source–detector pairs in the measurements. Indeed, we are now in the process of developing a multichannel NIR imaging system, along with the imaging reconstruction algorithm, so that tumor heterogeneity can be studied with better spatial resolution.

The time constants are not source–detector separation-sensitive. Equations (6), (7), and (11) demonstrate that ΔHbO and ΔHb are proportional to $1/d$, where d is the source–detector separation. This indicates that a different d value will only stretch or compress an entire temporal profile of ΔHbO, but it does not change the transient behavior of time response. The same argument can apply to DPF. Currently we have grouped DPF into the unit of [HbO] for simplicity. If the DPF value is larger than 1, the values of Δ[HbO] and $\Delta[\mathrm{Hb}]_{\mathrm{total}}$ will decrease by a factor of DPF. However, this decrease does not affect the time constants, τ_1 and τ_2 the dynamic responses of tumor Δ[HbO] to respiratory intervention.

[61] H. J. J. A. Bernsen, P. F. J. W. Rijken, T. Oostendorp, and A. J. van der Kogel, *Br. J. Cancer* **71,** 721 (1995).

[62] R. P. Mason, P. P. Antich, E. E. Babcock, A. Constantinescu, P. Peschke, and E. W. Hahn, *Int. J. Radiat. Oncol. Biol. Phys.* **29,** 95 (1994).

The simultaneous measurements of Δ[HbO] and ΔpO_2, shown in this chapter, demonstrate the compatibility of the NIRS system with the needle electrode and the FOXY fiber-optic oxygen-sensing system, without interference. All three systems are relatively inexpensive and provide real-time measurements, but the needle electrode and the three-channel FOXY system monitor pO_2 (viz., ΔpO_2) in specific locations, whereas the NIRS system provides global measurements. There are a few advantages of the FOXY system over the needle electrode: (1) it allows multiple locations to be interrogated simultaneously and (2) it is much easier to use than electrodes, particularly in calibration and stability. However, the FOXY probes may not provide accurate absolute pO_2 readings.

It is well known that measurements of tumor pO_2 have prognostic value in the clinic.[28,63] In this chapter, we have shown a linear correlation between tumor ΔHbO and mean ΔpO_2 (Fig. 10) when a tumor undergoes a hyperoxic respiratory intervention, and thus the noninvasive NIRS monitoring could have a potential value for clinical practice. The major deficiency in our current approach is lack of spatial resolution, so implementation of an NIR imaging system for tumor monitoring is our current effort.

NIRS provides a global assessment, in contrast to blood oxygenation level dependent (BOLD)-MRI, which can provide high-resolution images.[64,65] Although the latter approach can show heterogeneity in both temporal and spatial response, the results are often summarized to show mean values only. As such, an a priori global measurement can provide similar insight into dynamic tumor physiology or drug pharmacodynamics, while being more cost-effective, portable, and easier to implement and operate. For example, several groups of researchers have previously used NIR studies of tumors to observe the influence of chemotherapy,[52] pentobarbital overdose,[52] ischemic clamping,[66] and infusion of perfluorocarbon blood substitute.[67] All of these investigations demonstrate potential versatility of the NIRS application for diverse future studies.

Furthermore, the setup in our NIRS uses transmission mode between the source and detector, which we believe probes large and deep portions of the tumor, including the periphery on each side, as well as the center (see Fig. 3). This is in contrast to the setups used by most other investigators,

[63] M. Höckel and P. Vaupel, *J. Natl. Cancer Inst.* **93,** 266 (2001).
[64] S. P. Robinson, D. R. Collingridge, F. A. Howe *et al.*, *NMR Biomed.* **12,** 98 (1999).
[65] X. Fan, J. N. River, M. Zamora *et al.*, *Int. J. Radiat. Oncol. Biol. Phys.* **54,** 1202 (2002).
[66] F. Steinberg, H. J. Röhrborn, K. M. Scheufler, T. Otto, and C. Streffer, *Adv. Exp. Med. Biol.* **428,** 69 (1996).
[67] H. D. Sostman, S. Rockwell, A. L. Sylva, D. Madwed, G. Cofer, H. C. Charles, R. Negro-Villar, and D. Moore, *Magn. Reson. Med.* **20,** 253 (1991).

who apply reflectance mode,[21,66,68] which predominately detects the behavior of the peripheral vasculature. Indeed, the dynamic results measured from breast tumors reported by Hull *et al.*[21] are consistent with the fast component that we have observed and attributed to the well-perfused regions of our tumors.

Given the evidence for intratumoral heterogeneity from MRI[46,69] and histology,[70] it will be important to advance the NIRS system to an NIR imaging system so as to study not only dynamic, but also spatial aspects of blood oxygenation in tumor vasculature. In the meantime, we believe the preliminary results reported here are proof of principle for NIR imaging of tumor vascular oxygenation, laying a foundation for more extensive studies to correlate NIR imaging measurements with tumor heterogeneity and heterogeneous responses to various tumor therapeutic interventions and treatments.

Conclusions

In conclusion, we believe that NIRS presents a new potential imaging modality to examine tumor vasculature rapidly, noninvasively, and cost-effectively. Ease of implementation and operation permit rapid application to accessible tumors in cancer patients. The inherent compatibility of fiber-optics technology and light with other modalities, such as electrodes[20,24] and MRI,[71] will facilitate multiparametric multimodality investigations of tumor heterogeneity and vasculature in the near future.

In summary, we have demonstrated in this chapter that the NIR technology can provide an efficient, real-time, noninvasive means for monitoring vascular oxygenation dynamics in tumors during hyperoxic respiratory challenge. Concentration changes in HbO measured from both breast and prostate tumors often display a very prompt rise, followed by a gradual persistence throughout the intervention. By developing a hemoperfusion model with two exponential terms and fitting the model to the ΔHbO data, we have recognized two perfusion mechanisms in tumor vasculature and quantified the ratios of the two perfusion rates.

Furthermore, we have also obtained tumor pO_2 measurements using a needle electrode or multichannel, fiber-optic, FOXY probe in simultaneous conjunction with the noninvasive NIRS measurement. The comparative

[68] M. Kragh, B. Quistorff, and P. E. Kristjansen, *Eur. J. Cancer* **37,** 924 (2001).

[69] S. P. Robinson, F. A. Howe, L. M. Rodrigues, M. Stubbs, and J. R. Griffiths, *Semin. Radiat. Oncol.* **8,** 198 (1998).

[70] B. M. Fenton, *Radiother. Oncol.* **44,** 183 (1997).

[71] G. Gulsen, H. Yu, J. Wang, O. Nalcioglu, S. Merritt, F. Bevilacqua, A. J. Durkin, D. J. Cuccia, R. Lanning, and B. J. Tromberg, *Technol. Cancer Res. Treatment* **1,** 497 (2002).

results exhibit a linear correlation between ΔHbO and ΔpO_2 of the tumors under hyperoxic gas intervention, suggesting that the NIRS approach could have a good potential value in the clinic. Finally, the newly developed tumor hemodynamic model allows us to reveal tumor heterogeneities at different tumor locations based on the multichannel NIRS results. Through this chapter, we lay a foundation for an NIR imaging technique to be further developed to facilitate investigations of tumor heterogeneity and vascular perfusion. Such a noninvasive imaging approach can enhance our understanding of the dynamics of tumor oxygenation and the mechanism of tumor physiology under baseline and perturbed conditions.

Acknowledgments

This work was supported in part by the Department of Defense Breast Cancer Research grants BC990287 (HL) and BC000833 (YG), and NIH R01 CA79515 (NCI)/EB002762 (NIBIB) (RPM). We are grateful to Vincent Bourke for his collaborative work on multichannel pO_2 measurements and Dr. Anca Constantinescu for her assistance with all the tumor investigations. We also gratefully acknowledge Dr. Britton Chance for his technical support on the multichannel NIR system.

[18] Measuring Changes in Tumor Oxygenation

By DAWEN ZHAO, LAN JIANG, and RALPH P. MASON

Introduction

Significance of pO_2 in Oncology

It has long been appreciated that hypoxic tumor cells are more resistant to radiotherapy.[1] Indeed, a 3-fold increase in radio resistance may occur when cells are irradiated under hypoxic conditions compared with oxygen pressure $pO_2 > 15$ torr for a given single radiation dose. However, recent modeling has indicated that the proportion of cells in the range 0–20 torr may be most significant in terms of surviving a course of fractionated radiotherapy.[2] Certain chemotherapeutic drugs also present differential efficacy, depending on hypoxia.[3,4] Increasingly, there is evidence that hypoxia also

[1] L. Gray, A. Conger *et al.*, *Br. J. Radiol.* **26,** 638 (1953).
[2] B. G. Wouters and J. M. Brown, *Radiat. Res.* **147,** 514 (1997).
[3] B. Teicher, J. Lazo *et al.*, *Cancer Res.* **41,** 73 (1981).
[4] A. C. Sartorelli, *Cancer Res.* **48,** 775 (1988).

0076-6879/04 $35.00

Appendix 3

Yueqing Gu, Ralph Mason, and Hanli Liu, "Estimated fraction of tumor vascular blood contents sampled by near infrared spectroscopy and ^{19}F magnetic resonance spectroscopy," *Optics Express* 13(5), 1724-1733 (2005).
http://www.opticsexpress.org/abstract.cfm?URI=OPEX-13-5-1724.

Estimated fraction of tumor vascular blood contents sampled by near infrared spectroscopy and ^{19}F magnetic resonance spectroscopy

Yueqing Gu[1,3], Ralph Mason[2], and Hanli Liu[1]

[1]*Joint Program of Biomedical Engineering, University of Texas at Arlington, Arlington, TX 76019*
[2]*Dept.of Radiology, University of Texas Southwestern Medical Center, Dallas, TX 75390*
[3]*School of Life Science and Technology, China Pharmaceutical University, Nanjing, PR.China 21009*
yueqing@uta.edu, Ralph.mason@utswmed.edu, hanli@uta.edu

Abstract: This study introduces an experimental approach to estimate percentage of hemoglobin content and volume sampled by near infrared spectroscopy (NIRS). Carbogen (5% CO_2, 95% O_2) respiratory intervention was used to induce physiological changes in a group of six Fisher rat breast tumors. Changes in total hemoglobin concentration, $\Delta[Hb]_{total}$, and in total blood volume, $\Delta V_{T\text{-}blood}$, of the tumors were measured by NIRS and ^{19}F magnetic resonance spectroscopy of perflubron, respectively. The ratio of $\Delta[Hb]_{total}/\Delta V_{T\text{-}blood}$ was used to calculate the fraction of hemoglobin contents sampled by NIRS. The results showed that the mean value of estimated fractions is within a range of 15~30% of total hemoglobin content in the tumor tissues. Based on the results, we suggest that NIRS does not sample the entire hemoglobin volume of the tissue vasculature, but is more sensitive to microvasculature. This study helps to understand the blood vascular volume sampled by NIRS, and demonstrates that the low cost, portable NIRS system may be a reliable, non-invasive, real-time, monitoring tool for changes in tumor blood contents.

OCIS codes: (000.0000) optical path length, Near infrared spectroscopy, MRS, breast tumor.

References and links

1. W. Cheong, S. A. Prahl, and A. J. Welch,."A review of the optical properties of biological tissue," IEEE J. Quantum Electron. **26**, 2166-2183 (1990).
2. N. Ramanujam, "Fluorescence spectroscopy of Neoplastic and non-Neoplastic tissue," Neoplasia. **2**, 89-117 (2000).
3. A. M. Siege, J. J. A. Marota, and D. A. Boas. "Design and evaluation of a continuous wave diffuse optical tomography system," Opt. Express. **4**, 287-298 (1999).
4. B. Chance, E. Anday, S. Nioka, S. Zhou, L. Hong, K. Worden, C. Li, T. Murray, Y. Ovetsky, D. Pidikiti, and R. Thomas, "A novel method for fast imaging of brain function, non-invasively, with light," Opt. Express. **2**, 411-423 (1998).
5. V. Ntaiachristors, H. Ma, and B. Chance, "Multichannel photon counting instrument for spatially resolved near infrared spectroscopy," Rev. Sci. Instrum. **70**, 1444-1451 (1999).
6. B. W. Pogue, M. Testorf, and T. McBride, "Instrumentation and design of a frequency domain diffuse optical tomography imager for breast cancer detection," Opt. Express. **1**, 391-403 (1999).
7. K. Sokolov, R. Drezek, and K. Gossage, "Reflectance spectroscopy with polarized light: is it sensitive to cellular and nuclear morphology," Opt. Express. **5**, 302-317 (1999).
8. A. Mayevsky, S. Lebourdais, and B. Chance, "The interrelation between brain PO_2 and NADH oxidation-reduction state in the Gerbil," J. Neurosci. Res. **5**, 173-182 (1980).
9. E. M. Sevick, B. Chance, J. Leigh, and M. Maris, "Quantitation of time- and frequency- resolved optical spectra for the determination of tissue oxygenation," Anal. Biochem. **195**, 330-351 (1991).
10. H. Liu, Y. Song, K. L. Worden, X. Jiang, A. Constantinescu, and R. P. Mason, "Noninvasive investigation of blood oxygenation dynamics of tumors by near-infrared spectroscopy," Appl. Opt. **39**, 5231-5243 (2000).

#6289 - $15.00 US Received 11 January 2005; revised 25 February 2005; accepted 28 February 2005

11. J. G. Kim, Y. Song, D. Zhao, A. Constantinescu, R. P. Mason, and H. Liu, "Interplay of Tumor Vascular Oxygenation and pO_2 in Tumors Using NIRS, ^{19}F MR pO_2 Mapping, and pO_2 Needle Electrode," J. Biomed. Opt. **8**, 53-62 (2003).
12. Y. Gu, V. Bourke, J. Kim, A. Constantinescu, R. P. Mason, and H. Liu, "Dynamic response of breast tumor oxygenation to hyperoxic respiratory challenge monitored with three oxygen-sensitive parameters," Appl. Opt. **42**, 2960-67 (2003).
13. H. Liu, A. H. Hielscher, F. K. Tittel, S. L. Jacques, and B. Chance, "Influence of blood vessels on the measurement of hemoglobin oxygenation as determined by time-resolved reflectance spectroscopy," Med. Phys. **22**, 1209-1216 (1995).
14. M. Firbank, E. Okada, D. T. Delpy, "Investigation of the effect of discrete absorbers upon the measurement of blood volume with near-infrared spectroscopy," Phys. Med. Biol. **42**, 465-477(1997).
15. B. W. Pogue, E. A. White, U. L. Osterberg, K. D. Paulsen, "Absorbance of opaque microstructures in optically diffuse media," Appl. Opt. **40**, 4616-4621 (2001).
16. M. C. Van Beekvelt, W. N. Colier, R. A. Wevers and B. G. Van Engelen, "Performance of near infrared spectroscopy in measuring local O2 consumption and blood flow in skeletal muscle," J. Appl. Physiol. **90**, 511-519 (2001).
17. R. A. De Blasi, M. Ferrari, A. Natali, G. Conti, A. Mega, A. Gasparetto, "Noninvasive measurement of forearm blood flow and oxygen consumption by near infrared spectroscopy," J. Appl Physiol. **76**, 1388-1393 (1994).
18. C. Thomas, C. Counsell, P. Wood, G.E. Adams, "Use of F-19 NMR spectroscopy and hydralazine for measuring dynamic changes in blood perfusion volume in tumors in mice," JNCI **84,**174-80(1992).
19. N. J. Baldwin, Y. Wang, and T. C. Ng, "In situ ^{19}F MRS measurement of RIF-1 tumor blood volume: Corroboration by radioisotope-labeled [^{125}I]-albumin and correlation to tumor size," Magn. Reson. Imaging, **14**, 275-280 (1996).
20. D. T. Delpy, M. Cope, P. van der Zee, S. Arridge, S. Wray, and J. Wyatt, "Estimation of optical pathlength through tissue from direct time of flight measurement," Phys. Med. Biol. **33**, 1433-1442 (1988).
21. Y. Gu, Z. Qian, J. Chen, D. Blessington, N. Ramanujam, and B. Chance, "High resolution three dimensional scanning optical image system for intrinsic and extrinsic contrast agents in tissue," Rev. Sci. Instrum. **73**, 172-178 (2002).
22. H. P. Shukla, R. P. Mason, D. E. Woessner, and P. P. Antich, "A comparison of three commercial perfluorocarbon emulsions as high field NMR probes of oxygen tension and temperature," J. Magn. Reson. B, **106**, 131-141 (1995).
23. E. W. Hahn, P. Peschke, R. P. Mason, E. E. Babcock,, and P.P.Antich, "Isolated tumor growth in a surgically formed skin pedicle in the rat: A new tumor model for NMR studies," Magn.Reson. Imaging **11**, 1007-1017 (1993).
24. B. L. Horecker, "The absorption spectra of hemoglobin and its derivatives in the visible and near infrared regions," J. of Biol. Chem. **148**, 173-183 (1943).
25. E. J. Van Kampen, and W. G. Zijlstra, "Determination of hemoglobin and its derivatives," Adv. Clin. Chem. **8**, 141-187 (1965).
26. R. Benesch, G. Macduff, and R. E. Benesch, "Determination of oxygen equilibria with a versatile new tonometer," Anal. Biochem. **11**, 81-87 (1965).
27. R. E. Benesch, R. Benesch, and S. Yung, "Equations for the spectrophotometric analysis of hemoglobin mixtures," Anal. Biochem. **55**, 245-248(1973).
28. O. W. Van Assendelft, and W. G. Zijlstra, "Extinction coefficients for use in equations for the spectrophotometric analysis of haemoglobin mixtures," Anal. Biochem. **69**, 43-48 (1975).
29. W. G. Zijlstra, A. Buursma, H. E. Falke and J. F. Catsburg, "Spectrophotometry of hemoglobin: absorption spectra of rat oxyhemoglobin, deoxyhemoglobin, carboxyhemoglobin, and methemoglobin," Comp. Biochem. Physiol. **107B**, 161-166 (1994).
30. M. Cope, "The application of near infrared spectroscopy to non invasive monitoring of cerebral oxygenation in the newborn infant," Ph.D. thesis, Appendix B, 316-323, University College London (1991).
31. S. I. Fox, Human Physiology, 6th edition, McGraw-Hill Companies, Inc. Chapter 13, Heart and Circulation, 388-391(1999).
32. S. R. Arridge, M. Cope, and D. T. Delpy, "The theoretical basis for the determination of optical pathlengths in tissue: temporal and frequency analysis," Phys. Med. Biol., **37**, 1531-1560 (1992).
33. M. Ferrari, Q. Wei, L. Carraresi, R. A. de Blasi, and G. Zaccanti, "Time-resolved spectroscopy of the human forearm," J. Photochem. Photobiol. B:Biol., **16**, 141-153 (1992).
34. P. van der Zee, M. Cope, S. R. Arridge, M. Essenpreis, L. A. Potter, A. D. Edwards, J. S. Wyatt, D. C. McCormick, S. C. Roth, E. O. R. Reynolds, and D. T. Delpy, "Experimentally measured optical pathlengths for the adult head, calf and forearm and the head of the newborn infants as a function of inter optode spacing," Adv. Exp. Med. Biol., **316**, 143-153 (1992).
35. M. Kohl, C. Nolte, H. R. Heekeren, S. Horst, U. Scholz, H. Obrig, and A. Villringer, "Determination of the wavelength dependence of the differential pathlength factor from near-infrared pulse signals," Phys. Med. Biol., **43**, 1771-1782 (1998).
36. J. S. Ultman, and C. A. Piantadosi, "Differential pathlength factor for diffuse photon scattering through tissue by a pulse-response method," Math. Biosci. **107**, 73-82 (1991).

#6289 - $15.00 US Received 11 January 2005; revised 25 February 2005; accepted 28 February 2005

37. P. van der Zee, S. R. Arridge, M. Cope, and D. T. Delpy, "The effect of optode positioning on optical pathlength in near infrared spectroscopy of brain," Adv. Exp. Med. Biol. **277**, 79-84 (1990).
38. L. A. Paunescu, "Tissue blood flow and oxygen consumption measured with near infrared frequency-domain spectroscopy," Degree of Doctor of Philosophy (University of Illinois, Urbana, 2001).
39. H. Liu, M. Miwa, B. Beauvoit, N.G. Wang, and B. Chance, "Characterization of absorption and scattering properties of small-volume biological samples using time-resolved spectroscopy," Anal. Biochem. **213,** 378-385 (1993).
40. R. G. Steen, K. Kitagishi, and K. Morgan, "In vivo measurement of tumor blood oxygenation by near-infrared spectroscopy: Immediate effects of pentobarbital overdose or carmustine treatment," J. Neuro-Oncol. **22**, 209-220 (1994).
41. R. P. Choudhury, V. Fuster; J. J. Badimon, E. A. Fisher; Z. A. Fayad, "MRI and Characterization of Atherosclerotic Plaque," Arteriosclerosis, Thrombosis, and Vascular Biology **22**,1065-1072 (2002).
42. J. R. Forder and G. M. Pohost, "Cardiovascular nuclear magnetic resonance: basic and clinical applications," J. Clin. Invest. **111**, 1630–1639 (2003).

1. Introduction

In biomedical research, optical spectroscopy and imaging can potentially provide rapid, economical, and non-invasive diagnostic links between crucial tissue characteristics and cancer detection or diagnosis [1-7]. Near infrared (NIR) light in the range of 700 nm to 900 nm has an optimal penetrating depth in tissue (up to 15 centimeters) since photon transport in tissue is dominated by light scattering rather than absorption in the NIR region. Therefore, the use of NIR light enables us to sample large tissue volumes, such as the breast, the brain, and skeletal muscles as well as tumors deep in the tissue. In the NIR spectral range, two important endogenous tissue chromospheres, i.e., oxygenated and deoxygenated hemoglobin (HbO_2 and Hb, respectively), display oxygen-dependent absorption features [8,9]. Experimental determination of absorption quantities of tissue can provide quantification of several physiological parameters, such as hemoglobin/myoglobin concentrations, vascular oxygenation, and blood volume changes. Such quantification could be important for cancer prognosis and treatment monitoring, as we have demonstrated in our previous reports [10-12].

Because of large scattering of NIR light in tissue, however, it is not clear how much of the total vascular volume within a tissue is sampled by the NIR signals. It has been reported that the NIR detection is most sensitive to microvessel density, i.e., arterioles, capillaries, and venules [13-14]. The opaque microstructures in tissue also have contributions to the absorption [15]. The measured absorption is actually a volume-weighted average of absorption of the sampled vessels and the surrounding tissue. Thus, the measured (apparent) chromophore concentration may be less than the actual concentration. Moreover, the blood flow measured by NIR spectroscopy (NIRS) was reported 2~3 times lower than the plethysmographic flow [16-17]. These reports motivated us to investigate what fraction of blood volume in tissue is sampled by NIR . In particular, tumor tissue is recognized as highly heterogeneous. Better understanding and accurate determination of tumor vascular blood volume sensed by the NIRS could provide crucial information for assessing tumor progress and guiding tumor therapy and treatment.

Several investigators have shown that vascular volume can be estimated using ^{19}F Magnetic Resonance spectroscopy (MRS) following infusion of a perfluorocarbon blood substitute emulsion [18-19]. Our previous studies have demonstrated that NIRS can be used to monitor changes in total (*i.e.*, oxygenated and deoxygenated) hemoglobin concentrations within tumor vasculature. Thus, correlations between MRS and NIRS measurements may allow us to investigate the relationship between the blood volumes sampled by these two respective methods. Specifically, in this paper, we will report our measurements of changes in total hemoglobin concentration, $\Delta[Hb]_{total}$, and changes in tumor blood volume, $\Delta V_{T\text{-}blood}$, induced by hyperoxic gas intervention in rat breast tumors using NIRS and ^{19}F MRS of perflubron (formerly called perfluorooctyl bromide or PFOB), respectively. The ratio of rat tumor $\Delta[Hb]_{total}/\Delta V_{T\text{-}blood}$ will be estimated to quantify the fractions of tumor blood volume sampled by NIRS and MRS in tumors.

#6289 - $15.00 US Received 11 January 2005; revised 25 February 2005; accepted 28 February 2005

2. Experimental materials and methods

2.1 Near Infrared spectroscopy for the measurement of $\Delta[Hb]_{total}$

A homodyne, frequency-domain NIRS system (NIM, Philadelphia, PA) was used in our experiments, as described in detail previously [10-12]. Briefly, the amplitude-modulated light at 140 MHz from two NIR laser diodes at 758 nm and 785 nm was projected on one side of the tumor through a delivery fiber bundle. The diffused light through the tumor was collected and propagated to a photomultiplier tube (PMT) by a second fiber bundle. The signal from the PMT was demodulated through an In-phase and Quadrature-phase circuit, and the amplitude and phase were recorded, as shown in Fig. 1. Based on modified Beer-Lambert's law [10, 20-21] and the recorded amplitude, changes in oxygenated, deoxygenated, and total hemoglobin concentrations, $\Delta[HbO_2]$, $\Delta[Hb]$ and $\Delta[Hb]_{total}$, due to respiratory intervention were estimated, as described below. In this NIRS system, only amplitude signal was used for the calculation since phase signal was very noisy.

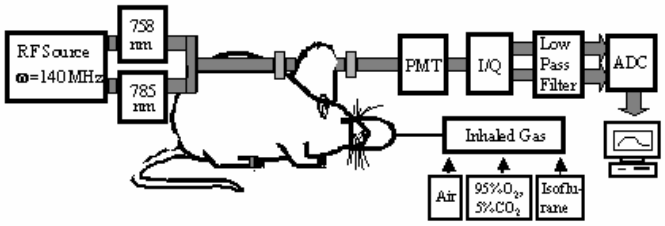

Fig. 1. Schematic diagram of experimental setup for the NIRS system. A 3 mm-diameter fiber bundles delivered and detected the laser light through the rat tumor in transmittance geometry. PMT represents a photomultiplier tube. I/Q is an in-phase and quadrature phase demodulator for retrieving amplitude information.

2.2 ^{19}F MRS of perflubron for the measurement of tumor blood volume $V_{T\text{-}blood}$

An Omega CSI 4.7 T superconducting magnet system (Acustar™, Bruker Instrument, Inc., Fremont, CA) was used for the measurement of tumor blood volume. An emulsion of perflubron (Oxygent™, Alliance Pharmaceutical Corp., San Diego, CA) (2 ml) was infused into tumor-bearing rats i.v. as a blood volume indicator. The tumors were placed within a frequency-tunable ($^1H/^{19}F$), single-turn, solenoid coil, together with a sealed capillary containing sodium trifluoroacetate (TFA), which was used as an external standard reference for calibrating tumor blood volume.

Under fully relaxed conditions, integration of ^{19}F signal from the tumor was linearly proportional to the total number of ^{19}F nuclear spins of perflubron in the tumor, which, in turn, was linearly proportional to the total blood volume in the tumor, assuming that the perflubron emulsion had reached an equilibrium state with the blood throughout the tumor.. To ensure full relaxation a repetition time (TR) of 30 seconds was used [22]. The spectral peaks of perflubron were integrated in the data post-processing. Following the tumor measurement, the rat was removed, leaving the reference TFA capillary in the original position within the RF coil. A small amount of blood (0.5 ml) was drawn from the rat tail vein and placed in the RF coil without disturbing the reference TFA capillary. Another quantitative ^{19}F spectrum was then acquired. Thus, the tumor blood volume can be calculated based on the following Eq.:

$$V_{T\_blood} = V_{S\_blood} \cdot \left(\frac{I_{T\_blood}}{I_{S\_blood}}\right) \cdot \left(\frac{I_{S\_TFA}}{I_{T\_TFA}}\right), \quad (1)$$

where V_{T_blood} and V_{S_blood} were the tumor blood volume and blood sample volume (ml), respectively, I_{T_blood} and I_{S_blood} were the integrated MRS signal of ^{19}F taken from the rat

#6289 - $15.00 US Received 11 January 2005; revised 25 February 2005; accepted 28 February 2005

tumor and blood sample, respectively, and I_{blood_TFA} and I_{Tumor_TFA} were the integrated ^{19}F MRS signals from the TFA capillary for the two respective measurements.

2.3 Animal model and protocols

Mammary adenocarcinomas 13762NF were implanted in skin pedicles [23] on the forebacks of female Fisher 344 rats (~150 g). Once the tumors reached 1~2 cm diameter, rats were anesthetized with ketamine hydrochloride (100 mg/ml, i.p.) and maintained under general gaseous anesthesia with 1.3% isoflurane in air (1 dm^3/min). Tumors were shaved to improve optical contact for NIR light transmission. Tumor volume, V, was estimated using an ellipsoid approximation as V=(π/6).a.b.c from the three orthogonal diameters, i.e., a, b, c, measured with a caliper.

In this study, breast tumor bearing Fisher rats were challenged with carbogen (95% O_2 + 5% CO_2) using a sequence of air-carbogen–air. The $\Delta[Hb]_{total}$ values in response to the carbogen inhalation were monitored by NIRS. For the rats that exhibited a significant change in $[Hb]_{total}$ induced by carbogen (n=6), they were re-anesthetized the next day after the NIRS measurement and infused with 2 ml of perflubron emulsion for the tumor blood volume determination. The ^{19}F MRS. experiment was performed on the rat 30 min after the emulsion injection allowing sufficient time for the perflubron emulsion to reach an equilibrium state within the tumor blood vasculature. The same inhaled gas sequence was repeated during the MRS measurements.

3. Algorithms for calculations of $\Delta[Hb]_{total}$ and fraction of sampled blood volume

3.1 Calculations for tumor $\Delta[Hb]_{total}$

Based on Beer-Lambert's law, optical attenuation, presented by Optical Density (OD), can be expressed as a function of concentration of chromospheres (24-28),

$$Optical\ Density\ (OD) = Log(A_0/A) = \varepsilon c l \tag{2}$$

where A_0 and A are light intensities of the incident and transmitted light, respectively, ε is the extinction coefficient of chromophore, c is the concentration of chromophore, and l is the optical path-length through the measured sample. When the measured sample has a mixture of chromophores, e.g., oxygenated and deoxygenated hemoglobin in tumor tissue, the changes in oxygenated and deoxygenated hemoglobin concentrations (i.e., $\Delta[HbO_2]$ *and* $\Delta[Hb]$) can cause a change in optical density, which can be presented as [26-28]:

$$\Delta OD(\lambda) = log(A_B/A_T) = \{\varepsilon_{Hb}(\lambda)\Delta[Hb] + \varepsilon_{HbO2}(\lambda)\Delta[HbO_2]\}\, l\,, \tag{3}$$

where $\Delta OD(\lambda)$ represents a change in optical density at the specific wavelength, λ. A_B and A_T correspond to light intensities measured under the baseline and transient conditions. $\varepsilon_{Hb}(\lambda)$ and $\varepsilon_{HbO2}(\lambda)$ are extinction coefficients at wavelength λ for molar concentrations of deoxygenated hemoglobin and oxygenated hemoglobin, respectively. By employing two wavelengths in Eq. (3), both $\Delta[HbO_2]$ and $\Delta[Hb]$ can be determined by measuring the ΔOD values at the two specific wavelengths, provided that the values for $\varepsilon_{Hb}(\lambda)$ and $\varepsilon_{HbO2}(\lambda)$ are known:

$$\Delta[HbO_2] = \frac{\varepsilon_{Hb}(\lambda_2)\Delta OD(\lambda_1) - \varepsilon_{Hb}(\lambda_1)\Delta OD(\lambda_2)}{l\left[\varepsilon_{Hb}(\lambda_2)\varepsilon_{HbO2}(\lambda_1) - \varepsilon_{Hb}(\lambda_1)\varepsilon_{HbO2}(\lambda_2)\right]}, \tag{4}$$

$$\Delta[Hb] = \frac{\varepsilon_{HbO2}(\lambda_2)\Delta OD(\lambda_1) - \varepsilon_{HbO2}(\lambda_1)\Delta OD(\lambda_2)}{l\left[\varepsilon_{Hb}(\lambda_1)\varepsilon_{HbO2}(\lambda_2) - \varepsilon_{Hb}(\lambda_2)\varepsilon_{HbO2}(\lambda_1)\right]}. \tag{5}$$

#6289 - $15.00 US Received 11 January 2005; revised 25 February 2005; accepted 28 February 2005

Note that in principle, *l* represents the optical path length between the source and detector. While *l* is simply the physical separation, *d*, between the source and detector through a non-scattering medium, exact quantification of *l* for an intact tissue or organ is complex because of light scattering in tissue. Since *l* is in proportion to the separation, *d*, we can associate *l* to *d* as *l=DPF*d*, where *DPF* is a differential path length factor to account for light scattering [20]. It has been well accepted [9, 10, 20] that together with *DPF*, Eq. (3) can be treated as modified Beer-Lambert's law; and consequently, Eqs. (4) and (5) can be used to quantify changes in *[Hb]* and *[HbO$_2$]* in highly scattering media, such as in intact tissue or organs.

To be consistent with our previous work, we adopt in this paper the ε values published by Zijlstra *et al*. [29]. We had to interpolate the ε values at the two wavelengths employed in our study, i.e., ε_{Hb}(758 nm) = 1.418, ε_{HbO2}(758 nm) = 0.6372, ε_{Hb}(785 nm) = 1.111, and ε_{HbO2}(785 nm) = 0.766, all in $mM^{-1}cm^{-1}$. Note that a factor of 4 has been multiplied for each of the ε's at the respective wavelengths to account for light absorption from 4 hemes per hemoglobin molecule [30] since the extinction coefficients published in the field of biochemistry were expressed on a per heme basis [26-30].

Because of the interpolation of ε values, necessary calibration is needed to assure the accuracy of *Δ[HbO$_2$], Δ[Hb], and Δ[Hb]$_{total}$* calculation as given in Eqs. (4)-(5). We conducted a set of phantom experiments, as previously described in ref. 11. The empirical calibration has resulted in two correction factors β_1 and β_2, where β_1=1.103 and β_2=0.9035, as expressed below:

$$\Delta[HbO_2] = \frac{\frac{\varepsilon_{Hb}(785nm)}{\beta_1}\times\Delta OD(758nm) - \varepsilon_{Hb}(758nm)\times\Delta OD(785nm)}{l\left[\varepsilon_{Hb}(785nm)\varepsilon_{HbO2}(758nm) - \varepsilon_{Hb}(758nm)\varepsilon_{HbO2}(785nm)\right]}, \tag{6}$$

$$\Delta[Hb] = \frac{\frac{\varepsilon_{HbO2}(785nm)}{\beta_2}\times\Delta OD(758nm) - \varepsilon_{HbO2}(758nm)\times\Delta OD(785nm)}{l\left[\varepsilon_{Hb}(758nm)\varepsilon_{HbO2}(785nm) - \varepsilon_{Hb}(785nm)\varepsilon_{HbO2}(758nm)\right]}. \tag{7}$$

After substituting all of the parameters into Eqs. (6) and (7), we arrived at Eqs. (8) and (9) to quantify changes in hemoglobin concentration:

$$\Delta[HbO_2] = \frac{-2.658\times\Delta OD(758nm) + 3.743\times\Delta OD(785nm)}{d\times DPF}, \tag{8}$$

$$\Delta[Hb] = \frac{2.238\times\Delta OD(758nm) - 1.683\times\Delta OD(785nm)}{d\times DPF}. \tag{9}$$

where *l* has been replaced by *d×DPF*. Notice that the difference in the coefficients between these equations and those published earlier [10-12] results from the factor of 4 in ε values. *Δ[Hb]$_{total}$* can also be obtained by adding Eqs. (8) and (9):

$$\Delta[Hb]_{total} = \Delta[HbO_2] + \Delta[Hb] = \frac{-0.42\times OD(758nm) + 2.06\times OD(785nm)}{d\times DPF}. \tag{10}$$

In principle, units of *Δ[HbO$_2$], Δ[Hb], and Δ[Hb]$_{total}$* are in mM with ε in $cm^{-1}.mM^{-1}$. Since DPF is so far an unknown parameter for tumors, we include it within the unit as mM/DPF for the relative measurements. Thus, Eq. (10) becomes Eq. (11), and it permits us to obtain *Δ[Hb]$_{total}$* with a unit of mM/DPF for breast tumors under carbogen intervention.

#6289 - $15.00 US Received 11 January 2005; revised 25 February 2005; accepted 28 February 2005

$$\Delta[Hb]_{total} = \Delta[HbO_2] + \Delta[Hb] = \frac{-0.42 \times OD(758nm) + 2.06 \times OD(785nm)}{d}. \quad (11)$$

3.2 Calculations for the fraction of vascular blood volume sampled by NIRS

The determination of $\Delta[Hb]_{total}$ can further lead to estimation of changes in total hemoglobin content within a rat tumor, $\Delta[C_{Hb}]_{tumor}$, since total hemoglobin content of a tumor, $[C_{Hb}]_{tumor}$, is directly associated with hemoglobin concentration and tumor physical volume. Namely, $[C_{Hb}]_{tumor}$ determined by NIRS should be a product of tumor vascular hemoglobin concentration, $[Hb]_{total}$ in mole/liter=10^3 mM, hemoglobin molecular weight, M in gram/mole, and the tumor physical volume, $V_{T\text{-}physical}$ in cm^3, and can be expressed as

$$[C_{Hb}]_{tumor\_NIRS} = [Hb]_{total} \times M \times V_{T\text{-}physical}, \quad (12a)$$

or

$$\Delta[C_{Hb}]_{tumor\_NIRS} = \Delta[Hb]_{total} \times M \times V_{T\text{-}physical}, \quad (12b)$$

where $[C_{Hb}]_{tumor\_NIRS}$ and $\Delta[C_{Hb}]_{tumor\_NIRS}$ are in gram, and $\Delta[C_{Hb}]_{tumor\_NIRS}$ is induced by carbogen intervention.

On the other hand, the total tumor blood volume, $V_{T\text{-}blood}$ in liters, can be quantified from the ^{19}F MRS measurement with and without carbogen inhalation. The corresponding hemoglobin content determined by the MRS can be written as:

$$[C_{Hb}]_{tumor\_MRS} = V_{T\text{-}blood} \times K, \quad (13a)$$

or

$$\Delta[C_{Hb}]_{tumor\_MRS} = \Delta V_{T\text{-}blood} \times K, \quad (13b)$$

where K is hemoglobin concentration in gram/liter for liquid blood, $V_{T\text{-}blood}$ can be determined using Eq. (1) based on the MRS measurements, and $\Delta V_{T\text{-}blood}$ results from respiratory intervention.

To quantify the fraction of tumor blood volume sampled by NIRS and MRS in tumors, we introduce a variable, γ, to associate $[C_{Hb}]_{tumor\_NIRS}$ with $[C_{Hb}]_{tumor\_MRS}$ as:

$$[C_{Hb}]_{tumor\_NIRS} = \gamma [C_{Hb}]_{tumor\_MRS}. \quad (14a)$$

Since γ is expected to be a constant for a given tumor, it follows that

$$\Delta[C_{Hb}]_{tumor\_NIRS} = \gamma \Delta[C_{Hb}]_{tumor\_MRS}. \quad (14b)$$

Then, we can obtain Eq. (15) by taking the ratio of Eqs. (13b) and (12b) to determine the percentage of tumor hemoglobin content, sampled by NIRS and by MRS:

$$\gamma = \frac{\Delta[C_{Hb}]_{tumor\_NIRS}}{\Delta[C_{Hb}]_{tumor\_MRS}} * 100\% = \frac{M \times V_{T-physical}}{K} \times \frac{\Delta[Hb]_{total}}{\Delta V_{T-blood}} \times 100\%, \quad (15)$$

where K is often given as 150 g/l [30], M is taken as 68000 g/mol [31], $\Delta[Hb]_{total}$ and $\Delta V_{T\text{-}blood}$ are obtained from our NIRS and MRS experimental measurements, respectively, and $V_{T\text{-}physical}$ is measured from the tumor physical volume. With Eq. (15), we are able to compare and estimate the fraction of hemoglobin content or blood volume of the tumor, γ, sampled by near infrared spectroscopy and ^{19}F magnetic resonance spectroscopy.

4. Experimental results

Changes of total hemoglobin concentration, $\Delta[Hb]_{total}$, and blood volume, $V_{T\text{-}blood}$, of six selected rat tumors were monitored by NIRS and ^{19}F MRS of perflubron on consecutive days, respectively. Figure 2 shows the time course profiles of $\Delta[Hb]_{total}$ and $V_{T\text{-}blood}$ from a representative breast tumor (V=2.6 cm^3) with respect to carbogen intervention. When the inhaled gas was switched from air to carbogen, $\Delta[Hb]_{total}$ increased significantly (p<0.0001)

#6289 - $15.00 US Received 11 January 2005; revised 25 February 2005; accepted 28 February 2005

from a baseline value of 0.0005 ± 0.0015 mM/DPF to a maximal value of 0.020 ± 0.001 mM/DPF over the period of carbogen intervention, with a maximal $\Delta[Hb]_{total}$ of 0.0185 mM/DPF. After the gas was switched back to air, a significant drop ($p< 0.0001$) of $\Delta[\mathrm{Hb}]_{\mathrm{total}}$ occurred, followed by a plateau at 0.009 ± 0.001 mM/DPF. A similar temporal pattern in response to carbogen intervention was found for $V_{T\text{-blood}}$ derived from the MRS measurement. Specifically, $V_{T\text{-}blood}$ increased significantly ($p<0.0001$) from a baseline of 0.809 ± 0.004 cm^3 to a maximum of 0.837 ± 0.004 cm^3 during carbogen intervention, having a maximal $\Delta V_{T\text{-}blood}$ of 0.028 cm^3.

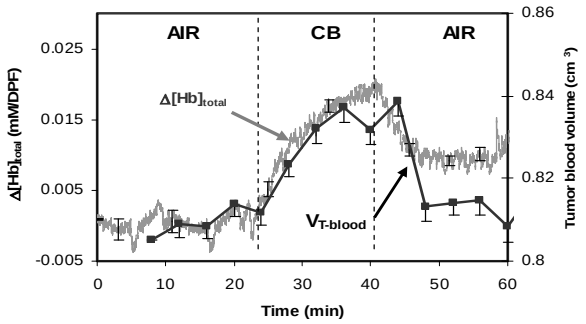

Fig. 2. Temporal profile of $\Delta[\mathrm{Hb}]_{\mathrm{Total}}$ and $V_{T\text{-blood}}$ for a representative rat breast tumor (2.6 cm^3) with respect to carbogen (CB) intervention, monitored by NIRS and ^{19}F MRS of perflubron, respectively. Error bars indicate the standard deviation.

By substituting $\Delta[Hb]_{total}$, $\Delta V_{T\text{-}blood}$, K, M, and the corresponding $V_{T\text{-}Physical}$=2.6 cm^3 into Eq. (15), we obtain

$$\gamma = \left| \frac{[C_{Hb}]_{tumor\_NIRS}}{[C_{Hb}]_{tumor\_MRS}} \times 100\% \right| = \left| \frac{\Delta[C_{Hb}]_{tumor\_NIRS}}{\Delta[C_{Hb}]_{tumor\_MRS}} \times 100\% \right|$$

$$= \frac{68000\,[g/mole] \times 2.6[cm^3]}{150\,[g/l]} \times \frac{0.0185\,[mM/DPF]}{0.028\,[cm^3]} 100\% \cong \frac{77.9\%}{DPF}. \qquad (16)$$

Typical values of DPF for the brain and muscle have been reported in the range of 4-6 and 3-4, respectively [32-35], independent of the source-detector separation when d is larger than 2.5cm [36-37]. However, the DPF values for tumors, DPF_{tumor}, are not well studied. It is still reasonable to assume DPF_{tumor} to be in the range of 2-4 because of 1) higher blood content, 2) denser blood vasculature, and 3) the finite size of solid tumors in this study. Thus, the percentage of tumor vascular content or volume sampled by NIRS over that by ^{19}F MRS is within the range of 19%~39%, based on the result of Eq. (16), for a given DPF_{tumor} of 4 and 2, respectively.

Data for all six rat breast tumors are shown in *Table 1*. The percentage of tumor vascular hemoglobin content sampled by NIRS and by MRS is within the range of 17~48% if considering a DPF_{tumor} of 2, and 8~24% if considering a DPF_{tumor} of 4. The mean value of the percentage, γ, is about 15±6% and 30±12%, depending on the DPF values of actual tumors. No obvious correlation was found between percentage values and tumor volume.

#6289 - $15.00 US Received 11 January 2005; revised 25 February 2005; accepted 28 February 2005

Table 1. Percentage of tumor vascular blood volume sampled by NIRS over that by ^{19}F MRS

Tumor physical volume (cm^3)	$\Delta[Hb]_{total}$ from NIRS (mM/DPF)	$\Delta V_{T\text{-}blood}$ from MRS (cm^3)	γ (%) with *DPF*=2	γ (%) with *DPF*=4
1.6	0.026	0.056	16.8	8.4
1.2	0.062	0.067	25.2	12.6
1.9	0.053	0.081	28.2	14.1
2.5	0.038	0.045	47.9	23.9
2.6	0.019	0.028	40.0	20.0
2.2	0.022	0.056	19.6	9.8
Mean ± S.D.[+]	0.037 ± 0.018	0.056 ± 0.018	30 ± 12	15 ± 6

[+]S.D. indicates standard deviation.

5. Discussion

In this study, changes in total hemoglobin concentration, $\Delta[Hb]_{total}$, and in total blood volume, $\Delta V_{T\text{-}blood}$, of rat breast tumors in response to carbogen intervention were determined by NIRS and by ^{19}F MRS of perflubron, respectively. The ratio of $\Delta[Hb]_{total}/\Delta V_{T\text{-}blood}$ was used to calculate the fraction of vascular hemoglobin contents sampled by NIRS and MRS. Since ^{19}F MRS of perflubron samples all blood volume in the tumor [18-19], the MRS measurement may be considered as a "gold standard" for the complete total blood volume within the tumor, provided that the entire rat tumor was placed within the RF coil. Then, this experimental approach provides evidence that the vascular blood content or volume sampled by the NIR system is about 15~30% of the total blood volume (Table 1). This estimation should be applicable not only to tumor tissues but also to other kinds of tissues, providing us with important information for better understanding of blood vascular volume sampled by NIRS. Moreover, the consistent trends between $\Delta[Hb]_{total}$ and $\Delta V_{T\text{-}blood}$ during hyperoxic gas intervention (Fig. 2) demonstrate that the low cost, portable NIRS system provides a non-invasive, real-time, monitoring tool to detect changes in tumor blood content.

Is it reasonable to believe that NIRS samples only 15~30% of the total blood content or volume in tissue vasculature? It has been reported that NIR light is most sensitive to microvessel densities, such as arterioles, capillaries, and venules [13-14] and surface areas of microstructures in tissue [15]. The size of micro blood vessels is often in the range of ~100 μm, which is in the same order of magnitude as the average scattering length of NIR light in tissue [15, 31]. So NIR light is scattered more frequently by the small blood vessels than large vessels, whereas large vessels have larger chances to terminate the NIR light due to high absorption. Thus, multiple scattering from micro vasculature permits better sensitivity to be sampled by NIR light. Moreover, small vessels have lower hematocrit compared to big vessels because of reduction of hematocrit with the decrease of vessel diameters [38]. Thus, based on our experimental measurements, it is reasonable to conclude that the NIR system samples 15-30% portion of total hemoglobin contents in tissue vasculature, mainly sensing the signals in microvessels.

DPF is a very important parameter for quantifying NIR measurements. As mentioned earlier, many investigators have conducted research on the estimation of optical path length of the brain and muscle of both human subjects and animal models [20, 32-37]. However, the NIR light propagated in tumor tissue is different from that in brain and muscle. Due to tumor angiogenesis, tumor tissues possess more blood vessels and have higher light absorption than the normal brain and muscle. Furthermore, the solid tumors in the study have a finite size, where "photon escape" from the measured volume can take place [39]. The term of "photon escape" has been used to refer to the situation where the sample size under study is finite, and a large amount of light may escape from the sample and never be detected, leading to a shorter path length in comparison with the path length existing in a large volume of tissues. Steen et al took DPF = 2.5 for their tumor study [40]. Therefore, we believe that

#6289 - $15.00 US Received 11 January 2005; revised 25 February 2005; accepted 28 February 2005

DPF_{tumor}=2~4 is a reasonable range used in our estimation of hemoglobin contents for breast tumors.

The errors in the percentage measurement may be potentially reduced by conducting measurements of NIRS and ^{19}F MRS simultaneously, eliminating experimental variations between the two kinds of measurements. One might also apply ^{1}H MRI of vascular volume markers such as super paramagnetic iron oxide particles (SPIOs) [41-42] in place of the ^{19}F NMR approach used here. Since agents, such as Combidex, are in clinical use, correlation studies with NIRS could allow examination of percentage of blood content/volume sampled by the NIRS system in human tumors. Also, the uncertainty in both the size measurement and volume calculation of the tumors should be reduced since they all contribute critically to the error in the estimated fraction of blood vascular contents.

In our study, not all tumors showed significant changes in $[Hb]_{total}$ accompanying challenge with hyperoxic gas. This is mainly due to both heterogeneity and irregularity of breast tumors, which have leaky, broken, and dis-functioning blood vasculatures. The inconsistency of changes in tumor $[Hb]_{total}$ induced by hyperoxic gas interventions has been observed throughout our research studies over several years. Thus, we believe it is reasonable to select rat breast tumors, which show significant changes in $[Hb]_{total}$, for this study in order to obtain estimated fraction of vascular blood contents sampled by NIRS.

In conclusion, we have introduced a new experimental approach to estimate the percentage of tumor blood content or volume sampled by the NIRS system by combining the measurements of NIRS with ^{19}F MRS. The results gave rise to an estimated range of 15~30%, suggesting that NIRS does not sample the entire blood hemoglobin content/volume of the tissue, but it senses more toward microvasculature. The study helps better understand blood vascular volume sampled by NIRS, and demonstrates that the low cost, portable NIRS system can be a reliable, non-invasive, real-time, monitoring tool on changes in tumor blood contents.

Acknowledgments

This work was supported in part by the Department of Defense Breast Cancer Research grants DAMD17-01-1-0423 (YG) and DAMD17-00-1-0459 (HL), and in part by NIH RO1 CA79515/EB2762 (RPM). Tumor cells were provided by the Division of Cancer Therapeutics, NIH, and perflubron emulsion (Oxygent™) was kindly provided by Alliance Pharmaceuticals. The authors would like to acknowledge Yulin Song's initial work and useful discussion for this publication.

Appendix 4

Mengna Xia, Yueqing Gu, Hanli Liu, Vikram Kodibagkar, Anca Constantinescu, Ralph Mason, “Tumor oxygen dynamics measured simultaneously by near-infrared spectroscopy and MR EPI imaging,” in Biomedical Topical Meetings on CD-ROM (The Optical Society of America, Washington, DC, 2004), ThF33.

Tumor oxygen dynamics measured simultaneously by near-infrared spectroscopy and ^{19}F MR EPI imaging

Mengna Xia, Yueqing Gu, Hanli Liu
Biomedical Engineering Graduate Program, University of Texas at Arlington, Arlington, TX 76013
Tel: (817) 272-2054; Fax: (817) 272-2251; email address: hanli@ uta.edu

Vikram Kodibagkar, Anca Constantinescu, Ralph Mason
Department of Radiology, UT Southwestern Medical Center at Dallas, Dallas, Texas, United States
Tel: (214) 648-8926; Fax: (214) 648-2991; email address: Ralph.Mason@UTSouthwestern.edu

Abstract: We demonstrate the ability to simultaneously investigate tumor oxygen dynamics by Near-infrared spectroscopy and Fluorocarbon Relaxometry using Echo planar imaging for Dynamic Oxygen Mapping in breast tumors, with close correlations between the two techniques.

OCIS codes: (170.1470) blood/tissue constituent monitoring; (170.6510) Spectroscopy, tissue diagnostics

1. Introduction

Tumor oxygenation has been well recognized as a crucial factor governing the efficacy of radiotherapy [1,2]. Accordingly, accurate evaluation of tumor oxygenation could provide a better understanding of tumor response to therapy. Because of its importance, many techniques have been developed for monitoring tumor oxygenation [3]. In recent years, near-infrared spectroscopy (NIRS) has been developed as a promising non-invasive and real-time technique to quantify tumor vascular oxygenation [4,5]. Comparatively, magnetic resonance imaging (MRI) offers alternative noninvasive approaches to monitor tumor oxygenation, with its strength of high spatial resolution but weakness in low temporal resolution. By using Fluorocarbon Relaxometry using Echo planar imaging for Dynamic Oxygen Mapping (FREDOM), MRI can provide quantitative pO_2 readings at multiple specific locations simultaneously with millimeter spatial resolution. It is of interest to correlate NIRS and FREDOM in order to improve and complement their individual strength for tumor physiology and pathology under therapeutic interventions.

2. Materials and Methods

2.1 Animal Preparation and experimental setup

Ten adult female Fisher 344 rats were planted with mammary adenocarcinomas 13762NF in surgically prepared foreback pedicles. When the tumors reached ~1 cm in diameter, the rats were anesthetized with ketamine hydrochloride i.p. (1.5ml; 100mg/ml; Aveco, Fort Dodge, IA) and were maintained under general gaseous anesthesia (air and 1% isoflurane; Baxter International Inc., Deerfield, IL). Tumor hair was trimmed for the ease of optical contact for transmitting NIR light and HFB injection. The rats were placed in the magnet on their side, and body temperature was maintained using a warm water blanket. A Helmholtz coil with a diameter of 3 cm was designed to facilitate simultaneous MRI and NIRS measurements. We measured tumor oxygenation parameters simultaneously by FREDOM and NIRS during respiratory challenge with oxygen or carbogen. The response was characterized with both the signal magnitude and rate of oxygenation.

2.2 NIRS for measuring changes in tumor vascular oxygenation (ΔHbO_2)

We used a homodyne, frequency-domain system (NIM, Philadelphia, PA) to monitor global changes of oxy- and deoxy-hemoglobin concentration of tumors in response to different gas interventions. Light from 785 nm and 758 nm laser diodes was modulated at 140 MHz and was coupled into a 22-foot, bifurcated fiber bundle. The probe tips were made with a non-metallic material and in good contact on the surface of tumor. After being absorbed and scattered in the tumor tissue, the transmitted light was collected by another fiber bundle and amplified by a photomultiplier tube (PMT). An In-phase and Quadrature (IQ) demodulator chip was used to demodulate the measured signal from PMT. More details about this system have been described previously [4,6].

2.3 Mathematical model for the blood oxygenation dynamics of tumors

In our previous study, we derived a simplified model to relate the time constants to tumor blood perfusion rates [4].

$$\Delta[HbO_2(t)]^{vasculature} = \gamma_1 H_0[1-e^{\frac{-f_1 t}{\gamma_1}}] + \gamma_2 H_0[1-e^{\frac{-f_2 t}{\gamma_2}}] = A_1[1-e^{\frac{-f_1 t}{\gamma_1}}] + A_2[1-e^{\frac{-f_2 t}{\gamma_2}}], \quad (1)$$

where H_0 is the arterial oxygenation input, f_1 and γ_1 are the blood perfusion rate and the vasculature coefficient in a well-perfused region, and f_2 and γ_1 are the blood perfusion rate and the vasculature coefficient in a poorly perfused region. Also, $A_1=\gamma_1 H_0$, $A_2=\gamma_2 H_0$, and the two time constants in eq. (1) are equal to $\tau_1=\gamma_1/f_1$ and $\tau_2=\gamma_2/f_2$. Since A_1, A_2 and the two time constants can be determined from our NIR dynamic measurements, we arrive at the ratios for the two vasculature coefficients and the two blood perfusion rates,:

$$\frac{\gamma_1}{\gamma_2} = \frac{A_1}{A_2}, \quad \frac{f_1}{f_2} = \frac{A_1/A_2}{\tau_1/\tau_2}. \quad (2)$$

Therefore, by studying tumor oxygenation dynamics with NIRS and obtaining the time constants together with their amplitudes, we are able to gain important information on regional blood perfusion and vascular structures of the tumor within the measured volume.

2.4 FREDOM for measuring oxygen tension of tumors (pO_2)

Simultaneous MRI experiments were performed on an Omega CSI 4.7T horizontal bore system equipped with actively shielded gradients (Acustar™, Bruker Instrument, Inc. Fremont, CA). Before the experiment, HFB (50μl, 99.9%, Aldrich Chemical Co., St. Louis, MO) was administered along two or three tracks in central and peripheral regions of the tumors in a single plane (transverse to the rat's tumor, and in the region of NIR photon pathway) using a Hamilton syringe with a fine sharp 32 G needle. The tumor was placed inside a Helmholtz coil designed to facilitate simultaneous MRI and NIRS measurements. T1-weighted images were acquired with TR=200 ms, TE=10 ms, and 128x128 points over a 40x40 mm area, giving 312x312 μm resolution. Following ^{1}H MR imaging, the corresponding ^{19}F MR imaging (188.252 MHz) was performed to show the distribution of HFB in the tumor. *FREDOM* used an MBEST spin echo planar imaging sequence with pulse burst saturation recovery (PBSR) signal preparation, a variable recovery time and spin echo acquisition. The Alternated R1 Delays with Variable Acquisitions to Reduce Clearance effects (ARDVARC) protocol was applied to improve the precision of R1 measurements [7]. R1 was calculated on a pixel–by-pixel basis using nonlinear least-squares data fitting by the Gauss-Newton method. Readings for pO_2 were estimated using the equation pO_2 = (R1-0.0835)/0.001876, as described in detail previously [8]. Three baseline pO_2 maps were generated over 24 mins for all tumors, and then the rats were exposed to inhaled gas interventions. Five *FREDOM* readings were taken during each gas breathing period. A total of 23 maps were obtained during a complete five-phase imaging session over about 2.5 hours.

3. Results

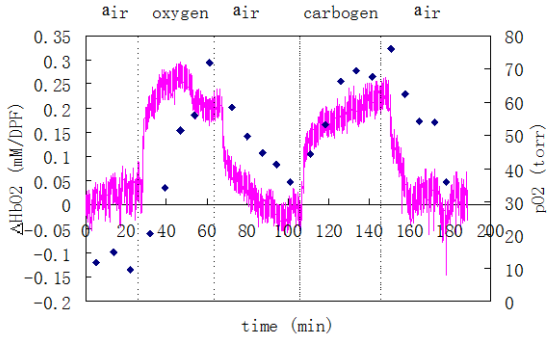

Fig.1 Time course of ΔHbO_2 and pO_2 in response to respiratory challenge for tumor No.1, simultaneous measured by NIRS (curve) and FREDOM (symbols).

Figure 1 shows simultaneous readings of mean pO_2 and relative changes of $\Delta[HbO_2]$ of a breast tumor in response to respiratory challenge measured by FREDOM and NIRS. This tumor showed a rapid response to the hyperoxic gas interventions with a significant increase in $\Delta[HbO_2]$. The pO_2 readings increased significantly, but more slowly. These changes can be characterized by their magnitude of response and kinetics. Namely, eq.(1) can be used to fit $\Delta[HbO_2]$, whereas the pO_2 data can be quantified by a rising rate, which is the slope of best-linear-fit in the pO_2 time course during oxygen or carbogen intervention. Compared with A_1/τ_1 and A_2/τ_2 by fitting the ΔHbO_2 readings, the

pO_2 rising rate has a significant positive correlation with A_1/τ_1 in the well-perfused region, but no correlation with that in the poorly-perfused region within the tumor, as shown in Figure 2.

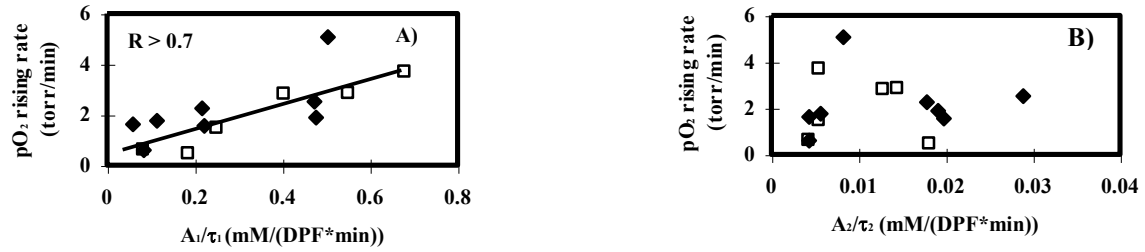

Fig. 2 **A)** pO_2 rising rate vs A_1/τ_1 with a positive correlation between the two variables ($R>0.7, p<0.02$). **B)** pO_2 rising rate vs A_2/τ_2 with no correlation between them.

Furthermore, Figure 3 shows that a good correlation existed between the tumor perfusion rate ratio (f_1/f_2) and tumor pO_2, where the latter values are the average oxygen tensions determined in the non-hypoxic regions of tumor during the hyperoxic interventions.

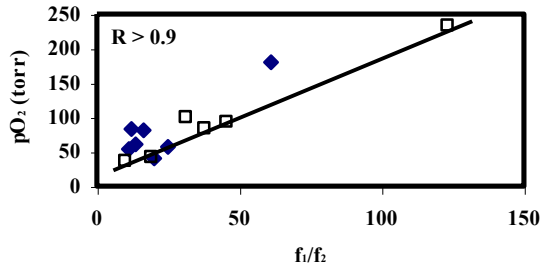

Fig.3 Tumor pO_2 vs perfusion rate ratio (f_1/f_2) ($R>0.9$, $p<0.001$). The pO_2 readings are the average of maximal pO_2 values in selected voxels, which have pO_2 increased to more than 10 torr during oxygen (solid points) or carbogen intervention (open points).

4. Discussion

This study shows that the two techniques, i.e., NIRS and MRI, are consistent and complementary with one another for tumor oximetry. It also demonstrates the feasibility to correlate tumor vascular oxygenation with tumor tissue pO_2, indicating the potential applications of the NIRS technique for clinical cancer practice and providing valuable insights into tumor patho-physiology and response to therapy.

5. Acknowledgements: This work was supported in part by the Department of Defense Breast Cancer Research grant BC990287 (HL), and NIH RO1 CA79515 (RPM). MR experiments were conducted at the Rogers MR Center, an NIH BTRP Facility (P41-RR02584) in conjunction with Cancer Image Program P20 CA86354. Tumor cells were provided by the Division of Cancer Therapeutics, NIH.

6. References

1. Hall EJ, " the oxygen effect and reoxygenation", in *Radiobiology for the Radiologist*, 4th ed., (J. B. Lippincott, Philadelphia, 1994).
2. D Zhao, A Constantinescu, C-Hui Chang, E W. Hahn*a* and R P. Mason, "Correlation of Tumor Oxygen Dynamics with Radiation Response of the Dunning Prostate R3327-HI Tumor", Radiat Res., 2003 **159**(5):621-31.
3. Stone HB, Brown JM, Phillips T and Sutherland RM, " Oxygen in human tumors: correlation between methods of measurement and response to therapy." Radiat. Res. **136**, 422-434(1993).
4. Liu H, Song Y, Worden KL, Jiang X, Constantinescu A and Mason PR, " Noninvasive investigation of blood oxygenation dynamics of tumors by near-infrared spectroscopy", App. Opt. **39**, 5231-43(2000)
5. Gu Y, Bourke VA, Kim JG, Constantinescu A, Mason RP and Liu H, " Dynamic response of breast tumor oxygenation to hyperoxic respiratory challenge monitored with three oxygen-sensitive parameters", Apply Opt., **42**, 2960-2967(2003)
6. Yang Y, Liu H, Li X and Chance B, " Low-cost frequency-domain photon migration instrument for tissue spectroscopy, oximetry, and imaging", Opt. Eng. 36, 1562-69(1997)
7. Hunjan S, Zhao D, Constantinescu A, Hahn EW, Antich PP and Mason RP, " Tumor oximetry: demonstration of and enhanced dynamic mapping procedure using fluorine-19 echo planar magnetic resonance imaging in the Dunning prostate R3327-AT1 Rat tumor." Int. J. Radiat. Oncol. Biol. Phys. 49,1097-1108(2001).
8. Zhao D, Constantinescu A, Jiang L, Hahn EW and Mason RP, " Prognostic Radiology: quantitative Assessment of tumor Oxygen Dynamics by MRI", Am J Clin Oncol, **24**: 462-466 (2001).

Appendix 5

Yueqing Gu, Mengna Xia, Hanli Liu, Vikram Kodibagkar, Anca Constantinescu, Ralph P. Mason, “Correlation of NIR spectroscopy with BOLD MR imaging of assessing breast tumor vascular oxygen status,” in Biomedical Topical Meetings on CD-ROM (The Optical Society of America, Washington, DC, 2004), FB6.

Correlation of NIR spectroscopy with BOLD MR imaging of assessing breast tumor vascular oxygen status

Yueqing Gu, Mengna Xia, Hanli Liu
Joint Graduate Program in Biomedical Engineering, University of Texas at Arlington, Arlington, TX 76019
Tel: (817) 272-2054; FAX: (817) 272-2251; email address: ***hanli@uta.edu***

Vikram Kodibagkar, Anca Constantinescu, Ralph P. Mason
Department of Radiology, University of Texas Southwestern Medical Center at Dallas, Dallas, TX 75390
Tel: (214) 648-8926; FAX: (214) 648-2991; e-mail address: ***Ralph.Mason@UTSouthwestern.edu***

Abstract: Dynamic changes of oxygenated and deoxygenated hemoglobin concentrations in response to hyperoxic gas interventions on rat breast tumors were simultaneously investigated by near infrared spectroscopy and BOLD (blood oxygenation level dependent) contrast MR imaging.

OCIS codes: (170.1470) blood/tissue constituent monitoring; (170.3660) light propagation in tissues; (170.4580) optical diagnostics for medicine; (170.5280)

1. Introduction

Hyperoxic gases have been investigated as potential contrast agents in magnetic resonance (MR) imaging. Manipulation of oxygen (O_2) content in the inhaled gas can provide qualitative and quantitative information on regional oxygenation. During hypoxia, the concentration of deoxyhemoglobin ([Hb]) is increased, causing decreased signal intensity (SI) on T2*-weighted MR images[1,2]. Oxygenation, on the other hand, increases local T2*, resulting in increased SI[3]. Inhalation of O_2 or carbogen (95%O_2, 5%CO_2) in tumor-bearing rats alters blood deoxy-hemoglobin concentration, resulting in SI changes on T2* weighted images of the measured tumors. Therefore, blood oxygenation level dependent (BOLD) contrast MR imaging has been utilized to detect hemodynamic changes in the brain and tumor tissues[4,5]. It has also used to evaluate the physiologic parameters of tissue metabolic activities, such as cerebral blood flow (CBF) and O_2 consumption. Results of BOLD MR imaging for CBF and O_2 consumption are compatible to those obtained with animal models and PET[6,7]

While MR imaging provides a noninvasive *in vivo* imaging modality for mapping tumor hemodynamic changes, the signal from BOLD contrast MRI is also influenced by variations in blood volume (, hemoglobin concentration) and blood flow. This confusion may limit its wide clinic application. Near Infrared spectroscopy (NIRS) provides an alternative noninvasive, real time, monitoring means for tumor vascular hemoglobin concentration. Moreover, the signals from NIRS are independent of blood flow. Therefore, simultaneous measurements by NIRS and BOLD MRI will allow us to correlate the signals from both non-invasive modalities and to better interpret the signals of BOLD MRI. In this way, the ability of understanding BOLD signal better will increase the potential of BOLD MRI to be used for clinical applications, particularly for cancer research.

In this study, we performed simultaneous measurements of dynamic oxygenated and deoxygenated hemoglobin concentrations, $\Delta[HbO_2]$ and $\Delta[Hb]$, using NIRS and BOLD contrast MRI, in response to carbogen inhalation on rat breast tumor vasculature. The average signals from the BOLD MR imaging were correlated well with the tumor global $\Delta[HbO_2]$ signals obtained from the NIRS and BOLD MR imaging revealed the heterogeneity of tumor hypoxia.

2. Material and Methods

2.1 Near Infrared Spectroscopy for global measurements of tumor $\Delta[HbO_2]$ and $\Delta[Hb]_{total}$

The changes of oxygenated, deoxygenated hemoglobin concentrations and total hemoglobin in tumor tissue, $\Delta[HbO_2]$, $\Delta[Hb]$ and $\Delta[Hb]_{total}$, caused by external interventions were determined by a homodyne frequency-domain (NIRS system (NIM, Philadelphia, PA)[8,9,10]. Briefly, the RF-modulated light at the wavelengths of 758 nm and 785 nm was projected on the tumor surface through a delivery fiber bundle. The light diffusing through the rat tumor tissue was collected and propagated to a photomultiplier tube (PMT) through another fiber bundle. The signal from the PMT was demodulated through an In-phase and Quadrature-phase circuit, and the amplitude and phase were recorded in real time. Based on modified Beer-Lambert's law and recorded amplitudes, the values of $\Delta[HbO_2]$, $\Delta[Hb]$ and $\Delta[Hb]_{total}$ due to respiratory intervention were derived previously[9].

2.2 Magnetic resonance imaging system

BOLD contrast was measured by using a Varian IVOVA 4.7 T super-conducting magnet system single turn solenoid RF coil. The coil was tuned at proton resonance frequency (200.13 MHz at 4.7 T). The paramagnetic deoxyhemoglobin creates local magnetic field variations in the proximity of blood vessels, producing additional phase dispersion of water proton signals in the surrounding tissue. Gradient recalled echo (GRE) ^{1}H MR imaging sequences are sensitive to these local susceptibility variations near the vessels; hence, an increase in concentration of deoxyhemoglobin, due to oxygen desaturation or blood flow changes, leads to a signal attenuation in gradient echo or T_2^* (apparent spin-spin relaxation time)-weighted image. The parameters for data acquisition of T_2^*- weighted image were: TR (Recycle time)=300ms, TE (Echo time)=30ms, Flip angle=20 ^{0}.

2.3 Animal model and protocol

Mammary adenocarcinomas 13762NF were implanted in skin pedicles on the forebacks of female Fisher 344 rats (~150 g). Once the tumors reached 1~2 cm diameter, rats were anesthetized with ketamine hydrochloride (100 mg/ml, i.p.) and maintained under general gaseous anesthesia with 1.3% isoflurane in air (1 dm^3/min). Tumors were shaved for better optical contact and placed in the frequency-tunable (^{1}H/^{19}F), single-turn solenoid RF coil. The delivering and detecting fiber bundles of the NIRS were touched firmly to the surface of the shaved tumors (without compression of tumor) for the measurement of $\Delta[Hb]_{total}$ and $\Delta[HbO_2]$. BOLD MRI was performed simultaneously with NIRS during hyperoxic gas interventions. Specifically, two experiments were setup in each of the tumor measurements: the BOLD MRI, was first performed on a single thick slice equivalent to the volume interrogated by NIR and then from three thinner slices (2 mm) were selected to study the heterogeneity of tumor oxygenation.

3. Results

3.1 Consistency of tumor vascular oxygenations obtained from NIRS and BOLD MRI

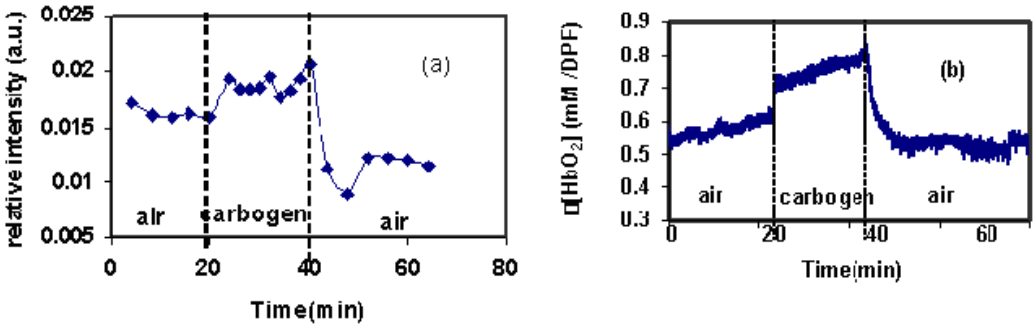

Figure 1 Simultaneous measurements with BOLD MRI and NIRS of a rat breast tumor (No. 2, 4.8 cm ^{3}) for its vascular oxygenation status with respect to carbogen intervention. (a) Average intensity of BOLD MR images within the tumor region. (b) The changes in oxygenated hemoglobin concentration, $\Delta[HbO_2]$, measured by NIRS.

The whole tumor was first observed as one thick slice for the simultaneous measurements. Figure 1 shows the time course profiles of average SI from BOLD MR images (a) and $\Delta[HbO_2]$ obtained from NIRS (b). Analysis of ROI (region of interest) on whole tumors gave rise to the mean SIs of each MR image (Fig. 1(a)). During the first 20 minutes, when the rat breathed air as baseline, the mean intensity of BOLD signals is about 0.0162±0.0005. Carbogen intervention after the baseline breathing produced a significant increase ($p<0.001$) in BOLD MRI intensity, to about 0.0189±0.0008. The signal decreased significantly to 0.011±0.001 when the inhaled gas was switched back to air ($p<0.001$). A similar tendency in $\Delta[HbO_2]$ was observed by NIRS (Fig.1(b)), indicating that both BOLD MRI and NIRS provide consistent results for oxygenation dynamics in tumor vasculature.

3.2 Heterogeneity of tumor oxygenation dynamics

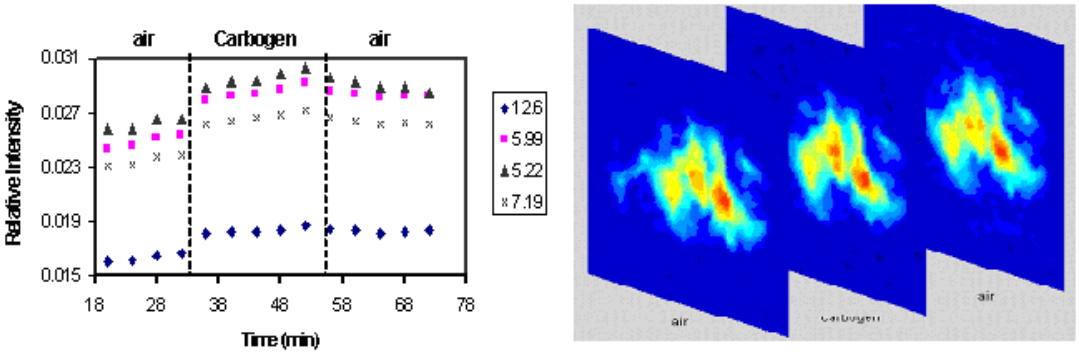

Figure 2 (a) Relative signal intensity of BOLD MR images at different tumor regions in response to carbogen intervention for a representative breast tumor (3.2 cm ^{3}). (b) Typical cross-sectional intensity images of BOLD MRI under three different gas inhalations for the same breast tumor.

The heterogeneity of tumor oxygenation with respect to carbogen intervention for a representative breast tumor (3.2 cm^3) was demonstrated in Fig.2. Several locations exhibit increased signals, whereas others remain unchanged, when the breathing gas was switched to carbogen and then back to air.

4. Summary

We have demonstrated the ability to correlate NIR and 1H MRI investigations simultaneously. This preliminary study demonstrates that the global signals of breast tumors obtained by NIRS and BOLD MRI in response to respiratory intervention are in good agreement. These two techniques may be complementary to one another for *in vivo* measurements of tumor oxygenation dynamics. MRI can be applied to deep tumors with special pulse sequences, whereas NIRS can be used to monitor acute responses of tumors to different therapeutic interventions. The correlation of NIRS and BOLD MRI techniques could provide a new prognostic tool for assessing efficacy of tumor therapies and could help us better interpret BOLD MRI signals. Furthermore, the heterogeneity of tumor vascular oxygenation dynamics to external interventions can be investigated directly by BOLD MRI, while the development of NIR imaging for tumor oximetry has also great potential to reveal tumor vascular heterogeneities.

5. Acknowledgements

This work was supported in part by the Department of Defense Breast Cancer Research grants BC000833 (YG) and BC990287 (HL), and NIH RO1 CA79515 (RPM). MR experiments were conducted at the Rogers MR Center, an NIH BTRP Facility (P41-RR02584) in conjunction with Cancer Image program P20 CA86354. Tumor cells were provided by the Division of Cancer Therapeutics, NIH.

Reference

[1] A. J. De Crespigny, M.F. Wendland, N. Derugin, E. Kozniewska, M.E. Moseley, "Real time observation of transient focal ischemia and hyperemia in cat brain," Magnetic Resonance in Medicine **27**, 391-397, 1992.

[2] G.C. Houston, N.G. Papadakis, T.A. Carpenter, L.D. Hall, B. Mukherjee, M. F. James, C. L Huang, "Mapping of the cerebral response to hypoxia measured using graded asymmetric spin echo EPI," Magnetic Resonance Imaging **18**, 1043-1054, 2000.

[3] R. P. Kennan, B. E. Scanley, J.C. Gore. "Physiologic basis for BOLD MR signal changes due to hypoxia/hyperoxia: separation of blood volume and magnetic susceptibility effects". Magnetic Resonance in Medicine **37**,953-956, 1997.

[4] S. Ogawa, T. M. Lee, A. R. Kay, D. W. Tank, "Brain magnetic resonance imaging with contrast dependent on blood oxygenation. Proceeding of the National Academy of Sciences of the United States of America **87**, 9868-9872, 1990.

[5] S. Kim, K. Ugurbil, "Functional magnetic resonance imaging of the human brain," J. Neuroscience Methods. **74**,229-243, 1997.

[6] R. D. Hoge, J. Atkinson, B. Gill, G. R. Crelier, S. Marrett, G. B. Pike, "Investigation of BOLD signal dependence on cerebral blood flow and oxygen consumption: the deoxyhemoglobin dilution model," Magnetic Resonance in Medicine **42,** 849-863, 1999.

[7] F. Hyder, R. P. Kennan, I. Kida, G. F. Mason, K. L. Behar, D. Rothman, "Dependence of oxygen delivery on blood flow in rat brain: A 7 tesla nuclear magnetic resonance study," Journal of Cerebral Blood Flow & Metabolism **20**, 485-498, 2000.

[8] H. Liu, Y. Song, K. L. Worden, X. Jiang, A.Constantinescu, and R. P. Mason, "Noninvasive investigation of blood oxygenation dynamics of tumors by near-infrared spectroscopy," Appl. Opt. **39**, 5231-5243, 2000.

[9] J. G. Kim, Y. Song, D. Zhao, A. Constantinescu, R. P. Mason, and H. Liu, "Interplay of Tumor Vascular Oxygenation and pO_2 in Tumors Using NIRS, ^{19}F MR pO_2 Mapping, and pO_2 Needle Electrode," J. Biomed. Optics, 8(1), 53-62, 2002.

[10] Y. Gu, V. Bourke, J. Kim, A. Constantinescu, R. P. Mason, H. Liu, "Dynamic response of breast tumor oxygenation to hyperoxic respiratory challenge monitored with three oxygen-sensitive parameters", Applied Optics. **42**(16), 2960-67, 2003.

Appendix 6

Yulin Song, Yueqing Gu, Jae G. Kim, Hanli Liu, Anca Constantinescu, and Ralph P. Mason, "Correlation between total hemoglobin concentration and blood volume of breast tumors measured by NIR spectroscopy and ^{19}F MRS of PFOB," *OSA Biomedical Topical Meetings*, Technical Digest, SuH5, Miami Beach, FL, April 7-10, 2002.

Correlation between total hemoglobin concentration and blood volume of breast tumors measured by NIR spectroscopy and ^{19}F MRS of PFOB

Yulin Song, Yueqing Gu, Jae G. Kim, Hanli Liu
Joint Graduate Program in Biomedical Engineering, University of Texas at Arlington, Arlington, TX 76019
Tel: (817) 272-2054; FAX: (817) 272-2251; email address: ***hanli@uta.edu***

Anca Constantinescu, Ralph P. Mason
Department of Radiology, University of Texas Southwestern Medical Center at Dallas, Dallas, TX 75390
Tel: (214) 648-8926; FAX: (214) 648-2991; e-mail address: Ralph.Mason@UTSouthwestern.edu

Abstract: Correlation between total hemoglobin concentration and blood volume in solid mammary tumors was explored using both NIRS and ^{19}F MRS of PFOB, respectively, while studying dynamic changes in tumor vascular volume induced by a vasoactive agent, carbogen. A close correlation between the results obtained from the two methods indicates the potential utility of NIRS for non-invasive *in vivo* quantification of tumor blood volume.

OCIS codes:(170.1470) blood/tissue constituent monitoring; (170.3660) light propagation in tissues; (170.4580) optical diagnostics for medicine; (170.5280)

1. Introduction

Tumor blood volume is an important physiological parameter that affects not only tumor growth and survival, but also efficacy of cancer treatments that alter oxygen delivery and chemotherapeutic agents to tumor cells. The ability to measure tumor blood volume may provide a valuable diagnostic tool for cancer treatment planning. Longitudinal measurements could reveal insight into tumor development and perhaps provide a prognostic indicator for tumor therapy. For many years, the most commonly used methods of measuring tumor blood volume involved the use of radioactive labeled tracers and also required the excision of the tumor[1,2].

Recently, several new techniques have been developed for *in vivo* measurements associated with tumor blood volume, including near infrared spectroscopy (NIRS)[3], position emission tomography (PET), and ^{19}F NMR of perfluorocarbons (PFCs)[4]. Since NIRS is entirely noninvasive, inexpensive, portable, and real-time, it would be a useful and desirable technique in cancer research and practice if direct readouts of tumor blood volume *in vivo* could be obtained. However, the current NIRS can measure quantitative values of only total hemoglobin concentration, [Hb_{total}], and oxygenated hemoglobin concentration, [HbO_2]. Few studies have reported on how to quantitatively convert or correlate tumor Hb_{total} to tumor blood volumes. In this paper, we report our preliminary investigation on the correlation between the Hb_{total} and blood volume in solid mammary tumors using both NIRS and ^{19}F MRS of PFOB, respectively, while a vasoactive agent, carbogen, was employed to induce dynamic changes in tumor vascular volume. A close correlation between the results obtained from the two methods supports the ability of NIRS for *in vivo* quantification of tumor blood volumes. Also, the vascular density of breast tumors was obtained as a function of the tumor volume.

NIRS is based on the endogenous chromophores, i.e., oxygenated and deoxygenated hemoglobin. The absorption of light by these intrinsic chromophores can be altered to determine important physiological indicators, such as Hb_{total} changes. Others have shown that perfluorocarbon emulsions provide a valid indicator of tumor vascular volume for some time after infusion. ^{19}F NMR can be applied to measure signal intensity, which is related to blood concentration. In this study, a perfluorooctylbromide (PFOB) ($C_8F_{17}Br$) emulsion was used as a tumor blood volume indicator based on the earlier work of Baldwin *et al*.[4] PFOB is extremely inert chemically, and biochemically, and ideally suited for *in vivo* biological studies.

2. Materials and Methods

2.1 Animal Preparation

Mammary adenocarcinomas 13762NF were implanted in skin pedicles on the forebacks of female Fisher 344 rats (~250 g). Once the tumors reached ~ 2 cm diameter, tumor $[Hb]_{Total}$ and [HbO_2] were measured by dual-wavelengths NIRS in anesthetized rats (isoflurane/air). On the next day, the rats were re-anesthetized and intravenously infused with 2 ml of a PFOB emulsion by tail vein injection. The ^{19}F MRS measurements were performed 30 min later to

give sufficient time for the PFOB emulsion to reach an equilibrium state within the blood stream. To study the dynamic change of blood volume, the inhaled gas was alternated in the order of air -> carbogen -> air -> carbogen -> air.

2.2 Near Infrared Spectroscopy

$[HbO_2]$ and $[Hb_{total}]$ can be determined with multi-wavelength NIR spectroscopy based on their absorption properties. The instrument setup was described elsewhere[3], but the algorithms used in this paper to obtain $\Delta[Hb_{total}]$ were modified in the light of *in vitro* laboratory calibration. The equation for $\Delta[Hb_{total}]$ is given below:

$$\Delta[Hb_{total}] = [-2.12*Ln(A_B/A_T)^{758} + 8.25*Ln(A_B/A_T)^{785}] / L, \quad (1)$$

where A_B = baseline amplitude; A_T = transient amplitude; L = optical pathlength between source/detector; the constants given in the equations were computed with the extinction coefficients for oxy- and deoxy-hemoglobin at the two wavelengths used. In principle, the unit of $\Delta[Hb]_{total}$ is mM, and L is equal to the source–detector separation multiplied by a Differential Pathlength Factor (DPF)[5]. Little is known about the DPF for tumors, though a DPF value of 2.5 has been used by others[6]. Since our focus is on dynamic changes of tumor $[Hb_{total}]$ with respect to carbogen intervention, we include the DPF in the unit, i.e., modifying eq. (1) as follows:

$$\Delta[Hb_{total}] = [-2.12*Ln(A_B/A_T)^{758} + 8.25*Ln(A_B/A_T)^{785}] / d, \quad (2)$$

where d is the direct source-detector separation in cm, and the unit of $\Delta[Hb_{total}]$ in eq. (2) is mM/DPF.

2.3 *^{19}F MRS of PFOB*

The rats were placed on their sides in an animal bed and the body temperature was maintained at 37° C. A frequency tunable (^{1}H/^{19}F) single turn solenoid coil was placed around the tumors and a sealed capillary containing sodium trifluoroacetate (TFA) used as an external standard for the purpose of quantifying tumor blood volume. The rats were positioned in the magnet (Omega CSI 4.7 T, Bruker Instrument, Inc., Fremont, CA) with the tumors at the isocenter of the magnet. Spectra were acquired with a long repetition time (TR = 30 s) to ensure that changes in T1 due to variable oxygenation would not interfere with volume measurements (ref Shukla)[7]. The rats were removed from the magnet and the RF coil, with the reference TFA capillary left in the original position. 0.5 ml blood sample drawn by tail vein was put into the RF coil without disturbing the reference TFA capillary. The RF coil was then placed back into the magnet in the same position as with the rats. A quantitative ^{19}F spectrum was acquired. Given a set of data acquisition parameters, the integration of ^{19}F signal from the tumor was linearly proportional to the total number of ^{19}F nuclear spins of PFOB in the tumor, which, in turn, was linearly proportional to the total blood volume in the tumor, assuming that the PFOB emulsion had reached an equilibrium state with the blood throughout the tumor.

The tumor blood volume is given as $V_{T\_blood} = V_{S\_blood} \cdot \left(\frac{I_{T\_blood}}{I_{S\_blood}}\right) \cdot \left(\frac{I_{S\_TFA}}{I_{T\_TFA}}\right)$, (2)

where I_{S_blood} and I_{T_blood} were the integration of NMR signal from ^{19}F in the blood sample and in the tumor, V_{S_blood} and V_{T_blood} were the blood sample volume and total tumor blood volume (ml), respectively. I_{blood_TFA} and I_{Tumor_TFA} were the integration of NMR signal from ^{19}F in the reference TFA capillary acquired with the blood sample and the tumor.

3. Results and Discussion

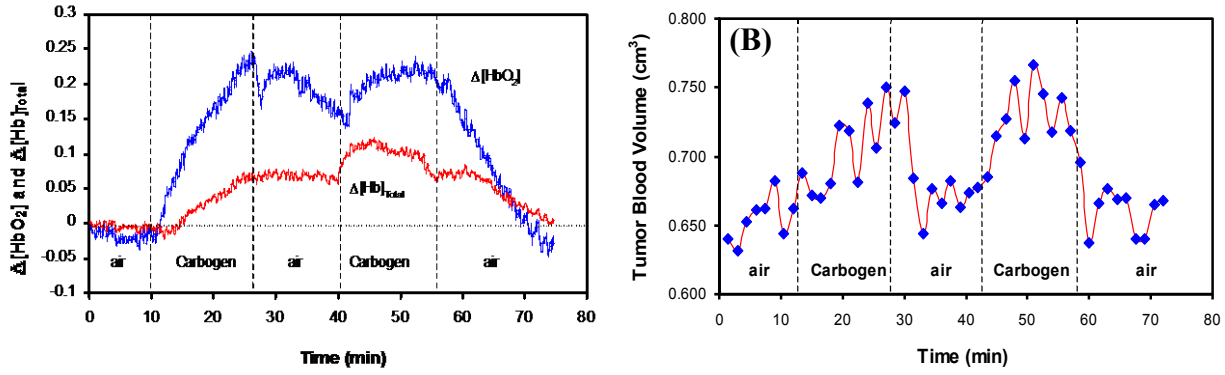

Fig 1. (A) Time course profiles of tumor vascular $\Delta[HbO_2]$ and $\Delta[Hb]_{Total}$ determined by NIRS; **(B)** tumor blood volume V_{TBlood} measured by ^{19}F MRS of PFOB for breast tumor No. 1 (4.2 cm^3).

The rat with mammary tumor first breathed air, and the values of [Hb_{total}] and [HbO_2] in the tumor were measured for baseline. The inhaled gas was alternated from air to carbogen, and the dynamic changes in [Hb_{total}] and blood volume of the tumor were monitored by NIRS and ^{19}F MRS of PFOB, respectively. **Figure 1(A)** shows the time course profiles of $\Delta[HbO_2]$ and $\Delta[Hb_{Total}]$ in response to carbogen intervention measured by NIRS for a representative breast tumor No. 1 (4.2 cm^3). **Figure 1(B)** shows the tumor blood volume, V_{T_blood}, as a function of time as measured by ^{19}F MRS of PFOB for the same breast tumor. In spite of fluctuation, the overall trend of V_{TBlood} was similar to that of $\Delta[Hb_{Total}]$. The correlation between the $\Delta[Hb_{Total}]$ measured by NIRS and V_{T_blood} measured by ^{19}F MRS of PFOB is shown in **Figure 2**, which shows reasonable consistency between the results obtained from the two methods.

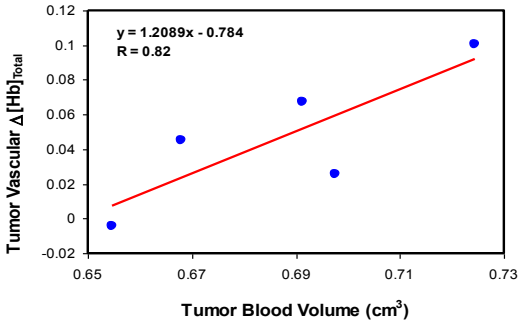

Fig. 2 Correlation between mean $\Delta[Hb]_{Total}$ measured by NIRS and mean V_{T_blood} measured by ^{19}F MRS of PFOB for each gas switch for breast tumor No. 1 (4.2 cm^3).

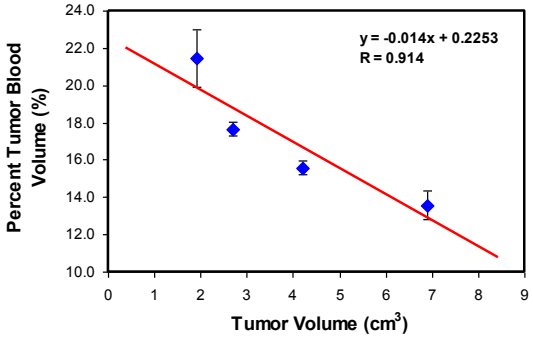

Fig. 3. Relationship between tumor vascular density versus tumor volume for a group of four breast tumors.

Furthermore, a number of breast tumors were investigated with ^{19}F MRS of PFOB, and the results are compared and shown in Figure 3. The tumor physical volumes were calculated from the three dimensions of the tumor. We can calculate the vascular density of the tumors as the ratios of the tumor blood volume (measured with air inhalation) to the tumor physical volume. The relationship between the tumor vascular density and the tumor physical volume is plotted in **Figure 3.** The strong negative linear relationship suggested that tumors became increasingly poorly perfused, and thus, poorly oxygenated as they grew in size.

4. Summary

In summary with this preliminary study, the agreement between the results obtained by ^{19}F MRS of PFOB and NIRS suggests that NIRS is a valid technique for *in vivo* measurement of changes in [Hb_{Total}] and tumor vascular volume. ^{19}F MRS of PFOB can be applied to deep tumors with special pulse sequences and NIRS can be used to monitor the acute response of tumors to drug intervention. The correlation of NIRS and ^{19}F MRS of PFOB techniques could provide a new prognostic tool for assessing efficacy of tumor therapy and could reveal the relationship between percent tumor blood volume and other tumor kinetic and physiological parameters.

5. Acknowledgements

This work was supported in part by NIH RO1 CA79515 (RPM), and the Department of Defense Breast Cancer Initiative grants BC962357 (YS) and BC990287 (HL). Tumor cells were provided by the Division of Cancer Therapeutics, NIH.

References

[1] G.M. Tozer, and C.C. Morris, "Blood flow and blood volume in a transplanted rat fibrosarcoma: Comparison with various normal tissues", *Radiother. Oncol*., **17**:153-166 (1990).
[2] H. Sands, S. A. Shah, B. M. Gallagher, "Vascular volume and permeability of human and murine tumors grown in athymic mice", *Cancer Lett.,* **27**:15-21 (1985).
[3] H. Liu, Y. Song, K.L. Worden, X. Jiang, A. Constantinescu, and R.P. Mason, "Noninvasive Investigation of Blood Oxygenation Dynamics of Tumors by Near-Infrared Spectroscopy", *Applied Optics*, 39(28):5231-5243 (2000).
[4] N.J. Baldwin, Y. Wang, and T.C. Ng, "In situ ^{19}F MRS measurement of RIF-1 tumor blood volume: Corroboration by radioisotope-labeled [^{125}I]-albumin and correlation to tumor size", *Magn. Reson. Imaging*, 14(3):275-280 (1996).
[5]. D.T. Delpy, M. Cope, P. van der Zee, S. Arridge, S. Wray, and J. Wyatt, "Estimation of optical pathlength through tissue from direct time of flight measurement," Phys. Med. Biol. 33(12), 1433-1442 (1988).
[6]. R. G Steen, K. Kitagishi and K. Morgan, " *In vivo* measurement of tumor blood oxygenation by near-infrared spectroscopy: Immediate effects of pentobarbital overdose or carmustine treatment", *J. Neuro-Oncol.,* **22**, pp. 209-220 (1994).
[7] H. P. Shukla, R. P. Mason, D. E. Woessner & P. P. Antich, "A comparison of three commercial perfluorocarbon emulsions as high field NMR probes of oxygen tension and temperature", J. Magn. Reson. B, 106, 131-141 (1995).

Appendix 7

Yueqing Gu, Wei R. Chen, Mengna Xia, Sang W. Jeong, and Hanli Liu, “Effect of Photothermal therapy on breast tumor vascular contents: non-invasive monitoring by near infrared spectroscopy,” *Photochemistry and Photobiology* 81(4), 1002–1009 (2005).

Photochemistry and Photobiology, 2005, 81: 000–000

Effect of Photothermal Therapy on Breast Tumor Vascular Contents: Noninvasive Monitoring by Near-infrared Spectroscopy¶

Yueqing Gu[1,3], Wei R. Chen[2], Mengna Xia[1], Sang W. Jeong[2], and Hanli Liu*[1]

[1]Biomedical Engineering Program, University of Texas at Arlington, Arlington, TX
[2]Biomedical Engineering Program, Department of Physics and Engineering, University of Central Oklahoma, Edmond, OK
[3]Biomedical Engineering Laboratory, China Pharmaceutical University, Nanjing, P.R. China

Received 16 March 2005; accepted 20 March 2005

ABSTRACT

?1 **The goal of this study was to investigate the effect of photothermal laser irradiation on rat breast tumor (DMBA-4) vascular contents. An 805-nm diode laser was used in our experiment with a power density ranging from 0.32 to 1.27 W/cm^2. The dynamic changes of oxygenated hemoglobin and total hemoglobin concentrations, $\Delta[HbO_2]$ and $\Delta[Hb]_{total}$, in rat tumors during photothermal irradiation were *noninvasively* monitored by a near-infrared spectroscopy system. A multichannel thermal detection system was also used simultaneously to record temperatures at different locations within the tumors. Our experimental results showed that: (1) photoirradiation did have the ability to induce hyperthermic effects inside the rat breast tumors in a single exponential trend; (2) the significant changes ($P < 0.005$) of $\Delta[HbO_2]$ and $\Delta[Hb]_{total}$ in response to a low dosage of laser irradiation (0.32 W/cm^2) have a single exponential increasing trend, similar to that seen in the tumor interior temperature; and (3) the increase in magnitude of $\Delta[HbO_2]$ is nearly two times greater than that of $\Delta[Hb]_{total}$, suggesting that photoirradiation may enhance tumor vascular oxygenation. The last observation may be important to reveal the hidden mechanism of photoirradiation on tumors, leading to improvement of tumor treatment efficiency.**

INTRODUCTION

Laser phototherapy, a nonsurgical modality for cancer treatment, is gaining widespread acceptance because of precise energy delivery into the tumor tissue (1–3). The laser energy delivered to the targeted tumors can induce localized photomechanical, photochemical and photothermal reactions, thus killing tumor cells. In general, photochemical reactions may cause the change of chemical bonds and form toxic radicals, such as release of singlet oxygen, leading to the death of organized tissues. Photomechanical reactions may induce tissue stress, resulting in the disruption of tissue cells and ejection of material. Photothermal reactions may induce hyperthermia and coagulation, causing cell destruction (4). In particular, thermal cytotoxicity effects are found to be more profound under acidotic (low pH) conditions, which are often present in poorly oxygenated tissues (5–7), such as in tumors. Many research studies have reported the existence of acute/chronic hypoxic regions within the majority of solid tumors (8–10). As a result, cytotoxicity induced by selective photothermal irradiation can be more effective in tumor tissue than in normal tissue. To further enhance the desirable photothermal effects, selective absorbers are often used in the targeted tumor tissue along with laser irradiation to cause selective and localized photon–tissue interactions (11,12). In addition, administration of an immunoadjuvant has been proved to increase systemic cancer cure and long-term resistance to cancer of the same origin, when combined with the selective photochemical treatment (13,14). Chen *et al*. have developed a laser immunotherapy by combining laser irradiation, a laser-absorbing dye and an immunoadjuvant to improve cancer therapy efficiency (11,12,15,16). The previous experimental results have demonstrated that this unique approach has positive effects on both primary and metastatic tumors.

Although the underlying mechanism of the laser irradiation has been intensively studied (17–20), the hemodynamic and physiological properties inside the tumors during phototherapy are poorly understood. Measuring the reduction of tumor size and survival rates is the current practice to evaluate the therapeutic outcome of therapy. Obviously, noninvasive, real-time monitoring of tumor hemodynamic characteristics before, during and after therapy is highly desirable. Such a technique may help reveal the tumor physiology and therapeutic process caused by the therapy, providing treatment prognoses and guidance to optimize the light dosimetry so as to improve the therapeutic outcome. Near-infrared spectroscopy (NIRS) has been demonstrated in our recent studies to be such a noninvasive means in monitoring tumor vascular oxygenation during therapeutic interventions (21–23).

In this study, we investigated the effects of photothermal therapy on tumor vascular contents and tumor temperature. An 805-nm diode laser was used for photothermal irradiation of mammary tumors in rats. The dynamic changes caused by the laser irradiation in oxygenated, deoxygenated and total hemoglobin concentrations, $\Delta[HbO_2]$, $\Delta[Hb]$, and $\Delta[Hb]_{total}$, in the tumor vasculature were

¶Posted on the website on ???

*To whom correspondence should be addressed: Biomedical Engineering Graduate Program, 501 West First, ELB-220, P.O. Box 19138, University of Texas at Arlington, Arlington, TX 76019, USA. Fax: 817-272-2251; e-mail: Hanli@uta.edu

Abbreviations: NIR, near infrared; NIRS, near-infrared spectroscopy; I&Q, in phase and quadrature phase; $[HbO_2]$, oxygenated hemoglobin concentration; [Hb], deoxygenated hemoglobin concentration; $[Hb]_{total}$, total hemoglobin concentration.

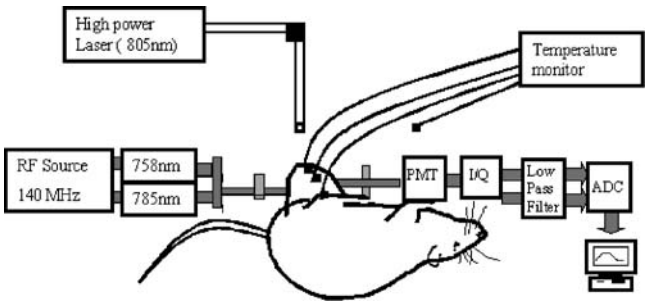

Figure 1. Experimental setup for the simultaneous NIRS and thermal measurements of breast tumors under photothermal therapy. PMT represents a photomultiplier tube; I&Q is an in-phase and quadrature-phase demodulator for retrieving amplitude and phase information. The thermal detection system comprises multiple thermal sensing probes, three of which are inserted into different regions of the tumor, and one probe was used to measure room temperature. The power-adjustable laser light (805 nm) is vertically delivered to tumor surface with a 2-cm beam diameter for photoirradiation.

monitored by an NIRS system. A multichannel, thermal monitor was also used simultaneously to record the temperatures at three different locations inside the breast tumors. The correlations between the optical irradiation dosages, tumor temperatures, and tumor vascular contents were studied. The dynamic features of tumor temperature and vascular oxygenation were quantified to reveal the dynamic effects within the tumors under the laser irradiation.

MATERIALS AND METHODS

NIRS. The changes of oxygenated, deoxygenated and total hemoglobin concentrations, $\Delta[HbO_2]$, $\Delta[Hb]$ and $\Delta[Hb]_{total}$, in tumor tissue caused by laser irradiation were determined by a near-infrared, homodyne, frequency-domain spectroscopy system (NIM, Philadelphia, PA), which has been described in detail elsewhere (21–23). Briefly, the amplitude-modulated light at 140 MHz at wavelengths of 758 nm and 785 nm illuminated the tumor surface through a light-delivery fiber bundle with output powers of 9 mW and 11 mW at 785 nm and 758 nm wavelengths, respectively, measured at the tip of the bundle by an optical power meter. The experimental setup is shown in Fig. 1. The 805-nm laser light was vertically applied on the tumor surface. The delivering and detecting fiber bundles of the NIRS system were placed horizontally and in good contact with the surface of the tumors in a transmittance mode, without compressing the tumors. The diffused light through the tumor tissue was collected and filtered by a sharp low-pass optical filter, which cut off the optical signal above 805 nm from the laser irradiation, and then propagated into a photomultiplier tube (PMT) through the detecting fiber bundle. The signal detected by the PMT was demodulated through an in-phase and quadrature-phase (I&Q) circuit, and the amplitude and phase of the signal were recorded.

Algorithms for calculations of $\Delta[HbO_2]$, $\Delta[Hb]$, and $\Delta[Hb]_{total}$. On the basis of the Beer-Lambert law, light attenuation, represented by optical density (OD), through a sample is proportional to the concentration of hemoglobin inside the sample (24–28),

$$\mathrm{OD} = \mathrm{Log}(A_0/A) = \varepsilon c l \tag{1}$$

where A_0 and A are light intensities of the incident and transmitted light, respectively, ε is the extinction coefficient of hemoglobin, c is the concentration of hemoglobin, and l is the length of light path through the measured sample. When the measured sample has a mixture of oxygenated and deoxygenated hemoglobin, Eq. (1) can be further evolved to (28–30),

$$\mathrm{OD}(\lambda) = \{\varepsilon_{Hb}(\lambda)[Hb] + \varepsilon_{HbO2}(\lambda)[HbO_2]\}l \tag{2}$$

where $\mathrm{OD}(\lambda)$ is the optical density at wavelength λ, $\varepsilon_{Hb}(\lambda)$ and $\varepsilon_{HbO2}(\lambda)$ are the extinction coefficients at wavelength λ for molar concentrations of deoxygenated hemoglobin, [Hb], and oxygenated hemoglobin, $[HbO_2]$, respectively, assuming ferrihemoglobin is minimal. By using two wavelengths, both $[HbO_2]$ and [Hb] can be determined by measuring the OD values at the two specific wavelengths, provided that the values for $\varepsilon_{Hb}(\lambda)$ and $\varepsilon_{HbO2}(\lambda)$ are known:

$$[HbO_2] = \frac{\varepsilon_{Hb}(\lambda_2)\mathrm{OD}(\lambda_1) - \varepsilon_{Hb}(\lambda_1)\mathrm{OD}(\lambda_2)}{l[\varepsilon_{Hb}(\lambda_2)\varepsilon_{HbO2}(\lambda_1) - \varepsilon_{Hb}(\lambda_1)\varepsilon_{HbO2}(\lambda_2)]}, \tag{3}$$

$$[Hb] = \frac{\varepsilon_{HbO2}(\lambda_2)\mathrm{OD}(\lambda_1) - \varepsilon_{HbO2}(\lambda_1)\mathrm{OD}(\lambda_2)}{l[\varepsilon_{Hb}(\lambda_1)\varepsilon_{HbO2}(\lambda_2) - \varepsilon_{Hb}(\lambda_2)\varepsilon_{HbO2}(\lambda_1)]}. \tag{4}$$

It follows that changes in [Hb] and $[HbO_2]$ can be consequently given as:

$$\Delta[HbO_2] = \frac{\varepsilon_{Hb}(\lambda_2)\Delta\mathrm{OD}(\lambda_1) - \varepsilon_{Hb}(\lambda_1)\Delta\mathrm{OD}(\lambda_2)}{l[\varepsilon_{Hb}(\lambda_2)\varepsilon_{HbO2}(\lambda_1) - \varepsilon_{Hb}(\lambda_1)\varepsilon_{HbO2}(\lambda_2)]}, \tag{5}$$

$$\Delta[Hb] = \frac{\varepsilon_{HbO2}(\lambda_2)\Delta\mathrm{OD}(\lambda_1) - \varepsilon_{HbO2}(\lambda_1)\Delta\mathrm{OD}(\lambda_2)}{l[\varepsilon_{Hb}(\lambda_1)\varepsilon_{HbO2}(\lambda_2) - \varepsilon_{Hb}(\lambda_2)\varepsilon_{HbO2}(\lambda_2)]}, \tag{6}$$

where $\Delta\mathrm{OD}(\lambda)$ represents a change in optical density at the specific wavelength, λ, and equals $\log(A_B/A_T)$. A_B and A_T correspond to light intensities measured under the baseline and transient conditions.

Note that in principle, l represents the optical path length between the source and detector. Whereas l is simply the physical separation, d, between the source and detector through a nonscattering medium, exact quantification of l for an intact tissue or organ is complex because of light scattering in tissue. Since l is in proportion to the separation, d, we can associate l to d as $l = DPF*d$, where DPF is a differential path length factor to account for light scattering. It has been well accepted that together with DPF, Eq. (2) can be treated as modified Beer–Lambert law; and consequently, Eqs. (5) and (6) can be correctly used to quantify changes in [Hb] and $[HbO_2]$ in highly scattering media (29,30), such as in intact tissue or organs.

To be consistent with our previous work, we adopted in this paper the ε values published by Zijlstra *et al*. (31). We had to interpolate the ε values at the two wavelengths used in our study, followed by certain corrections due to the interpolation errors by phantom calibration measurements (22). Specifically, we included two factors, β_1 and β_2, for the calibrated algorithm, as given below:

$$\Delta[HbO_2] = \frac{\frac{\varepsilon_{Hb}(785\ \mathrm{nm})}{\beta_1} \times \mathrm{OD}(758\ \mathrm{nm}) - \varepsilon_{Hb}(758\ \mathrm{nm}) \times \mathrm{OD}(785\ \mathrm{nm})}{l[\varepsilon_{Hb}(785\ \mathrm{nm})\varepsilon_{HbO2}(758\ \mathrm{nm}) - \varepsilon_{Hb}(758\ \mathrm{nm})\varepsilon_{HbO2}(785\ \mathrm{nm})]}, \tag{7}$$

$$\Delta[Hb] = \frac{\frac{\varepsilon_{HbO2}(785\ \mathrm{nm})}{\beta_2} \times \mathrm{OD}(758\ \mathrm{nm}) - \varepsilon_{HbO2}(758\ \mathrm{nm}) \times \mathrm{OD}(785\ \mathrm{nm})}{l[\varepsilon_{Hb}(785\ \mathrm{nm})\varepsilon_{HbO2}(758\ \mathrm{nm}) - \varepsilon_{Hb}(758\ \mathrm{nm})\varepsilon_{HbO2}(785\ \mathrm{nm})]}, \tag{8}$$

where $\varepsilon_{Hb}(758\ \mathrm{nm}) = 1.418$, $\varepsilon_{HbO2}(758\ \mathrm{nm}) = 0.6372$, $\varepsilon_{Hb}(785\ \mathrm{nm}) = 1.111$, and $\varepsilon_{HbO2}(785\ \mathrm{nm}) = 0.766$, all in $\mathrm{mM^{-1}cm^{-1}}$. Note that a factor of four has been multiplied for each of the εs at the respective wavelengths to account for light absorption from four hemes per hemoglobin molecule (34) since the extinction coefficients published in the field of biochemistry were expressed on a heme basis (24–28). Furthermore, we have used $\beta_1 = 1.103$ and $\beta_2 = 0.9035$ according to our phantom study (22). After substituting all of the parameters into Eqs. (7) and (8), we have arrived at the final equations to quantify changes in hemoglobin concentration: **?2**

$$\Delta[HbO_2] = \frac{-2.658 \cdot \mathrm{OD}(758\ \mathrm{nm}) + 3.743 \cdot \mathrm{OD}(785\ \mathrm{nm})}{d}, \tag{9}$$

$$\Delta[Hb] = \frac{2.238 \cdot \mathrm{OD}(758\ \mathrm{nm}) - 1.683 \cdot \mathrm{OD}(785\ \mathrm{nm})}{d}. \tag{10}$$

$\Delta[Hb]_{total}$ can also be obtained by adding Eqs. (9) and (10),

$$\begin{aligned}\Delta[Hb]_{total} &= \Delta[HbO_2] + \Delta[Hb] \\ &= \frac{-0.42 \cdot \mathrm{OD}(758\ \mathrm{nm}) + 2.06 \cdot \mathrm{OD}(785\ \mathrm{nm})}{d}.\end{aligned} \tag{11}$$

Notice that the units for $\Delta[HbO_2]$, $\Delta[Hb]$, and $\Delta[Hb]_{total}$ are mM; however, the values obtained from Eqs. (9) to (11) are scaled by a factor of

DPF. Since DPF is so far an unknown parameter for tumors, we include it within the unit as mM/DPF.

Laser photothermal irradiation system. The system used for the photothermal therapy consisted of an NIR diode laser, DIOMED 25 (DIOMEDICS, The Woodlands, TX), with an emitting peak wavelength at 805 nm and a maximum power output of 25 W. The laser light was coupled into an optical fiber, fitted with a microlens at the tip (Pioneer Optics, Windsor Locks, CT) to ensure a uniform beam density, and delivered onto the tumor surface. The laser beam diameter projected on the tumor surface was set as 2 cm in all the measurements by using the visible aiming light in the laser system. After the beam diameter was adjusted, the aiming light was turned off during NIR measurements.

Multichannel thermal monitor. A multichannel thermal monitor (Omega, Stamford, CT), incorporating an OM-700 Omega engineering data acquisition and control unit, was used simultaneously with the NIRS observation to monitor the internal temperatures at several locations within the tumors. Specifically, three thermal probes were inserted at the top (immediately below the overlaying skin), middle and bottom positions of the tumors, and one probe was located outside the tumor for room temperature recording. The data of each probe were recorded continuously, and the middle thermal probe recorded the internal tumor temperature near the center of the optical field of NIRS.

Animal model. The transplantable, metastatic mammary tumor cells (DMBA-4) (33–35) were implanted in one of the inguinal fat pads of female Wistar Furth rats (Harlan Sprague Dawley, Indianapolis, IN). Once the tumors reached 0.5 to 0.8 cm in diameter, the rats were anesthetized for the experiments. Hairs around tumors were removed for better probe contact in the NIRS measurement and for more efficient tumor exposure to the laser irradiation. The tumor diameters along the three major orthogonal axes (*a, b, c*) were measured to determine the volume of the tumors by using an ellipsoid approximation with the formula of $V = (\pi/6)abc$.

In this study, 16 rat breast tumors were used in two different treatment protocols. Ten rat tumors were first exposed to a single laser irradiation with a laser power of 0.32 W/cm^2 (1 W laser power in a 2-cm-diameter beam) for 10 min. Three or four days later, four of the treated tumors, along with other six untreated tumors, were exposed to repeated laser irradiations with a power density of 0.32, 0.64, 0.96 and 1.27 W/cm^2 (1 W, 2 W, 3 W, and 4 W in 2-cm-diameter beam) for 10 min with a recovery period of 10 min between two adjacent irradiations. Tumor temperatures, tumor vascular $\Delta[HbO_2]$, and $\Delta[Hb]_{total}$ were measured simultaneously in all the experiments.

Statistic analysis. A Student's *t*-test was applied in data analysis to determine whether the paired samples are significantly different. We considered $P < 0.05$ as the criteria for significant difference between the two sample groups. In addition, a mean and standard deviation (mean ± sd) were usually used to express the measured data and their dispersions.

RESULTS

Dynamic responses of $\Delta[HbO_2]$, $\Delta[Hb]_{total}$ and temperature to photothermal treatment

Using the experimental setup shown in Fig. 1 and Eqs. (9) and (11), tumor vascular $\Delta[HbO_2]$, $\Delta[Hb]_{total}$ and internal temperatures were quantified simultaneously. Figure 2 shows the temporal profiles of $\Delta[HbO_2]$, $\Delta[Hb]_{total}$ and the internal temperatures of a rat tumor under photothermal irradiation with a laser power density of 0.32 W/cm^2. The experimental data consisted of four temporal periods, as labeled in the Fig. In period 1, without irradiation, the thermal probes recorded the baseline temperatures at three different locations inside the tumor for about 6 min. In period 2, the NIRS system was turned on while the thermal recording continued, and the recorded thermal readings showed no obvious perturbation from the NIRS. After the NIRS signals were stabilized, a 10-min laser irradiation started. During the laser treatment, the tumor temperatures, $\Delta[HbO_2]$, and $\Delta[Hb]_{total}$ showed significant elevation (period 3 in Fig. 2a). Tumor temperatures increased significantly ($P < 0.0001$) with the irradiation. The tumor volumes near the tumor surface had more significant thermal effects: the temperature at the top (T-top) varied from 25.3 ± 0.1°C to 30.3 ± 0.1°C (mean ± sd), while the temperatures at the middle and bottom (T-middle and T-bottom) of the tumor were elevated from 26.1 ± 0.1°C to 29.8 ± 0.1°C and from 27.5 ± 0.1°C to 28.9 ± 0.1°C, respectively. The maximal changes in T-top, T-middle and T-bottom caused by the laser irradiation were 5.0 ± 0.1°C, 3.7 ± 0.1°C and 1.4 ± 0.1°C, respectively. Similarly, both $\Delta[HbO_2]$ and $\Delta[Hb]_{total}$ displayed significant increases over the entire irradiation period ($P < 0.005$), with the mean elevations of 0.04 ± 0.01 mM/DPF and 0.02 ± 0.01 mM/DPF, respectively. Notice that the maximal values of $\Delta[HbO_2]$ and $\Delta[Hb]_{total}$ shown in Fig. 2a are ~0.1 and 0.05 mM/DPF. When the laser beam was turned off in period 4, $\Delta[HbO_2]$, $\Delta[Hb]_{total}$ and temperatures all decreased, with the temperatures reaching the baselines quickly and $\Delta[HbO_2]$ and $\Delta[Hb]_{total}$ declining more gradually and not quite reaching the baselines within the 10-min recovery period.

To quantify the dynamic behaviors observed in Fig. 2a, single-exponential functions were applied to T-top, T-middle, $\Delta[HbO_2]$, and $\Delta[Hb]_{total}$ on both rising and falling periods, as shown in Fig. 2b,c. The time constants obtained from such fittings reveal the dynamic responses of signals to the initiation and termination of photothermal irradiation. As shown in Fig. 2b, T-top (time constant of 4.5 ± 0.5 min) has a faster response to laser irradiation than T-middle (time constant as 14.4 ± 0.6 min). The time constants for $\Delta[HbO_2]$ and $\Delta[Hb]_{total}$ are 3.85 ± 0.03 min and 3.95 ± 0.06 min, respectively. In response to the termination of laser irradiation, T-top and T-middle have a time constant of 3.9 ± 0.5 min and 12.3 ± 0.6 min, respectively (Fig. 2c). It is clearly seen that the dynamic thermal responses of the tumor to laser irradiation and to the termination of laser irradiation are well matched both at the tumor surface and within the tumor. However, the time constants for $\Delta[HbO_2]$ and $\Delta[Hb]_{total}$ to return to the baseline are much longer in the falling period, with 18.5 ± 0.5 min and 24.3 ± 0.8 min, respectively, also shown in Fig. 2c.

Similar protocols and measurements were performed on the other nine tumors. Figure 3 shows the average increases of the temperature at different locations. Temperatures near the tumor surface have maximal increases, whereas local temperatures near the bottom of the tumors have minimal increases observed from all the 10 tumors. The average elevations for T-top and T-bottom are 7 ± 3°C and 3 ± 2°C, respectively. The thermal readings from the middle position (T-middle) represent the average temperatures in the tumor volumes probed by the NIRS beams, and the average increase in T-middle for the 10 rats is 5 ± 2°C. The statistical analysis indicates significant differences between T-top, T-middle, and T-bottom ($P < 0.05$).

To investigate dynamic behaviors of the tumors in response to the initiation and termination of laser irradiation, the time constants of T-top, T-middle, $\Delta[HbO_2]$, and $\Delta[Hb]_{total}$ obtained from the rising and falling periods are summarized in Table 1. The results demonstrate several points: (1) an average dynamic change in T-top is significantly ($P < 0.05$) faster than that in T-middle in the rising period, with a time constant of 3.7 ± 1.1 min for T-top and 6.4 ± 3.2 min for T-middle. A similar significant difference ($P < 0.01$) also holds in the falling period with a time constant of 3.8 ± 1.2 min for T-top and 6.6 ± 2.7 min for T-middle, respectively. (2) The dynamic responses of $\Delta[HbO_2]$, $\Delta[Hb]_{total}$, and T-middle have no significant differences during the initiation of photoirradiation ($P > 0.4$). (3) The average time constant of T-top in the rising period is similar ($P > 0.9$) to that in the falling period, and so is that of T-middle ($P > 0.7$). However, (4) the dynamic response of

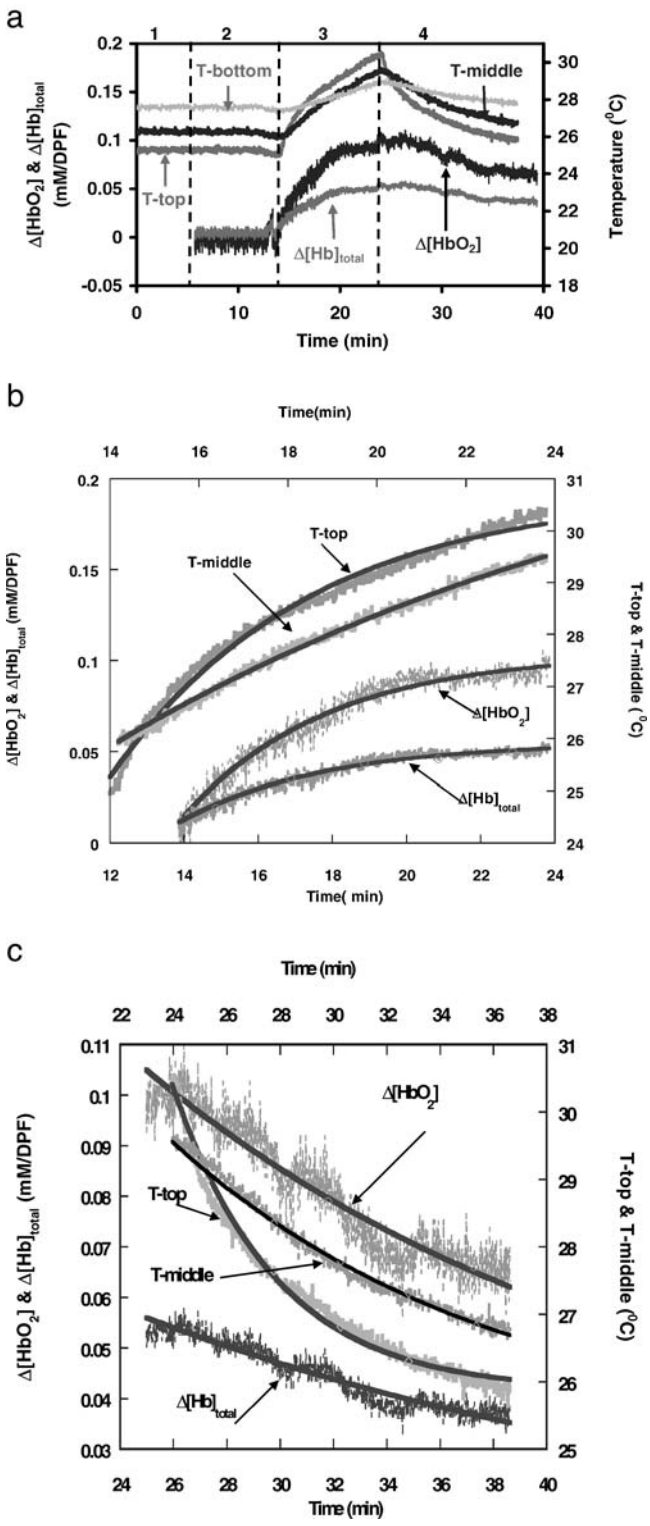

Figure 2. (a) Temporal profiles of the changes in tumor oxygenation and total hemoglobin concentrations, $\Delta[HbO_2]$ and $\Delta[Hb]_{total}$, and three intratumor temperatures during photothermal intervention in a representative DMBA-4 rat breast tumor (2.4 cm^3). The profile is divided into four periods, and the laser irradiation was applied only in period 3. (b) Respective single-exponential curve fittings for the rising period of T-top, T-middle, $\Delta[HbO_2]$ and $\Delta[Hb]_{total}$ displayed in (a). The top *x*-axis is used for the T-top and T-middle curves, whereas the bottom *x*-axis is for $\Delta[HbO_2]$ and $\Delta[Hb]_{total}$. Single exponential fitting yields: T-top = 5.76*(1 − exp[−{*t* − 147}/4.49]) + 24.95 with R = 0.99; T-middle = 7.28*(1 − exp[−{*t* − 14}/14.3]) + 25.98 with R = 0.99; $\Delta[HbO_2]$ = 0.093*(1 − exp[−{*t* − 14}/3.85]) + 0.013 with R = 0.98; $\Delta[Hb]_{total}$ = 0.044*(1 − exp[−{*t* − 14}/3.95]) + 0.012 with R = 0.98; (c) Respective single-exponential curve fittings for the falling period of T-top, T-middle, $\Delta[HbO_2]$ and $\Delta[Hb]_{total}$ displayed in (a). Single exponential fitting yields: T-top = –4.48*(1 − exp[−{*t* − 25}/3.86]) + 29.23 with R = 0.98; T-middle = –3.83*(1 − exp[−{*t* − 25}/12.29]) + 30.42 with R = 0.99; $\Delta[HbO_2]$ = –0.163*(1 − exp[−{*t* − 25}/18.5]) + 0.10 with R = 0.94; $\Delta[Hb]_{total}$] = –0.114*(1 − exp[−{*t* − 25}/24.3]) + 0.06 with R = 0.92.

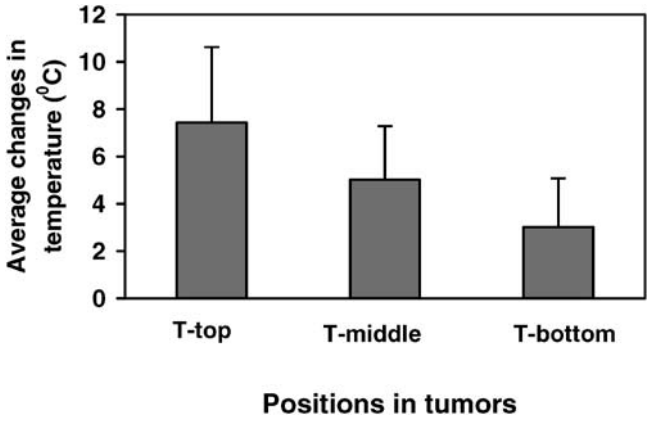

Figure 3. Average changes in temperature from the 10 rats for T-top, T-middle and T-bottom.

$\Delta[HbO_2]$ in the falling period (a time constant of 28 ± 22 min) is significantly slower ($P < 0.01$) than that in the rising period (a time constant of 5.3 ± 2.8 min), and so is $\Delta[Hb]_{total}$ response, with a time constant of 6.2 ± 3.7 min and 41 ± 32 min for the rising and falling periods, respectively ($P < 0.01$).

Furthermore, although $\Delta[HbO_2]$ and $\Delta[Hb]_{total}$ have similar dynamic trends in response to photoirradiation, a difference between their magnitudes exists. A strong correlation ($R^2 = 0.95$) between $\Delta[HbO_2]$ and $\Delta[Hb]_{total}$ has been observed, as shown in Fig. 4, where the amplitude in $\Delta[HbO_2]$ is nearly twice that of $\Delta[Hb]_{total}$ for all 10 tumors (with a slope of the fitted curve being 0.54).

Effect of the optical power density on tumor $\Delta[HbO_2]$, $\Delta[Hb]_{total}$ and temperatures

Repeated laser irradiation was applied to the 10 tumors, 4 of which were used in the previous single-irradiation treatment 3 or 4 days earlier. Figure 5a shows the profiles of the tumor vascular $\Delta[HbO_2]$, $\Delta[Hb]_{total}$ and tumor temperatures in response to irradiations under power densities of 0.32, 0.64, 0.96 and 1.27 W/cm^2, with an irradiation period of 10 min and a recovery period of 10 min between each treatment. Tumor temperatures (T-top, T-middle and T-bottom) increased significantly ($P < 0.0001$) from the baseline to different maximum values under different laser powers. The maximal changes in temperature in the middle of the tumor (T-middle) due to consecutive irradiation displayed a strong linear dependence on the laser power density, as shown in Fig. 5b. However, $\Delta[HbO_2]$ and $\Delta[Hb]_{total}$ showed interesting behaviors in response to the thermal irradiation at different light dosages. Under relatively low laser power irradiations (0.32, 0.64, 0.96 W/cm^2), both $\Delta[HbO_2]$ and $\Delta[Hb]_{total}$ increased significantly ($P < 0.0001$) with respect to the baselines, and they both declined significantly under a high laser power irradiation (1.27 W/cm^2), as shown in

Table 1. Time constants (minutes) of T-top, T-middle, $\Delta[HbO_2]$, and $\Delta[Hb]_{total}$ with respect to photoirradiation and termination

Tumor size(cm^3)	Rising part (in response to irradiation)				Falling part (in response to termination)			
	T-top	Tmiddle	$\Delta[HbO_2]$	$\Delta[Hb]_{total}$	T-top	Tmiddle	$\Delta[HbO_2]$	$\Delta[Hb]_{total}$
2.4	4.49	14.3	3.85	3.95	3.86	12.29	18.5	24.3
2.5	2.47	6.77	1.99	1.53	3.17	8.27	50	74
0.68	4.83	4.83	1.76	1.66	3.87	4.45	20	25
0.53	4.61	7.62	1.84	1.91	4.56	8.37	3.63	2.75
1.2	3.28	5.17	6.9	9.8	4.20	6.30	80	120
3.3	4.70	6.65	7.34	7.83	3.58	4.45	11.3	29.9
1.9	1.89	3.85	10.0	12.0	1.30	3.43	28	37
3.4	2.69	3.13	6.76	7.81	2.96	4.58	35	45
2.1	3.25	4.31	7.32	7.58	4.52	5.65	23.5	30
3.0	4.50	7.80	5.60	8.40	5.50	8.30	15.5	23.4
Average	3.7	6.4	5.3	6.2	3.8	6.6	28.	41
SD*	1.1	3.2	2.8	3.7	1.2	2.7	22.	33

*SD = standard deviation.

Fig. 5b. Similar to the feature observed in single irradiation, $\Delta[HbO_2]$ values had greater magnitude than $\Delta[Hb]_{total}$, whereas their dynamic trends were consistent.

To investigate the accumulative effects on $\Delta[HbO_2]$ and $\Delta[Hb]_{total}$ from several thermal irradiations given 10 min apart (Fig. 5a), we had also taken a direct reading for $\Delta[HbO_2]$ and $\Delta[Hb]_{total}$ with a high laser power of 1.27 W/cm^2 without any preirradiation. Figure 5c shows an example of this case, demonstrating that $\Delta[HbO_2]$ indeed decreases after an initial increase for a few minutes, whereas $\Delta[Hb]_{total}$ has less trend to drop within the 10-min treatment. The similarity for the ratio of $\Delta[HbO_2]$ to $\Delta[Hb]_{total}$ close to a factor of 2 still exists.

Temperature data for all 10 tumors under different power irradiations are plotted in Fig. 6a. The maximum changes in T-middle increase linearly with the optical radiation dosages, with a correlation of $R^2 > 0.91$ for all the cases and having an average slope of 13 ± 3 (°C/[W/cm^2]). To distinguish the tumors pretreated and nonpretreated with a single low-power irradiation (0.32 W/cm^2) 3 or 4 days before, the slopes of the linear regression for each of the tumors shown in Fig. 6a were classified into two groups, *i.e.* without pretreatment and with pretreatment (Fig. 6b). A Student's *t*-test showed that there is no significant difference ($P = 0.95$) between the two groups of slopes.

DISCUSSION

In this study, we have investigated vascular $\Delta[HbO_2]$, $\Delta[Hb]_{total}$ and internal temperature in response to photothermal therapy simultaneously in rat breast tumors by using an NIRS system and a thermal monitor, respectively. The results obtained in this study clearly demonstrate the compatibility of the NIRS system with the temperature monitoring system, without noticeable interference between the two systems (Fig. 2). The NIRS system offers a real-time measurement of $\Delta[HbO_2]$ and $\Delta[Hb]_{total}$ in tumor vasculature within the optical field of the NIR probes, while the multichannel thermal monitor records the temperatures at specific locations within the tumors in real time. The compatibility of the two systems permits simultaneous determinations of thermal and vascular characteristics of treated tumors under photothermal therapy, providing valuable insight into the dynamic relationship between the tumor vascular contents and the thermal effect in treated tumor tissues.

Thermal treatment to tumors has been demonstrated to cause cellular cytotoxicity, and thus, to destroy the tumor cells (36–38). Laser irradiation applied in this study proves its ability to induce photothermal effects inside the rat breast tumors. The single exponential increase in tumor temperature obtained in our results indicates that an extended exposure period to the laser beam may gradually stabilize the tumor temperature at a certain level, depending on both the laser power density and the individual tumors (as seen in Figs. 2a and 5a). Manipulation of the laser power may help adjust the internal tumor temperature, resulting in optimal tissue destruction. Although a strong linear relation between the maximum temperature increase within the tumors and the irradiation power density has been observed for all the tumors, the actual dependence of tumor temperature on the laser power density does vary from tumor to tumor (Fig. 6). Such intertumor variability demonstrates the necessity of real-time monitoring for tumor temperature under photothermal therapy. Moreover, the tumor temperatures near the surface (T-top) respond to the photoirradiation more rapidly and with a greater increase than those within deeper tumor tissue (T-middle) (as seen in Figs. 2, 3, and 5a, and Table 1). Such large thermal effects can cause tissue damage at the tumor surface. To avoid such thermal damage,

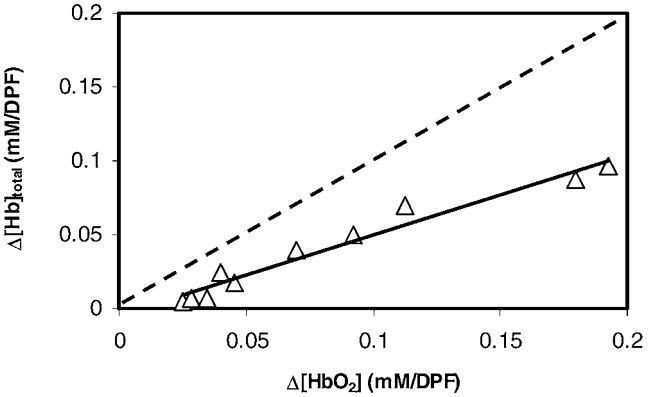

Figure 4. Relationship between $\Delta[HbO_2]$ and $\Delta[Hb]_{total}$ for the 10 rat tumors under single laser irradiation treatment (0.32 W/cm^2 for 10 min) with a linear fit of $\Delta[Hb]_{total} = 0.54*\Delta[HbO_2] - 0.0039$ (the solid curve) and a correlation of $R^2 = 0.96$. The dashed line represents the situation of $\Delta[HbO_2] = \Delta[Hb]_{total}$.

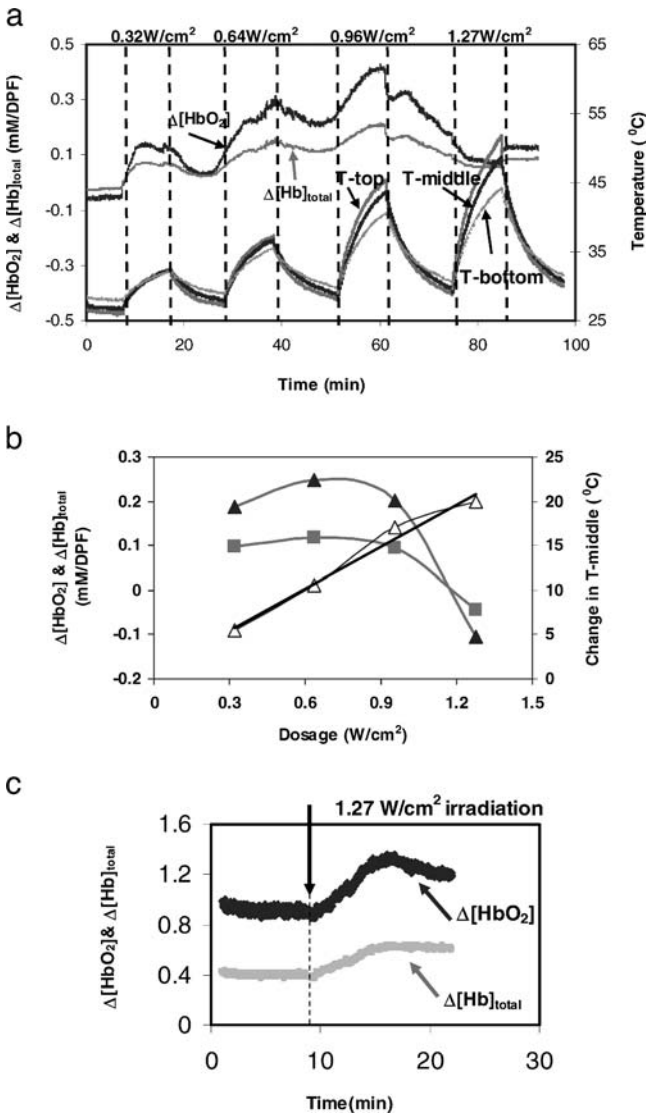

Figure 5. (a) The temporal profiles of vascular $\Delta[HbO_2]$, $\Delta[Hb]_{total}$ and temperatures of a tumor (#6, 3.0 cm^3) in response to repeated laser irradiations with different laser power densities (0.32, 0.64, 0.96 and 1.27 W/cm^2) for a 10-min treatment cycle with a 10-min recovery period between each treatment. (b). The correlations between the changes in $\Delta[HbO_2]$ (solid triangles), $\Delta[Hb]_{total}$ (squares), T-middle (open triangles), and laser irradiation power densities in the tumors. The thick straight line is the best-fitting curve for the tumor temperature increases as function of laser dosage. (c) The temporal profiles of vascular $\Delta[HbO_2]$ and $\Delta[Hb]_{total}$ of a tumor irradiated with a single laser power density of 1.27 W/cm^2.

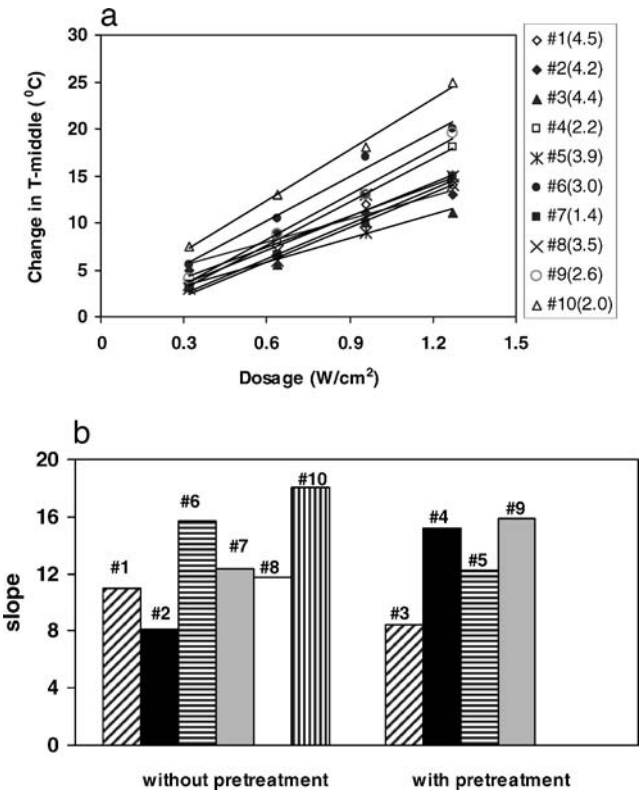

Figure 6. (a) Correlations between the maximum changes in T-middle reached at the end of each photothermal treatment cycle and the optical irradiation power density from the 10 treated rats. The numbers after the symbol ''#'' are labels for different tumors. The numbers inside the parentheses indicate the tumor volume, with unit of cm^3. Note that there are four tumors that had preirradiations 3–4 days earlier, and their tumor volumes have been possibly changed in comparison to those listed in Table 1. (b). The slopes in (a) for all the tumors were classified into two groups: without pretreatment and with pretreatment. A *t*-test between these two groups of slopes gives rise to $P = 0.95$.

intratumoral injection of selective absorbers, such as indocyanine green, has been used by Chen *et al*. to selectively manipulate the temperature within the tumor without severe damage at the tumor surface (11,12,39).

It is seen clearly in this study that tumor vascular contents, *i.e*. oxygenated and deoxygenated hemoglobin, are greatly affected by photothermal therapy. When the photothermal irradiation with a low power density (0.32 W/cm^2) was applied to the breast tumors, both $\Delta[HbO_2]$ and $\Delta[Hb]_{total}$ increased significantly ($P < 0.005$) in all the tumors (Figs. 2a, 4 and 5a). The dynamic behaviors of $\Delta[HbO_2]$ and $\Delta[Hb]_{total}$ in response to photo-irradiation, quantified by the time constants, are in the same order as those of tumor interior temperature, T-middle, while their behaviors in response to the termination of photoirradiation are much slower than those of T-middle (Fig. 2 and Table 1). In contrast to the lower laser power irradiation, higher laser power densities could cause interesting responses in tumor vascular contents. As seen in Fig. 5b,c, $\Delta[HbO_2]$ started to decrease when the laser power approached a certain level, either with or without preirradiation. Intriguingly, although $\Delta[HbO_2]$ has the same dynamic trend as $\Delta[Hb]_{total}$ in response to photoirradiation, the magnitude of $\Delta[HbO_2]$ is more profound than that of $\Delta[Hb]_{total}$ (Figs. 4, 5).

The analysis on the dynamic behaviors of tumor vascular contents and interior tumor temperature in response to photoirradiation allows us to better understand the mechanism of photothermal therapy. The time constants of $\Delta[HbO_2]$ as well as of $\Delta[Hb]_{total}$ have the same order as those of interior tumor temperature. We may speculate that an increase in tumor temperature may lead to vessel dilation within tumor vasculature, and thus, resulting in an increase in blood inflow. Such an increase in blood inflow will give rise to an increase in $\Delta[Hb]_{total}$ as well as $\Delta[HbO_2]$.

Besides thermal effects, it is reasonable to expect other photoactivation processes involved in the laser irradiation. It is known that direct exposure of vascular tissue to visible light causes vasodilation (40), whereas the thermal effect from visible light is minor. Photoactivation has also been reported to cause

upregulation of nitric oxide, and thus, produce vasodilation (41–43). The increase of tumor blood contents due to laser irradiation observed in our study may be attributed to the vessel dilation induced by the direct effect of heating as well as photoactivation. Consistently, the single-exponential trend of both $\Delta[Hb]_{total}$ and $\Delta[HbO_2]$ in response to laser irradiation indicated the existence of vessel dilation. The fact that the time constants of $\Delta[HbO_2]$ and $\Delta[Hb]_{total}$ in response to the laser termination are longer than those in response to the laser initiation (Table 1, Figs. 2a, 5a) implies a longer settling time needed for the recovery of dilated vessels.

In the laser thermal treatment, we realized that $\Delta[HbO_2]$ as well as $\Delta[Hb]_{total}$ did not completely return to the baseline during each of the recovery periods (Figs. 2a, 5a). Figure 5c was taken from a tumor that was exposed to a single high-power laser irradiation (1.27 W/cm^2), displaying somewhat different behavior in comparison to that under consecutive repeated treatments: the $\Delta[HbO_2]$ signals increased, followed by an obvious decrease. These phenomena lead us to a speculation that the previous laser exposure ''preconditions'' the treated tumor, with respect to consecutive treatments, and affects the response of tumor to subsequent high irradiation exposure, although the single lower-power irradiation pretreated 3 or 4 days earlier has no obvious influence on the later treatment (Fig. 6b). It is reasonable to believe that the ''preconditioning'' can be minimal if the time intervals between two repeated irradiations are two to three times longer than the time constants during the recovery periods, such as in the order of 1–1.5 h.

The interesting phenomenon, *i.e.* changes of oxygenated hemoglobin concentration are nearly two times greater than those of total hemoglobin concentration, allures us to speculate that the increase in $\Delta[HbO_2]$ comes partly from the increase of $\Delta[Hb]_{total}$, and partly from the conversion of deoxygenated hemoglobin to oxygenated hemoglobin. The correlation of magnitude between $\Delta[HbO_2]$ and $\Delta[Hb]_{total}$ unambiguously demonstrates that the increased total hemoglobin concentration, due to blood vessel dilation, is mostly oxygenated after the irradiation starts. It basically implies that photoirradiation may increase the tumor oxygenation, which will be beneficial to some nonsurgical treatments, such as chemotherapy and radiotherapy (37).

In summary, changes in breast tumor temperature and vascular oxygenation have been simultaneously measured using a multichannel thermal monitor and an NIRS system, while the tumors were under photothermal irradiation. The results have demonstrated that: (1) the compatibility of thermal monitoring system and the NIR system permits simultaneous determinations of thermal and vascular characteristics of the treated tumors; (2) photoirradiation did have the ability to induce thermal effects inside the rat breast tumors in a single exponential trend, thus leading to destruction of the tumor cells; (3) the response of $\Delta[HbO_2]$ and $\Delta[Hb]_{total}$ to photoirradiation may be attributed to vessel dilation under both thermal and photo effect; (4) low-power laser irradiations predelivered 3 or 4 days earlier have no effect on the later treatments; the previous laser exposures within a time interval of 10 min do influence the response of tumor vascular contents to subsequent high irradiation; (5) the fact that the change in the magnitude of $\Delta[HbO_2]$ is nearly two times greater than that of $\Delta[Hb]_{total}$ suggests that photoirradiation may enhance tumor vascular oxygenation. The primary results from this study clearly indicate that besides a considerable thermal effect, low-power density irradiation could also result in a significant enhancement of tumor vascular oxygenation; this enhancement may lead to improvement of treatment efficiency.

Acknowledgements—The authors acknowledge the support in part by the Department of Defense Breast Cancer Research Programs DAMD17-01-1-0423 (Y.G.) and DAMD17-00-1-0459 (H.L.), in part by Chinese National Science Foundation Committee (NSFC 30371362), in part by the Oklahoma Center for Advancement of Science and Technology (OCAST) AP01-016 (W.R.C.) and from the University of Central Oklahoma (W.R.C.), and in part by the National Institutes of Health P20 RR016478, the INBRE Program of the National Center for Research Resources (W.R.C.).

REFERENCES

1. Jacques, S. L. (1992) Laser-tissue interactions. Photochemical, photothermal, and photomechanical. *Surg. Clin. North Am.* **72**, 531–558.
2. Thomsen, S. L. (1991) Pathologic analysis of photothermal and photomechanical effects of laser–tissue interactions. *Photochem. Photobiol.* **53**, 825–835.
3. Chen, W. R., R. L. Adams, S. Heaton, D. T. Dickey, K. E. Bartels and R. E. Nordquist (1995) Chromophore-enhanced laser-tumor tissue photo-thermal interaction using an 808-nm diode laser. *Cancer Lett.* **88**, 15–19.
4. Chen, W. R., R. L. Adams, K. E. Bartels and R. E. Nordquist (1995) Chromophore enhanced in vivo tumor cell destruction using an 808-nm diode laser. *Cancer Lett.* **94**, 125–131.
5. Thistlethwaite, A. J., D. B. Leeper, D. J. Moylan and R. E. Nerlinger (1986) pH distribution in human tumors. *Int. J. Radiat. Oncol. Biol. Phys.* **11**, 1647–1652.
6. Reinhold, H. S. and B. Endrich (1986) Tumor microcirculation as a target for hyperthermia: a review. *Int. J. Hyperthermia* **2**, 111–137.
7. Anghileri, L. J. and J. Robert (1986) *Hyperthermia in Cancer Treatment*. CRC Press, Boca Raton, FL.
8. Thews, O., D. K. Kelleher and P. Vaupel (2002) Dynamics of tumor oxygenation and red blood cell flux in response to inspiratory hyperoxia combined with different levels of inspiratory hypercapnia. *Radiother. Oncol.* **62**, 77–85.
9. Hockel, M. and P. Vaupel (2001) Biological consequences of tumor hypoxia. *Semin. Oncol.* **28**, 36–41.
10. Wouters, B. G., S. A. Weppler, M. Koritzinsky, W. Landuyt, S. Nuyts, J. Theys, P. K. Chiu and P. Lambin (2002) Hypoxia as a target for combined modality treatments. *Eur. J. Cancer* **38**, 240–257.
11. Chen, W. R., R. L. Adams, R. Carubelli and R. E. Nordquist (1997) Laser-photosensitizer assisted immunotherapy: a novel modality for cancer treatment. *Cancer Lett.* **115**, 25–30.
12. Chen, W. R., H. Liu, J. W. Ritchey, K. E. Bartels, M. D. Lucroy and R. E. Nordquist (2002) Effect of different components of laser immunotherapy in treatment of metastatic tumors in rats. *Cancer Res.* **62**, 4295–4299.
13. Korbelik, M., V. R. Naraparaju, and N. Yamamoto (1997) Macrophage-directed immunotherapy as adjuvant to photodynamic therapy of cancer. *Br. J. Cancer.* **75**, 202–207.
14. Curry, P. M., A. J. Steward., L. Hardwicke, C. Smith and J. R. North (2001) Augmentation of tumor immunity with ENHANZYN adjuvant following verteporfin PDT: photodynamic vaccination (PDV). *SPIE* **4257**, 9–18.
15. Chen, W. R., A. K. Singhal, H. Liu and R. E. Nordquist (2001) Antitumor immunity induced by laser immunotherapy and its adoptive transfer. *Cancer Res.* **61**, 459–461.
16. Chen, W. R., W. G. Zhu, J. R. Dynlacht, H. Liu and R. E. Nordquist (1999) Long-term tumor resistance induced by laser photo-immunotherapy. *Int. J. Cancer* **81**, 808–812.
17. Fingar, V. H., T. J. Wieman and K. W. Doak (1991) Mechanistic studies of PDT-induced vascular damage: evidence that eicosanoids mediate this process. *Int. J. Radiat. Biol.* **60**, 303–309.
18. Yu, W., J. Naim and R. Lanzafame (1994) The effect of laser irradiation on the release of bFGF from 3T3 Fibroblasts. *Photochem. Photobiol.* **59**, 167–170.
19. Karu, T. (1988) Molecular mechanism of the therapeutic effect of low intensity laser radiation. *Laser Life Sci.* **2**, 53–74.
20. Margaret, T. T., W. Riley, X. Bai, E. Buchmann and H. T. Whelan (2001) Light-emitting diode treatment reverses the effect of TTX on cytochrome oxidase in neurons. *Neuroreport* **12**, 3033–3037.
21. Liu, H., Y. Song, K. L. Worden, X. Jiang, A. Constantinescu and R. P. Mason (2000) Noninvasive investigation of blood oxygenation

dynamics of tumors by near infrared spectroscopy. *Appl. Opt.* **39**, 5231–5243.
22. Kim, J. G., Y. Song, D. Zhao, A. Constantinescu, R. P. Mason and H. Liu (2003) Interplay of tumor vascular oxygenation and pO_2 in tumors using NIRS, ^{19}F MR pO_2 mapping, and pO_2 needle electrode. *J. Biomed. Opt.* **8**, 53–62.
23. Gu, Y., V. Bourke, J. G. Kim, A. Constantinescu, R. P. Mason and H. Liu (2003) Dynamic response of breast tumor oxygenation to hyperoxic respiratory challenge monitored with three oxygen-sensitive parameters. *Appl. Opt.* **42**, 2960–2967.
24. Horecker, B. L. (1943) The absorption spectra of hemoglobin and its derivatives in the visible and near infrared regions. *J. Biol. Chem.* **148**, 173–183.
25. Van Kampen, E. J. and W. G. Zijlstra (1965) Determination of hemoglobin and its derivatives. *Adv. Clin. Chem.* **8**, 141–187.
26. Benesch, R., G. Macduff and R. E. Benesch (1965) Determination of oxygen equilibria with a versatile new tonometer. *Anal. Biochem.* **11**, 81–87.
27. Benesch, R. E., R. Benesch and S. Yung (1973) Equations for the spectrophotometric analysis of hemoglobin mixtures. *Anal. Biochem.* **55**, 245–248.
28. Van Assendelft, O. W. and W. G. Zijlstra (1975) Extinction coefficients for use in equations for the spectrophotometric analysis of haemoglobin mixtures. *Anal. Biochem.* **69**, 43–48.
29. Sevick, E. M., B. Chance, J. Leigh, S. Nioka and M. Maris (1991) Quantitation of time- and frequency-resolved optical spectra for the determination of tissue oxygenation. *Anal. Biochem.* **195**, 330–351.
30. Gu, Y., Z. Qian, J. Chen, D. Blessington, N. Ramanujam and B. Chance (2002) High resolution three dimensional scanning optical image system for intrinsic and extrinsic contrast agents in tissue. *Rev. Sci. Instrum.* **73**, 172–178.
31. Zijlstra, W. G., A. Buursma, H. E. Falke and J. F. Catsburg (1994) Spectrophotometry of hemoglobin: absorption spectra of rat oxyhemoglobin, deoxyhemoglobin, carboxyhemoglobin, and methemoglobin. *Comp. Biochem. Physiol.* **107B**, 161–166.
?3 32. Cope, M. (1991) The application of near infrared spectroscopy to non invasive monitoring of cerebral oxygenation in the newborn infant. Ph.D. dissertation, University College London.
33. Chatterjee, S. K. and U. Kim (1976) Biochemical properties of cyclic nucleotide phosphodiesterase in metastasizing and nonmetastasizing rat mammary carcinomas. *J. Natl. Cancer Inst.* **56**, 105–110.
34. Chatterjee, S. K. and U. Kim (1977) Galactosyltransferase activity in metastasizing and nonmetastasizing rat mammary carcinomas and its possible relationship with tumor cell surface antigen shedding. *J. Natl. Cancer Inst.* **58**, 273–280.
35. Chatterjee, S. K. and U. Kim (1978) Fucosyltransferase activity in metastasizing and nonmetastasizing rat mammary carcinomas. *J. Natl. Cancer Inst.* **61**, 151–162.
36. Song, C. W., A. lokshina, J. G. Rhee, M. Patten and S. H. Levitt (1984) Implication of blood flow in hyperthermic treatment of tumors. *IEEE Trans. Biomed. Eng.* **31**, 9–16.
37. Dewey, E. C., L. E. Hopwood, S. A. Sapareto and L. E. Gerweck (1977) Cellular responses to combination of hyperthermia and radiation. *Radiology* **123**, 463–474.
38. Sapareto, S. A. and W. C. Dewey (1984) Thermal dose determination in cancer therapy. *Int. J. Radiat. Oncol. Biol. Phys.* **10**, 787–800.
39. Liu, V. G., T. M. Cowan, S. W. Jeong, S. L. Jacques, E. C. Lemley and W. R. Chen (2002) Selective photothermal interaction using an 805nm diode laser and indocyanine green in gel phantom and chicken breast tissue. *Lasers Med. Sci.* **17**, 272–279.
40. Furchgott, R. F., S. J. Ehrreich and E. Greenblatt (1961) The photoactivated relaxation of smooth muscle of rabbit aorta. *J. Gen. Physiol.* **44**, 499–518.
41. Chang, K.C., E. B. Koo, G. W. Lee, Y. J. Kang and H. Y. Lee (1998) Comparison of relaxations evoked by photoactivation of NO-containing compounds and nitrergic nerve stimulation in 5-hydroxytryptamine and potassium contracted rat gastric fundus. *Gen. Pharmacol.* **30**, 585–591.
42. Venturini, C. M., R. M. J. Palmer and S. Moncada (1993) Vascular smooth muscle contains a depletable store of a vasodilator which is light-activated and restored by donors of nitric oxide. *J. Pharmacol. Exp. Therap.* **266**, 1497–1500.
43. Matsunaga, K. R. and F. Furchgott (1991) Response of rabbit aorta to nitric oxide and superoxide generated by ultraviolet irradiation of solutions containing inorganic nitrite. *J. Pharmacol. Exp. Ter.* **259**, 1140–1146.